![TU/e Eindhoven University of Technology logo]

Bi-directional Transcutaneous Wireless Communication System for Intracortical Visual Prostheses

Document Version:
Publisher's PDF, also known as Version of Record (includes final page, issue and volume numbers)

Please check the document version of this publication:

• A submitted manuscript is the version of the article upon submission and before peer-review. There can be important differences between the submitted version and the official published version of record. People interested in the research are advised to contact the author for the final version of the publication, or visit the DOI to the publisher's website.
• The final author version and the galley proof are versions of the publication after peer review.
• The final published version features the final layout of the paper including the volume, issue and page numbers.

Link to publication

Download date: 17. Nov. 2023

Bi-directional Transcutaneous Wireless Communication System for Intracortical Visual Prostheses

PROEFSCHRIFT

ter verkrijging van de graad van doctor aan de
Technische Universiteit Eindhoven, op gezag van de
rector magnificus, prof.dr.ir. F. P. T. Baaijens, voor een
commissie aangewezen door het College voor
Promoties in het openbaar te verdedigen op
vrijdag 22 april 2022 om 16:00 uur

door

Adedayo Eberechukwu Omisakin

geboren te Lagos, Nigeria

Dit proefschrift is goedgekeurd door de promotoren en de samenstelling van de promotiecommissie is als volgt:

voorzitter: prof.dr.ir. S. Heemstra
promotor: prof.dr.ir. M.J. Bentum
copromotor: dr.ir. R.M.C. Mestrom
leden: prof.dr.ir. A.B. Smolders
                     prof.dr.ir. H.J. Visser
                     prof.dr.ir. W.A. Serdijn (Universiteit Delft)
                     dr.ir. P.J.A. Harpe
                     prof.dr.ir. F. Solzbacher (Universiteit Utah/ Blackrock Microsystems)

Contents

Summary

Restoring visual function in blind people using technology can be challenging but beneficial in improving their quality of life. For most cases of blindness, nerves between the eyes and brain are damaged, so the only option is to stimulate the visual cortex directly. Such a system requires external cameras, image processing and implanted electrodes. Powering, stimulating the brain (downlink), and recording neural activity (uplink) is preferably done wirelessly to avoid infections and is also more comfortable. The wireless communication to and from the implant is the core topic of this work. The wireless powering is subject to another PhD project.

The implanted electrodes in the visual cortex are grouped into 16 tiles, arrays of 64 electrodes totalling 1024 electrodes. There are a few possible configurations for the wireless system to communicate with these tiles. Our approach after discussion with neuro-surgeons is to place the central transceiver beneath the skin, with the electrode arrays tethered to it. This provides a scalable solution because it avoids multiple transceivers, and it avoids excessive attenuation or path loss through the skull. The main challenge, however, is the possible micro-motion of the implanted connecting wires, which can be partly alleviated with better packaging and implantation.

Based on a comparison between possible communication techniques and systems that meet the requirements for communication to and from the intracortical visual implant, the most viable solutions for downlink and uplink are investigated in detail. For the downlink, binary phase shift keying (BPSK) communication with an inductive link is selected. For the uplink, impulse radio ultra-wideband (IR-UWB) using on-off keying (OOK) modulation is proposed.

For the downlink part, a low-power non-coherent digital demodulator was designed for the implanted receiver. The downlink was experimentally demonstrated on a scaled-down version at a lower carrier frequency showing a promising data rate delivery. The experimental demonstration provides proof of principle for a future system that consumes under one mW at the receiver side in an integrated circuit (IC). Due to its digital architecture, the system is easily adjustable to an industrial, scientific and medical (ISM) frequency band, with its power consumption scaling linearly with the carrier frequency. The tested system uses off-the-shelf coils, which gave sufficient bandwidth while staying within safe specific absorption

rate (SAR) limits. The digital receiver achieved a reduction in power consumption by skipping clock cycles of redundant bits.

For the uplink part, the need for a low-power transmitter with high data rate was shown. Electromagnetic simulation of the transmit antenna, tissues and receive antenna resulted in about 20–30 dB path loss. The worst-case link budget of the IR-UWB demonstrates its system-level feasibility. A proposed IR-UWB transmitter demonstrated low-power consumption at its schematic stage and a high data rate (over 50 Mbps) potential. A proof of principle non-coherent external receiver was investigated, already delivering high data rate at its rudimentary stage. The uplink system promises to deliver a vital link for the compressed low data rate architecture to enable monitoring and calibration of the implanted intracortical prosthesis.

A sub-milliwatt transceiver IC for the intracortical visual prosthesis implant site was designed, fabricated and measured. It delivers 1 Mbps for the downlink (for stimulation) and 50 Mbps for the uplink (for recording), using a non-coherent BPSK demodulator and an IR-UWB transmitter, respectively. Its predominately digital components led to the low power consumption being sub-milliwatt using complementary metal–oxide–semiconductor (CMOS) technology for IC integration. Based on the transceiver IC in the implant, the system link budget analysis for both uplink and downlink shows achievable figures: 18–23 dB excess margin for uplink with 20 dB of path-loss, and 12–26 dB for downlink. These figures show that the link will be closed with an excess margin for the antenna/coil pair to communicate through 3 to 7 mm of skin.

In conclusion, the bi-directional communication using the proposed system comprises of IR-UWB for the uplink and BPSK communication with an inductive link for the downlink, and delivers sufficient data rates. We have developed a sub-milliwatt transceiver IC for the implant, which is the most power-constrained sub-system of the wireless part of the prosthesis. The communication system is reliable and physically secure when fully developed and integrated into an intracortical visual prosthesis due to closing the communication links with excess margin. The logical next step is to fabricate antennas/coils and a transceiver IC for the external side to realize the system link budget and also system packaging.

Samenvatting

Het herstellen van de visuele functie bij blinde mensen met behulp van technologie is een uitdaging, maar gunstig voor het verbeteren van hun kwaliteit van leven. Bij de meeste gevallen van blindheid zijn de zenuwen tussen de ogen en de hersenen beschadigd, waardoor de enige optie is om de visuele cortex direct te stimuleren. Een dergelijk systeem vereist externe camera's, beeldverwerking en geïmplanteerde elektroden. De energievoorziening, het stimuleren van de hersenen (downlink) en het opnemen van neurale activiteit (uplink) gebeurt bij voorkeur draadloos om infecties te voorkomen. Dat maakt het ook comfortabeler. De draadloze communicatie van en naar het implantaat is het kernonderwerp van dit werk. De draadloze energievoorziening is het onderwerp van een ander PhD-project.

De geïmplanteerde elektroden in de visuele cortex zijn gegroepeerd in 16 tegels, arrays van 64 elektroden, wat het totaal op 1024 elektroden brengt. Er zijn een paar mogelijke configuraties voor het draadloze systeem om met deze tegels te communiceren. Na overleg met neurochirurgen, is onze benadering om de centrale zendontvanger onder de huid te plaatsen, met de elektrode-arrays eraan vastgemaakt via verbindingsdraden. Dit biedt een schaalbare oplossing omdat het vermijdt dat er meerdere zendontvangers nodig zijn en voorkomt dat er overmatige signaalverzwakking (padverlies) door de schedel plaats vindt.. De grootste uitdaging is echter de mogelijke microbeweging van de geïmplanteerde verbindingsdraden, hetgeen gedeeltelijk kan worden beperkt door een betere verpakking en implantatie.

Op basis van een vergelijking tussen mogelijke communicatietechnieken en -systemen die voldoen aan de eisen voor communicatie van en naar de intracorticale visuele prothese, zijnde meest haalbare oplossingen voor downlink en uplink in detail onderzocht. Voor de downlink is binaire phase shift keying (BPSK) communicatie met een inductieve link geselecteerd. Voor de uplink wordt impulsradio ultrabreedband (IR-UWB) met behulp van aan-uit-sleuteling (OOK) modulatie voorgesteld.

Voor het downlink-gedeelte werd een niet-coherente digitale demodulator met laag vermogen ontworpen voor de geïmplanteerde ontvanger. De downlink werd experimenteel gedemonstreerd op een geschaalde versie bij een lagere draaggolffrequentie die een veelbelovende gegevenssnelheid liet zien. De experimentele demonstratie levert een principieel bewijs voor een toekomstig systeem dat minder dan één mW verbruikt aan de ontvanger zijde in een geïntegreerde schakeling (IC). Dankzij de digitale architectuur kan het systeem een-

voudig worden aangepast aan een industriële, wetenschappelijke en medische (ISM) frequentieband, waarbij het stroomverbruik lineair schaalt met de draaggolffrequentie. Het geteste systeem maakt gebruik van kant-en-klare spoelen, die voldoende bandbreedte gaven terwijl ze binnen veilige limieten voor specifieke energie-absorptie (SAR) van weefsel bleven. De digitale ontvanger zorgde voor een vermindering van het stroomverbruik door klokcycli van redundante bits over te slaan.

Voor het uplink-gedeelte is er duidelijk behoefte aan een zender met een laag vermogen en een hoge datasnelheid. Elektromagnetische simulaties met de zendantenne, tussenliggende weefsels en de ontvangstantenne resulteerde in ongeveer 20-30 dB padverlies. Het worst-case link budget van de IR-UWB toont de haalbaarheid op systeemniveau aan. Een voorgestelde IR-UWB-zender liet een laag stroomverbruik zien in de schematische fase samen met een potentieel voor een hoge datasnelheid (meer dan 50 Mbps). Een proof-of-principle niet-coherente externe ontvanger werd onderzocht, die al een hoge datasnelheid leverde in zijn rudimentaire fase. Hiermee geeft het uplink-systeem de belofte om te voorzien in een essentiële link voor de architectuur met gecomprimeerde lage datasnelheid. Dit zal monitoring en kalibratie van de geïmplanteerde intracorticale prothese mogelijk te maken.

Er is een sub-milliwatt zendontvanger-IC voor de intracorticale visuele prothese ontworpen, gefabriceerd en gemeten. Deze levert 1 Mbps voor de downlink (voor stimulatie) en 50 Mbps voor de uplink (voor opname), met respectievelijk een niet-coherente BPSK-demodulator en een IR-UWB-zender. De overwegend digitale componenten leidden tot een laag stroomverbruik van sub-milliwatt, gebruik makend van complementaire metaal-oxide-halfgeleider (CMOS) -technologie voor IC-integratie. Gebaseerd op de zendontvanger-IC in het implantaat, toont de analyse van het systeem link budget voor zowel uplink als downlink haalbare cijfers: 18-23 dB extra marge voor uplink met 20 dB padverlies, en 12-26 dB voor downlink. Deze cijfers laten zien dat een verbinding tot stand gebracht kan worden met een extra marge voor het antenne/spoelpaar om te communiceren door 3 tot 7 mm huid.

Ter conclusie omvat de bidirectionele communicatie van het voorgestelde systeem IR-UWB voor de uplink en BPSK-communicatie met een inductieve link voor de downlink, en levert deze voldoende hoge datasnelheden. We hebben een sub-milliwatt transceiver-IC ontwikkeld voor het implantaat, het meest beperkte subsysteem van het draadloze deel van de prothese. Het communicatiesysteem is betrouwbaar en fysiek veilig wanneer het volledig is ontwikkeld en geïntegreerd in een intracorticale visuele prothese en bevat voldoende marge in het link budget voor de communicatieverbindingen. Een logische volgende stap is het fabriceren van antennes/spoelen en een zendontvanger IC aan de buitenzijde van het hoofd om daarmee het systeem link budget en ook de systeemverpakking te realiseren.

List of Abbreviations and Symbols

Abbreviations and acronyms

ADC	analog-to-digital converter
ASK	amplitude shift keying
BER	bit error rate
BPF	band pass filter
BPSK	binary phase shift keying
CMOS	complementary metal–oxide–semiconductor
CW	continuous wave
DPSK	differential phase shift keying
FCC	federal communications commission
FSK	frequency shift keying
IC	integrated circuit
IF	intermediate frequency
IR-UWB	impulse radio ultra-wideband
ISM	industrial, scientific and medical
LNA	low noise amplifiers
MICS	microwave integrated circuits
NESTOR	NEuronal STimulation fOr Recovery of Function
NF	noise figure
OOK	on-off keying
PAM	pulse amplitude modulation
PL	path loss
PCB	printed circuit board
PDM	pulse delay modulation
PLL	phase locked loop
POR	power-on-reset
PPM	pulse position modulation
PSD	power spectral density
PSK	phase shift keying

RF	radio frequency
RFIC	radio frequency integrated circuits
RGC	retinal ganglion cells
SAR	specific absorption rate
SNR	signal-to-noise ratio
SPST	single-pole single-throw
UWB	ultra-wideband
VCO	voltage controlled oscillator
WiFi	wireless fidelity
WLAN	wireless local area network

List of symbols

Symbol	Description
$b(t)$	binary signal in time domain
$S_{OOK}(t)$	OOK signal in time domain
$S_{FSK}(t)$	FSK signal in time domain
$S_{BPSK}(t)$	BPSK signal in time domain
f_c	carrier frequency
T	bit duration
v	number of bit periods
E_b/N_0	normalized signal to noise ratio
ϕ_1	phase of a signal
f	frequency
f_{res}	resonant frequency
f_{peak}	frequency with a peak signal value
k	coupling factor
N	count-up number
T_{PSK}	period of PSK symbol
f_{PSK}	frequency of PSK symbol
f_{OSC}	frequency of the oscillator (clock)
T_{OSC}	period of the oscillator (clock)
p	number of carrier symbol skipped
c_{lower}	lower set-limit factor
c_{lower}	upper set-limit factor
f_U	upper frequency
f_L	lower frequency
λ	wavelength
ε_r	relative permittivity
S	receiver sensitivity
N_{floor}	noise floor
S11	reflection coefficient
S21	transmission loss
PL_{MAX}	maximum tolerable loss
P_{TX}	transmit power

CHAPTER ONE

Introduction

1.1 How to restore vision in the blind?

In recent decades, a radical change in biomedical engineering began around clinical applications to electrically stimulate the nervous system [1–6]. A plethora of clinical systems that have emerged from this revolution abound: cochlear implants to restore hearing, deep brain stimulators to alleviate symptoms of Parkinson's disease, and vagal nerve stimulators to ameliorate the effects of epilepsy [4–6]. A significantly more complex system already emerging is one to restore functional vision in visually impaired, or blind, individuals by electrically stimulating the visual pathway, based on input from a video system on a patient's head: a visual prosthesis [7].

Approximately 216 million people worldwide are visually impaired, 36 million of whom are blind [8, 9], and most would need an intracortical visual prosthesis to regain some (rudimentary) form of vision. The ultimate purpose of a visual prosthesis is to artificially produce a visual perception in individuals with profound loss of vision due to disease or injury. This will allow them to perform activities for which current assistive technologies have severe limitations, such as reading text, recognizing faces, and navigating through unfamiliar spaces. When the visual system is damaged by disease or trauma, blindness can be the ultimate result; this is further exacerbated by the inability of the neural elements of the visual system to repair or regenerate. In this way, the prosthesis can artificially generate visual perception where none would otherwise exist. While a visual prosthesis cannot replace the full complexity of the mammalian visual system (i.e. color, depth, textures), it should provide at least an amount of visual perception that will help an individual to perform day to day tasks more autonomously. Although the experience may be limited in scope, it should improve the quality of life of the individual nonetheless [7]. When implementing such a prosthesis, it is essential to consider the patient's point of view. For some blind patients, even a minor restoration of some of the vision can mean a lot. Therefore, any level of vision a prosthesis can provide could still improve the quality of life for a class of patients.

The desire to restore visual perceptions in blind individuals has a long history in biomedical engineering. Lessons learned from the first efforts to develop artificial vision systems have played an important role in the development of the current generation of these systems. The first efforts to provide a useful visual sense to blind individuals can be found in the early work of Brindley [1, 3] and his contemporary Dobelle [2, 11]. For both of their systems, a certain number of subdural stimulating electrodes (76 electrodes for Brindley, 57 electrodes for Dobelle) were placed over the occipital pole, where high acuity vision is thought to be processed. Both Brindley and Dobelle were able to stimulate the visual cortex in such a way that phosphenes were evoked. In addition, Dobelle was able to induce patterned perceptions by electrically stimulating the brain through a subset of his implanted electrodes [11].

In general, a visual prosthesis could be placed in several different ways: subretinal, epiretinal, on the optic nerve, or intracortical.

Subretinal prosthesis: Retinitis pigmentosa is a progressive degenerative disease of the eye, characterized by the gradual loss of retinal pigment epithelial cells. Vision loss progresses to blindness as more of these cells die and the capacity of the retina to transduce light into biologic signals is diminished. In what could be considered a bio-based approach to visual prostheses, consortia in the United States [13] and Germany [14] are determined to replace the lost retinal pigment epithelial cells with replacement cells of man-made origin. In such a prosthesis, a silicon micromanufactured device called a microphotodiode array is placed behind the retina, between the sclera and the bipolar cells. Incident light is transformed into graded electrical potentials that stimulate the bipolar cells to form a visual sensation [7].

Epiretinal prosthesis: An alternative approach to stimulating the retina from 'behind', as is the case with the subretinal implants, is to use an array mounted to the 'front' of the retina. In contrast to the subretinal approach, where the stimulating device is placed in the outer retina between the sclera and the bipolar cells, the epiretinal approach places the stimulating device on the inner retina between the vitria and the retinal ganglion cells (RGC) [15]. Based on published models of extracellular stimulation of the human retina [16, 17], the epiretinal implant will likely stimulate both RGC cell bodies and passing axons from RGC located on the periphery. This approach bypasses the damaged or missing photoreceptors as well as any remnant retinal circuitry (amacrine, bipolar, and horizontal cells) and directly stimulates the output layer of the retina. A commercially available epiretinal prosthesis is the Argus II Retinal Prosthesis System from Second Sight Medical Products [22]. It is the first that was commercially approved for the treatment for severe to profound retinitis pigmentosa. The system uses an array that has 60 platinum-based electrodes arranged in a 6×10 grid.

Optic nerve stimulation: One issue with electrically stimulating the retina or visual cortex is that the visual field is represented over a relatively large area, making coverage of the entire visual field nearly impossible with current electrode array technologies. In the visual pathway, the optic nerve is one place where the entire visual field is represented in a relatively small area. In a fairly novel approach to a visual prosthesis, it has been proposed that spiral cuff electrodes similar to those used in functional neuromuscular stimulation or vagus nerve stimulation could be used to electrically stimulate the optic nerve and produce visual

perceptions [18,19]. The objective is to place multi-electrode cuff electrodes around the optic nerve and, by using complex patterns of electrical stimulation, selectively stimulate subsets of axons, or even individual axons, in the optic nerve [20]. In a proof-of-concept experiment performed in a blind human volunteer, the ability to safely interface to the optic nerve and to evoke multiple phosphenes covering the entire visual space could be produced from a single cuff by varying the stimulation parameters [21].

Intracortical visual prosthesis: An implanted intracortical visual prosthesis is perhaps the only possible technological option for 90 percent of the blind, who cannot use other visual prosthesis systems. Stimulating the visual cortex can be the last resort when the visual pathway is damaged. Since the days of Brindley and Dobelle, progress in intracortical microstimulation of the visual cortex has concentrated on establishing the safety, long-term biocompatibility, and functionality of penetrating microelectrode arrays in the brain [24, 25, 41]. An integrated wired system with a large number of electrodes (65,536 electrodes) for neural recording and stimulation was reported in [37]. Second Sight Medical Products is developing the Orion Visual Cortical Prosthesis System, which is a chronically-implanted subdural electrode array intended to induce visual percepts in patients who are profoundly blind from various causes of non-cortical etiology [23]. The System leverages the technology and platform of the Argus II Retinal Prosthesis System (<100 electrodes). Other intracortical visual prosthesis projects include Monash vision project from Monash university [38] using 43 electrodes, and floating microelectrode array stimulator from the Troyk lab at the Illinois Institute of Technology [39]. An intracortical visual prosthesis system generally comprises a camera, an external processor, implanted electrode arrays, and a feedback loop [36]. Figure 1.1 illustrates an intracortical visual prosthesis system.

1.2 Different system layouts

A desirable aspect for the visual prosthesis is that the powering and communication to and from the implanted electrodes be done wirelessly, to avoid infections and to enable free movement [40]. Wireless enablement is part of the goal of the NESTOR project 5 of the NESTOR program (P15-42) which has the aim to implant a high count of electrodes ($\sim$1000) [42, 120], using 16 of Blackrock Microsystems' Utah arrays of 64 electrodes each [43].

The NESTOR project will develop the world's first large-scale, chronically implanted wireless device that directly imparts clinically relevant visual patterns to the visual cortex. The NESTOR project is in the "NWO Perspectief" programme, a Dutch government initiative bringing together academia and industry to solve research challenges with socio-economic impact. The NESTOR project involves partners including the National Institute of Neuroscience, Blackrock Microsystems Europe GmbH, Brain Innovation B.V., VicarVision, Elitac B.V., Twente Medical System International B.V., ATLAS Neuroengineering, BlueMark, AEMICS and Tiberion B.V.. Scientific partners include Radboud University, Maastricht University and the Netherlands Institute for Neuroscience. Patient organisations including Visio,
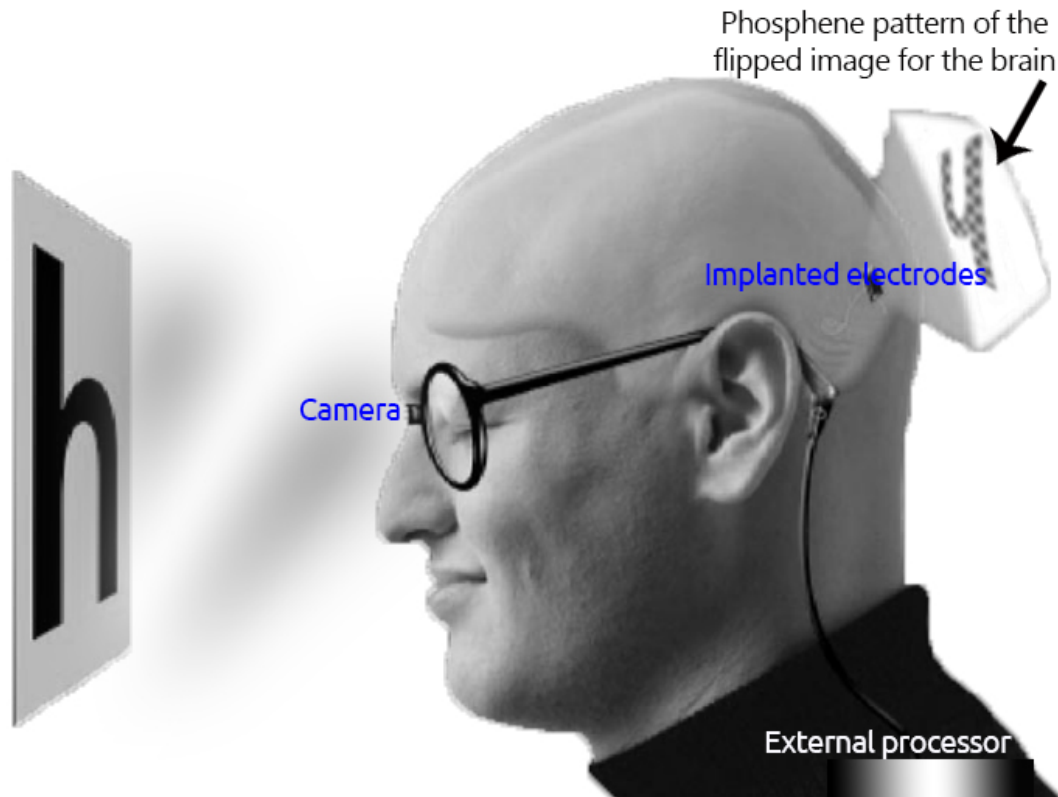
Figure 1.1: An illustration of an intracortical visual prosthesis (based on [7]).

Bartiméus and De Oogvereniging are also part of the NESTOR project [44–46].

The wireless-enabled visual prosthesis will need a communication link to send stimulation information to the implant (downlink), another link for retrieving recorded neural activity from the brain (uplink), and wireless powering of the implant. The uplink is needed for adaptation, monitoring, and calibration over time. This work focuses on the wireless communication part of the system. The wireless power transfer system is designed separately in another sub-project of the NESTOR project.

There are a few possibilities in laying out this wireless system, which may directly impact the communication technology used for transmitting stimulation information. Figures 1.2 through 1.4 shows three possible layouts with different levels of modularity and complexity. Table 1.1 highlights the advantages and disadvantages of each option.

One form (Option 1) as depicted in Figure 1.2 is that the tiles of electrodes (the electrode arrays) are each equipped with wireless capabilities and are independent. The Monash Vision group [38] developed a medium count (< 500 electrodes) prosthesis of this form. The main advantages of this implementation are that there will be no wires in the brain and that the surgical procedure is more straightforward than other implementations. However, a possible challenge is that it requires individual antennas/coils for each electrode array. This may face variable signal reception as the electrode arrays may have a different orientation, depending

on their position on the cortex. For example, arrays implanted on the medial surface of the occipital pole may be at a larger angle to the transmitting antenna or coil than those on the more lateral surface. If arrays are implanted more on the anterior of the medial calcarine cortex, these would be more distant from and orthogonal to the external coil than the more superficial arrays, resulting in poor coupling and energy transfer [61].

Another implementation (Option 2), as shown in Figure 1.3 is to tether the tiles of electrodes together with wires to a central transceiver placed beneath the skull. An advantage of this option is that both the electrodes and the transceiver are beneath the dura so that no wire will penetrate through the skull. The challenge of this approach is that there is less space for the central receiver placement. Surgical implantation in this space may not be convenient for the implanted transceiver if its components are bulky.

The last approach (Option 3) is to tether the electrodes to a central transceiver subsystem that is placed between the skull and the skin and to use a transcutaneous wireless link for communication. Figure 1.4 shows this option. This approach has advantages, such as a larger space for the wireless transceiver. Also, the transmission loss through 3–5 mm of skin tissue will be lower than transmission loss through 20 mm of tissue to reach the cortex [62]. This leads to 10 dB lower transmission loss compared to the other two implementations [123]. The challenge of this option is the possible micro-motion of the implanted connecting wires, which can be partly alleviated with better packaging and implantation using slack wires to mitigate mechanical stress (this statement followed from a discussion with a neurosurgeon). The micro-motion disadvantage is relevant for option 2 as well, but with shorter wires.

This last approach (Option 3) is the implementation proposed for the NESTOR project and is used throughout this work. The main reason for this is that the implanted electrodes array can remain passive, and a central transceiver just beneath the skin will enable lower transmission losses. Also, the current 1024 electrode count could still easily be tethered with wires beneath the skull to its central transceiver beneath the skin without causing severe micro-motion. In option 3, this is above the skull, under the skin, where there is more room without taking brain space. The space for the electrode arrays will always be necessary.

1.3 Research Objective

The research objective of this thesis is to design a bi-directional wireless communication system for the implanted prosthesis according to option 3 in Fig. 1.4. The design has to meet key requirements in terms of power consumption, data rate and co-existence with other technologies. These will be described in the next chapter. Figure 1.5 illustrates the focus of this thesis. The left-hand side of Figure 1.5 shows different categories of biomedical implants. The desired option (Fig. 1.4) is in the category of transcutaneous implants. The right-hand side of Figure 1.5 shows the main areas of application for wireless systems. Wireless power transfer is out of the scope for this thesis, although it is investigated within the NESTOR project [42](See Section 1.2). Here, we focus on the uplink and the downlink communication.
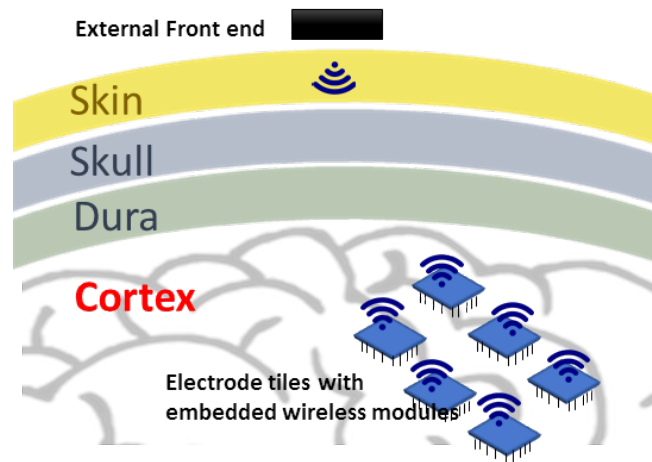
Figure 1.2: Option 1 for the system layout for the wireless enabled visual prosthesis: an implanted transceiver embedded into each electrode array.
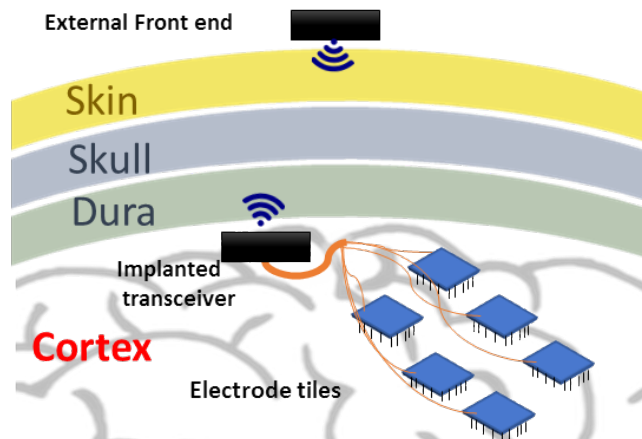
Figure 1.3: Option 2 for the system layout for the wireless enabled visual prosthesis: a central transceiver placed beneath the skull.
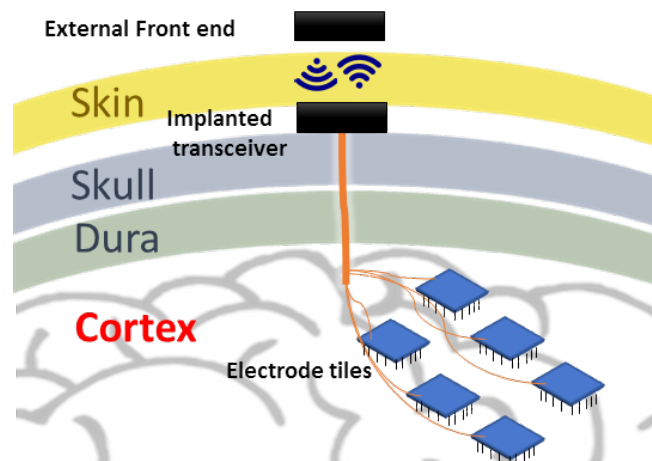
Figure 1.4: Option 3 for the system layout for the wireless enabled visual prosthesis: implanted transceiver placed beneath the skin.

Table 1.1: Comparing implementations of a wireless-enabled visual prosthesis.

	Advantages	Disadvantages
Option 1 (Fig. 1.2)	- Highly scalable - No wires in the brain - Straightforward surgical procedure - Highly flexible	- Low power efficiency (due to lossy media) - Variable power efficiency (very challenging link-budget) - Each tile needs a transceiver (more power consumption)
Option 2 (Fig. 1.3)	- Wireless module beneath the dura - Can be joined with the dura	- Limited available space - Low power efficiency (due to lossy media) - Wires in the brain - Mirco-motion of wires
Option 3 (Fig. 1.4)	- Higher power efficiency - Less transmission loss - More implantation space available	- Wires in the brain - Mirco-motion of wires

To achieve the research objective, our approach consists of the following steps:

- Investigate communication techniques and systems that will fit best with the requirements of the intracortical visual prosthesis context for both the uplink (sending out measurement data from the brain through the skin) and the downlink (sending stimulation data to the brain through the skin) parts of the total system.

- Carry out system level analysis for the downlink and uplink system, including link budgets of the proposed subsystems.

- Designing and testing the downlink system and the uplink system to show feasibility.
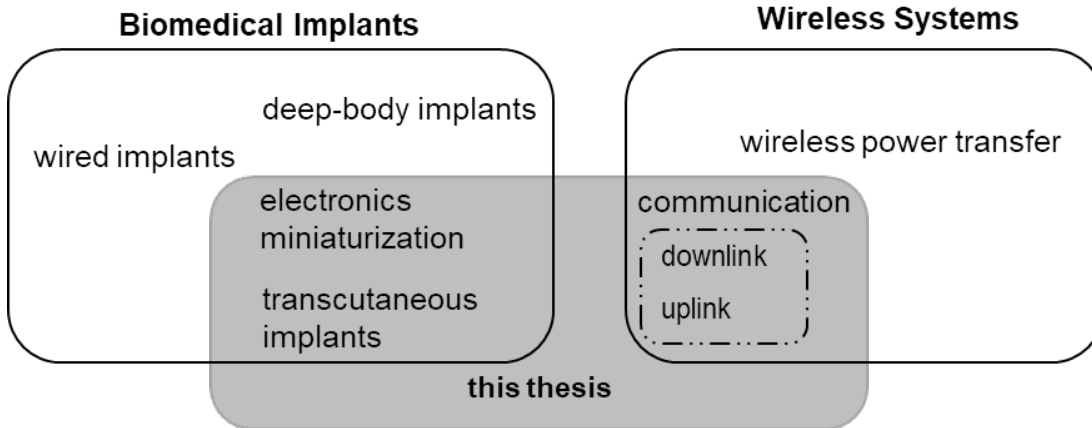
Figure 1.5: Research focus of the thesis: bi-directional transcutaneous wireless communication.

- Miniaturization of the implanted side and integration into an IC. Fabrication and validation of the core part of the IC, which is the uplink transmitter and the downlink receiver, to validate that requirements are met.

1.4 Outline of the Thesis

The thesis is structured along the steps that are required to meet the research objective, as described in the previous section. Figure 1.6 graphically illustrates the outline of the thesis.

In Chapter 2, relevant background on communication systems will be given and requirements for the bi-directional communication system will be detailed. Different options for downlink and uplink will be presented and judged against the requirements. This will lead to the key options for the system design. Finally, the selection of communication techniques most suitable for the intracortical visual prosthesis system will be motivated.

In the next two chapters, the downlink system and the uplink system will be designed, respectively. Chapter 3 is dedicated to the downlink communication system and the design considerations specific for this part of the visual prosthesis. The selected option, binary phase shift keying (BPSK) communication with a non-coherent receiver, is designed and demonstrated with off-the-shelf components. Exploratory investigation for the inductive link and considerations for coils for future application for the downlink in a scaled version will be carried out.

The design for the uplink communication system is presented in Chapter 4. We analyze the selected option, impulse radio ultra-wideband (IR-UWB), and the design considerations for its implanted side transmitter. System and link budget analysis of the IR-UWB System are carried out. In addition, the communication link through the skin will be investigated through simulations.

Chapter 5 focuses on the miniaturization of the implant side of both communication systems, of which the proof of principle was shown in Chapters 3 and 4. These systems have
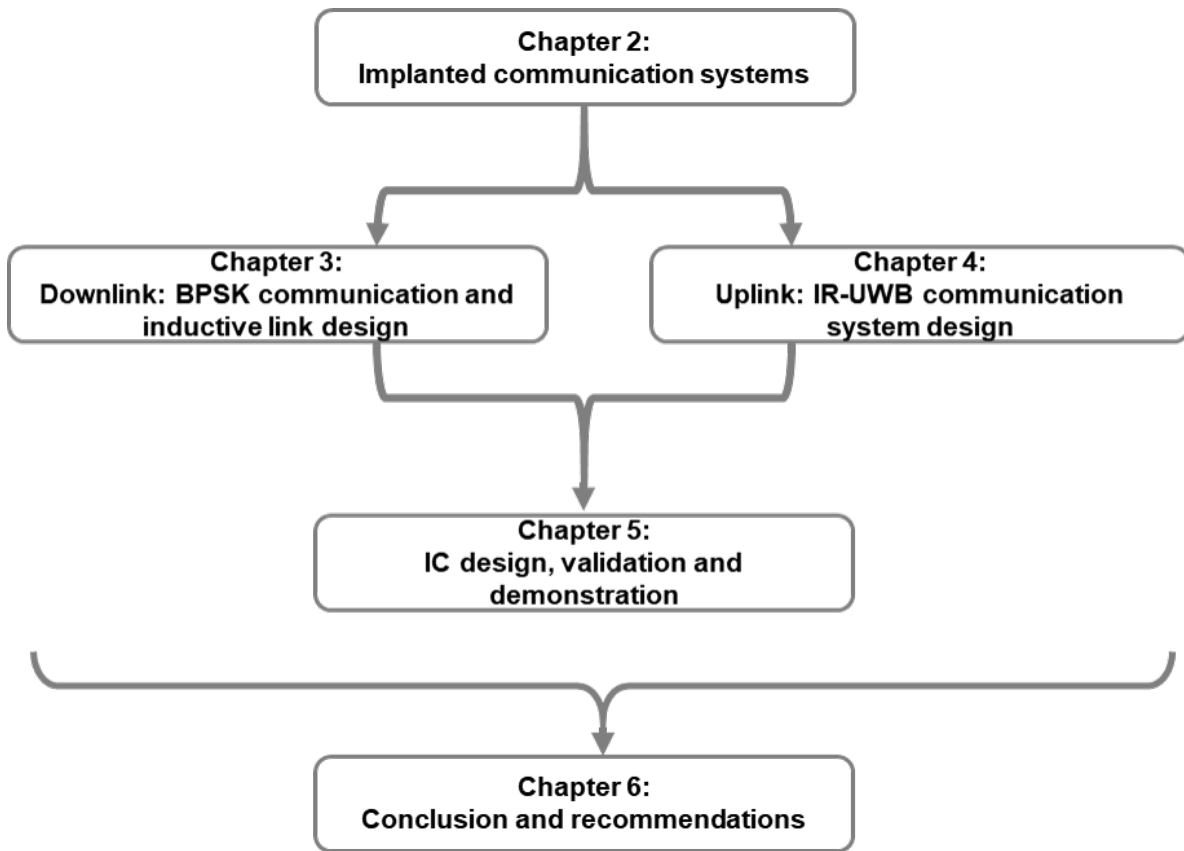
Figure 1.6: General outline of the thesis.

been integrated into a transceiver IC. The design was manufactured and tested with a demonstrator on a printed circuit board. This validates a low-power implant side communication that meets the minimum data rate requirements.

Finally, overall conclusions will be presented in Chapter 6, together with recommendations and an outlook for future work.

1.5 Original contribution of the Thesis

The work that is presented in this thesis contains the following original contributions.

- Determination of the system requirements and selection of communication techniques for the uplink and downlink for a 1024 - implanted electrode system in which the implanted transceiver is placed beneath the skin.

- System and link budget analysis of the uplink - IR-UWB System.

- Design and analysis of an improved non-coherent BPSK receiver for the downlink.

- Miniaturization of the core electronic parts and low-power demonstration of the implant side transceiver on an integrated circuit.

Table 1.2 shows the link between chapters and the research publications.

Table 1.2: Links between Chapters and Publications.

	Journal 1 [P1]	Journal 2 [P2]	Conf. 1 [P3]	Conf. 2 [P4]	Conf. 3 [P5]
Chapter 1			x		
Chapter 2		x			
Chapter 3	x		x	x	
Chapter 4					x
Chapter 5		x			

Implanted communication systems

This chapter explores implanted communications systems—literature survey including modulation techniques, low-power high data rate solutions and effect of the communication frequency. The wireless system requirements of the intracortical visual prosthesis are described. Next, key options are proposed, and the selected option for the uplink and the downlink system is motivated and discussed.

2.1 Literature survey

2.1.1 Background

Implanted communication systems have long been sought for various medical applications such as pacemakers [48], paralysis [50], hearing implants [52] and retinal prostheses [51]. The communication with the implant can be from outside the body to inside the body, mostly for stimulation purposes (downlink). The communication with the implant could also be the other way around, from inside the body to outside the body (uplink). The uplink is mostly for recording or monitoring of the stimulation process or the organ under stimulation. An implanted communication system is often designed for a particular communication depth into the body. For example, this could be only through the skin, like in Figure 1.4, but also for deeper implantations, see for instance [48]. The system, in general, could have a very low data rate, for instance below 100 kbps, in applications like pacemakers and audio implants, or much higher data rates of over Mbps like in the case considered in this thesis: neural recording for a visual prosthesis. Low power consumption is usually needed due to limited space available for a possible battery. Low power consumption can also help reduce the weight and size of the implant and improve lifetime [54]. In addition, low power consumption could even avoid the need for a battery [55,56] completely and the required power is obtained from wireless power transfer like in this work. Since the system has to be available for a very long time, solely powered by a battery can not be used.

For an intracortical visual prosthesis, low power consumption and high data rate are desired for uplink and downlink communication. The implant side would include the transmitter for the uplink and the receiver for the downlink. Generic biomedical telemetries have been proposed for the implanted transmitter for recording and also for an implanted receiver for stimulation. These will be described further on in this chapter. Based on relevant options from state-of-the-art related work, we propose a unique combination to form our proposed system for bi-directional communication in an intracortical visual prosthesis. The uniqueness lies in the fact that predominately digital components are used, and the system design is investigated to fit the system requirements of a visual prosthesis. The specific requirements for our work will be detailed in Section 2.2. In the following subsections, we will describe the state of the art in modulation techniques and we will look at available solutions that provide high data rate at low power consumption.

2.1.2   Modulation techniques

Modulation is one of the core techniques of any communication system. Since the input signals intended to be transmitted consist of digital data (bits) already, we only discuss digital modulation techniques. Digital modulation techniques impress the digital signal onto a carrier signal for data transmission. A sequence of digital data is used to alter parameters of the (analog) carrier signal at a high frequency, which is the desired data rate. Thus, signal transmission occurs by modulating different parameters like amplitude, phase and frequency of the signal. Different types of modulation techniques provide a range in performance in terms of transmission data rate, data security, signal quality, complexity of the architecture, power consumption, performance over a communication channel, channel capacity, accuracy in the presence of noise and distortion, etc. [57]. The main criteria for choosing the modulation schemes are based on power, bandwidth and system efficiency, among other parameters [80]. Figure 2.1 shows the three most common digital modulation techniques used in biomedical devices: amplitude shift keying (ASK), phase shift keying (PSK), and frequency shift keying (FSK). Each of these will be described briefly next and PSK will be subdivided further.

Let a general binary input bit signal have the following form:

$$b(t) = \begin{cases} \text{binary 1,} \\ \text{binary 0,} \end{cases} \tag{2.1}$$

where $b(t)$ is binary input bit signal in time domain, binary 1 and binary 0 are the possible states of a bit representing digital information.

On/off keying (OOK) modulation and demodulation

The technique of on/off keying (OOK) is a typical example of amplitude shift keying (ASK) and is the most straightforward digital modulation option used in wireless telemetry biodevices and biomedical implanted devices. In these modulation types, no carrier is used
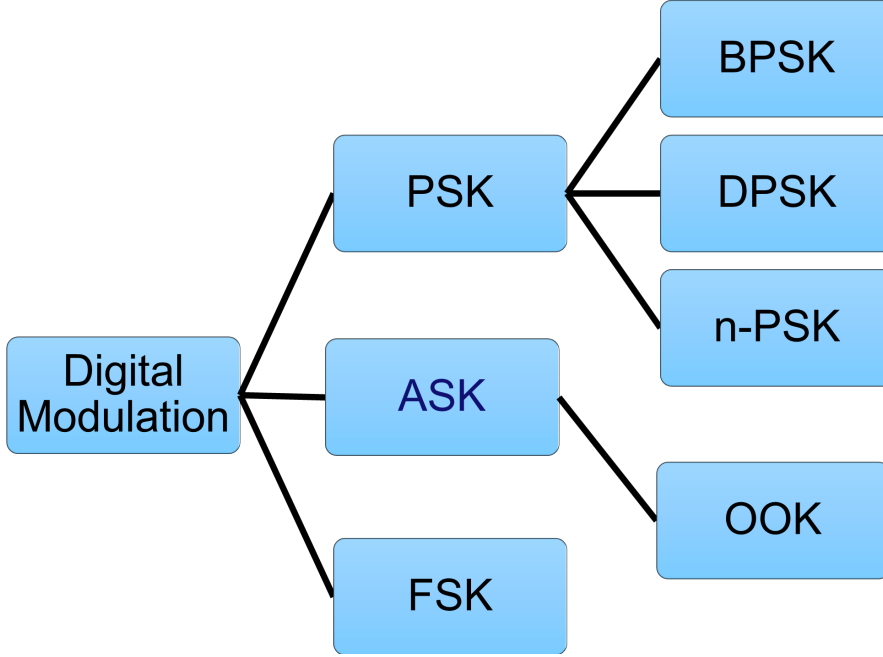
Figure 2.1: Digital modulation in biomedical implants.

during the binary 0 transmission, which minimizes the modulator's power consumption. The principle of OOK transmission is explained in [58] and can be represented as follows:

$$S_{OOK}(t) = \begin{cases} A\cos(2\pi f_c t), & vT \leq t \leq (v+1)T, \quad \text{binary 1,} \\ 0, & vT \leq t \leq (v+1)T, \quad \text{binary 0,} \end{cases} \tag{2.2}$$

where $S_{OOK}(t)$ is the OOK signal in time domain, T is the bit duration, f_c is the carrier frequency and v is an integer denoting the vth period. In general, OOK modulation is used in the implanted part for its simplicity, low power consumption, and better spectral efficiency. There are two methods of OOK demodulation: coherent and non-coherent detection. The coherent method uses carrier phase information for detection. This method uses a product detector and a phase-locked beat frequency oscillator for detection. In non-coherent methods, no carrier phase is used for detection. Most research reports the use of the non-coherent method due to its simplicity and low power consumption. Classical non-coherent methods are based on filtering signal energy within allocated spectra and envelope detectors. The performance degradation of these types of non-coherent method is about 1-3 dB compared to coherent detection [80], depending on the normalized signal to noise ratio (symbolized as E_b/N_0) [78], which is related to the bit error rate (BER). On-off keying will be used later on in this work for impulse radio ultra-wideband communication (see Section 4.4.1).

FSK modulation and demodulation

The frequency shift keying (FSK) modulation principle is based on sending binary data with two different frequencies. The resulting modulated signal is regarded as an amplitude mod-

ulation of different carrier frequencies. There are two types of FSK modulation: i.e. non-coherent or discontinuous, and coherent FSK modulation [78]. In non-coherent modulation, ϕ_1 and ϕ_2 are the initial phases of the signals at $t = 0$. These are not the same, in general. Such modulation can be generated by switching the modulator output line between two different oscillators. However, in the coherent type of FSK modulation, the two coherent signals have the same initial phase $\phi_1 = \phi_2$ at $t = 0$. In general, FSK modulation uses two different frequencies (f_1 and f_2). The FSK signal represents binary 1 and 0 as follows:

$$S_{FSK}(t) = \begin{cases} A\cos(2\pi f_1 t + \phi_1), & vT \leq t \leq (v+1)T, \quad \text{binary 1,} \\ A\cos(2\pi f_2 t + \phi_2), & vT \leq t \leq (v+1)T, \quad \text{binary 0,} \end{cases} \tag{2.3}$$

where $S_{FSK}(t)$ is the FSK signal in time domain, v is an integer denoting the v-th period, and ϕ_1 and ϕ_2 are the aforementioned initial phases. With FSK a low-data rate can be combined with power transfer through one of its carriers [60]. The combination with power transfer is in that one of the frequency carriers can also be made the frequency for power transfer. However, using one of the carriers in the FSK signal for the power transfer can be challenging if the desired power transfer frequency is much lower than the frequencies of the FSK carriers. The challenge is that the required channel bandwidth is now significantly increased due to the spreading of the signal over the band between both frequencies.

PSK modulation and demodulation

Phase shift keying (PSK) constitutes a large class of digital modulation techniques. Over the last decades, PSK modulation has been used extensively in wireless communication for biomedical applications [66, 79, 81, 84]. In PSK, to carry out coherent demodulation, one main implementation is to compare the received signal with a reference signal. This way of coherent modulation is done through a correlated or matched filter. The reference signal is generated by the carrier recovery circuit, which is synchronous to the received signal in terms of frequency and phase [80]. However, the differential coherent demodulator is non-coherent in the sense that phase-coherent reference signals are not required, which is used to overcome the adverse effect of the random phase in the received signal. The most common digital schemes appropriate for biomedical data transmission are binary PSK (BPSK), differential PSK (DPSK), and n-PSK.

For BPSK, binary data is represented by two signals with different phases in BPSK. Typically, with the two phases 0 and π, the signals have the following form:

$$S_{BPSK}(t) = \begin{cases} A\cos(2\pi f_c t), & vT \leq t \leq (v+1)T, \quad \text{binary 1,} \\ -A\cos(2\pi f_c t), & vT \leq t \leq (v+1)T, \quad \text{binary 0,} \end{cases} \tag{2.4}$$

where $S_{BPSK}(t)$ is the BPSK signal in time domain. These signals are called antipodal. They are chosen in this way, to have a correlation coefficient of -1, which leads to the minimum error probability for the same normalized signal to noise ratio E_b/N_0. These two signals have the same frequency and energy.

In DPSK, a variant of BPSK, differential encoding through a differential encoder is used in addition [97]. In n-PSK, more bits are encoded per symbol by using *n*-levels to increase the data rate in contrast with BPSK which has an $n = 2$. In this work, a particular type of BPSK receiver implementation is proposed and used. It is predominately digital and non-coherent with bandpass sampling and communication over an inductive link. Details will be given in Chapter 3.

Theoretical bit error rate performance comparison

Figure 2.2 compares the bit error rate performance of various modulation schemes from [78]. It can be observed that PSK requires a lower normalized signal to noise ratio E_b/N_0 for the same BER target of 10^{-3}, followed by DPSK and coherent OOK or FSK. Non-coherent FSK or OOK requires the highest E_b/N_0 compared to the PSK, with a difference of 4 dB at 10^{-3}. While PSK has the best theoretical BER performance and will be used for our downlink system, non-coherent OOK will be used in the uplink after ensuring there exists excess margin in the link-budget. This will become clear from Chapter 4.
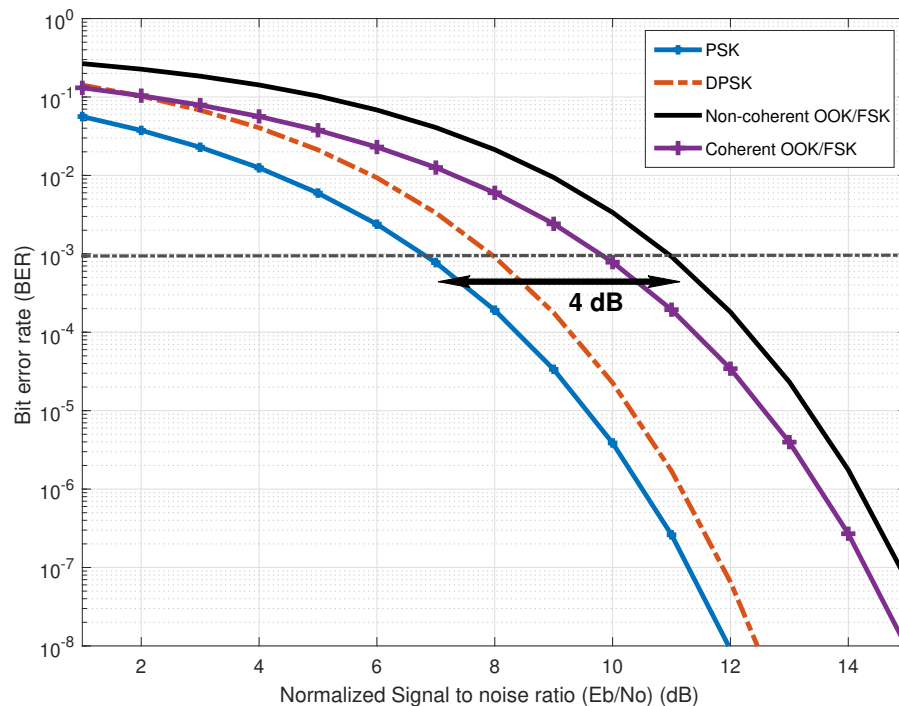
Figure 2.2: Comparing the theoretical bit error rate performance of various modulation schemes.

2.1.3 Low-power high data rate solutions

Downlink

In delivering low power consumption and high data rate for the downlink, we place emphasis on the receiver since this is the part of the system that will be implanted. Techniques for achieving low power consumption and high data rates involve the use of low-frequency carriers [67] and avoiding power-hungry coherent detection methods which may involve phase locked loops [79]. An addition could involve integrating the core parts of the system on a chip to realize the low power consumption [83].

Table 2.1 gives a summary of state-of-the-art implanted communication systems that were low-power and high data rate for the downlink (stimulation). For the downlink receiver, an analog differential phase-shift keying (DPSK) receiver was used in [79]. A non-coherent PSK receiver without a PLL, based on bandpass sampling theory, was presented. Sampling the analog PSK signal was done with a switch-capacitor array. The samples were then processed in the analog domain, which required no ADC for data demodulation. Pulse delay modulation (PDM) was used in [67]. The PDM receiver operated as a pulse delay detector and realized lower power consumption due to its low complexity. An FSK-ASK conversion receiver was presented in [83] for low power consumption. Dual injection locking was proposed to convert the FSK incident signal to an OOK modulated signal, allowing the implementation of a simple RF receiver architecture based on envelope detection. The conversion circuit, which represented a key component of envelope detection receivers, allowed high data rate transmission at low energy consumption in the reported receiver. However, for our implanted receiver we took an approach of a non-coherent digital receiver. This will be detailed in Section 2.3 and Chapter 3.

Table 2.1: State-of-the art medical implant receivers selected by high-data rate and low-power criterion.

	[67]	[79]	[83]
Data rate	13.56 Mbps	2 Mbps	8 Mbps
Power consumption	2.2 mW	6.2 mW	0.6 mW
Frequency	13.56 MHz	20 MHz	902–928 MHz
Modulation	PDM	DPSK	FSK–ASK
Technology	350 nm	350 nm	130 nm
Supply Voltage	1 V	-	3 V

Uplink

In building low-power, high data rate solutions for the uplink system, we place emphasis on the part of the system that will be implanted: the transmitter. Tackling low power consumption and high data rates often leads to using carrier-less techniques such as impulse

systems [35]. In this way, power-hungry high-frequency modulators and power amplifiers can be avoided [135]. An additional approach is to design the transmitter in IC technology rather than with discrete microwave components [26].

Table 2.2 gives a summary of state-of-the-art implanted communication systems that are low-power and high data rate for the uplink (recording). In [33] optical communication was attempted for the uplink. However, this faces a challenge of misalignment sensitivity. Impulse radio ultra-wideband (IR-UWB) was used in [73] around 3–5 GHz band showing a promising result, in [134] using the sub-GHz band and in [135] the 6.8–9 GHz band. A high data rate of 500 Mbps was achieved in [35] using an IR-UWB transmitter. In this work, IR-UWB is also proposed for the uplink. The approach will be detailed in Section 2.4 and Chapter 4.

Table 2.2: State-of-the medical implant transmitters, selected by high-data rate and low-power criterion.

	[134]	[73]	[35]	[135]	[33]
Mbps	30 Mbps	90 Mbps	500 Mbps	100 Mbps	100 Mbps
Power cons	30 mW	1.6 mW	5.4 mW	0.26 mW	2.1 mW
Freq	Sub-GHz	3–5 GHz	3–7 GHz	6.8–9 GHz	Light
Mod	UWB	UWB	UWB	UWB	-
Tech	350 nm	350 nm	130 nm	180 nm	-
Supply Volt.	3.3 V	1.65 V	1.8 V	1.5 V	-

2.1.4 Effect of the communication frequency

Low frequencies of below 100 MHz can be used for medical communication systems [67,79] and generally, for instance, in FM radios. The wavelength in free space is more than 3 m at these frequencies. Therefore, dipole-like or aperture-like antennas, whose dimensions scale with the wavelength, are not practical due to size constraints. So for these types of low-frequency communication, irrespective of the modulation technique, inductive coils provide a suitable alternative for antennas, since they can be designed having a few centimeters of diameter. Because inductive links operate with coils in close proximity [48, 63, 67], with transmission distances typically less than the coil diameter, they fit well with a 3–7 mm tran-scutaneous distance that is foreseen for the implantable system.

Very high data rates of tens of Mbps could be required in some applications. Achieving this at low frequencies (below 100 MHz) is quite challenging due to insufficient bandwidth in most cases. Therefore, it could lead to selecting higher carrier frequencies in the 1–10 GHz range. The wavelengths in the 1–10 GHz range could permit RF antennas such as dipole-like or aperture-like antennas at sizes that are suitable for implants and on-body antennas.

Optical frequencies could be used as well. The main reason they are sometimes used is due to the enormous bandwidth available at such frequencies. In such cases, neither coils nor RF antennas can be used. Instead, communication is done through a light emitter at the transmitter side and a light detector at the receiver side.

2.1.5 Robustness to interference to/from wireless power transfer

Wireless power transfer can be carried out at the 125 kHz ISM band [40], and the 6.78 MHz ISM band is also possible. At 125 kHz robustness can be created by filtering since data transfer can be done at a few MHz, giving sufficient spacing in frequency. In both the 6.78 MHz and 125 kHz cases, robustness can be created by physically separating data communication coils from wireless power transfer coils, e.g. by having a wire under the skin to a different location on the head.

There could be potential surface waves from the antenna-skin interface of the uplink, which need to be addressed for a fully assembled system. The possible interference to the wireless power transfer is expected to be low, as around a maximum of -9 dBm of signal power is generated by the uplink operating in the GHz range (see section 4.5.3), and about 20 dBm of wireless power transfer activity at under 10 MHz (see section 2.2).

Extensive tests and simulations need to be carried out on the complete, combined system. This is beyond the scope of this thesis, however, we give some directions for these tests here. These could encompass, for instance, the use of shielding to isolate parts of the data transfer subsystem from the wireless power transfer subsystem. Also, proper assembly of the fully integrated parts as in [40] using inner top/bottom shielding layers, could play a vital role in robustness to interference. Other tests include coupling between power and data coils, the effect of the generated higher harmonics, or the disturbance of the magnetic field of the wireless power transfer on circuits on the IC.

2.2 High-level wireless system requirements

In this section, an overview of the system-level considerations is given, which will lead to high-level requirements.

Power consumption: for any implanted device, power consumption is important due to battery size and capacity constraints, and an intracortical visual prosthesis is no different. The implanted intracortical visual prosthesis system of 1024 electrodes is estimated to consume 120 mW, a figure that is obtained as follows. A 128-electrode recording and stimulation array with embedded electronics but without a wireless module was designed in [72]. The embedded electronics included the neural amplifier, ADCs and memory elements. The total power consumption was 9.33 mW. From the estimation in [74], a 128-electrode array embedded with electronics will consume about 3 mW for its demultiplexing of the received stimulation signals. Less than 3 mW will also be required for multiplexing the recorded signals. Therefore, it is estimated that each electrode tile of 128 electrodes will consume no more than 15 mW (9

mW for stimulating and recording and 6 mW for multiplexing/demultiplexing). Combining 8 of these subsystems to reach the 1024 electrode goal will result in 120 mW total. The wireless part will increase the total power consumed. It is deemed acceptable that the power budget for the wireless system contributes up to an additional 10%, so around 10 – 12 mW. While power consumption is essential, it is about energy, i.e. power consumed over time eventually. In the use case of the visual prosthesis, the device is expected to be used during a typical 16-hour awake time of patients.

Data rate: an intracortical visual prosthesis with an electrode count of 1024 will already pose a much higher data rate than other implanted systems using 10 to 20 times fewer electrodes. From signal rate perspective, it could require for instance 5 bits for current levels × 200 Hz refresh rate × 1024 electrodes × 4 stimulation commands, which yields up to 4 Mbps. If the stimulation pulses are to be transmitted in raw form, the total number of commands for a stimulation is 4 for a biphasic signal: (1) turn on the cathodal current; (2) turn it off; (3) turn on the anodal current; (4) turn it off. Each electrode needs to be refreshed at a rate of about 200 Hz for physiological reasons [74]. An implanted neurostimulation driver could take care of the waveform for stimulation. Only wireless communication to the driver is considered here. Therefore, from a video rate perspective, coupled with a demultiplexing scheme on the implant side, such as reported in [74], stimulation will require 200 kbps. It is estimated based on [63] and [38] that the communication to each electrode will require about 10 bits (5 bits for amplitude level, 5 bits for other commands such as polarity and parity check). There will be 1024 electrodes. Humans will respond to as few as 4 frames/s through neural stimulation [36], but a frame rate of 20 frames/s is assumed for research purposes. This will, in total, lead to 10 bits/electrode × 1024 electrodes / frame × 20 frames/s = 200 kbps.

In addition, the uplink in the visual prosthesis denotes neural recording. This requires much higher data rates than mere stimulation. As a result of the need to digitize the recorded neural data, without compression this higher data rate could be up to 170 Mbps, and around 23 Mbps with compression. This will be explained next. Neural activity takes place typically between 0.1 Hz – 5 kHz [72]. If sampling is done above the Nyquist frequency to avoid aliasing, 10 ksample/s will be required. There will be 1024 electrodes, requiring 10 bits for channel separation/selection. In addition, a 7 bits ADC is foreseen for each sample. This will lead to a data rate of 10 ksample/s × 1024 electrodes × 17 bits = 170 Mbps. Uplink data rate reduction possibilities include: 1) Reducing the number of bits for the analog to digital signal: for example, reducing it to 5 bits. This reduces the resolution of the recorded signal and decreases the data rate to 150 Mbps; 2) Limiting the neural activity recording reduces the quality of the information that can be extracted from the signal. 3) Receiving from a subset of electrodes every second. Applying all three measures would lead to a compression of as low as 23 Mbps which is still considered acceptable information quality according to the NESTOR project proposal (see Appendix A).

Modulation Techniques: in theory, any modulation technique would be sufficient for data transmission. However, the complete system layout will determine whether the required data rate can be achieved. Some modulation techniques could be more advantageous if their

hardware implementation can be made low-power. For instance, an implementation using predominately digital blocks. This will be investigated in detail in the upcoming chapters, for both downlink and uplink of the visual prosthesis.

Bit error rate: neural scientists desire that only one percent of the phosphene pixels is an error in the worst case. If each electrode is encoded by 10 bits, then the worst-case bit error rate target is 10^{-3}. Going above 10^{-3} could cause severe distortion of the stimulation or recorded data, which implies that more than one percent of the phosphene pixels are in error.

Security: with the rise of worldwide security breaches, measures must be taken to avoid hacking and re-writing of the brain. One of such measures could be taken at the physical layer by employing close-range communication, which is inherently safer.

Co-existence with other subsystems: both the uplink and downlink and the wireless power transfer will operate at frequencies or frequency bands that have to be chosen. Careful selection of the optimal frequency has to take place, while taking into account the bandwidth requirement. This also involves considering the path loss at that frequency. For example, it will be beneficial that the uplink system is at a much higher frequency than the rest of the system. At higher frequencies, more bandwidth is available to meet the high data rate demands of the uplink.

Size: a final essential system parameter is the overall size of the implant side of the intra-cortical visual prosthesis. There is limited space to attach or implant this device beneath the skin. Solutions that could easily be miniaturized would therefore have priority. For example, using an inductive link at a frequency under 100 MHz could be beneficial as opposed to using antennas, which would be very bulky. The available volume for a practical implantation beneath the skin around the head is about 30 mm by 30 mm and some millimeters thick. This size is feasible because coils can be made as small as 10 mm by 10 mm and the PCB housing the IC as small as 15 mm by 15 mm, coupled with the idea of stacking in layers (i.e the coils above the electronics as in [40], which reported in 38 mm × 38 mm × 51 mm aluminum enclosure for head-mounted use.)

The above considerations and requirements are summarized in Table 2.3.

Table 2.3: Summary of system requirements.

	Uplink transmitter	Downlink receiver
Power consumption	<10 mW	<10 mW
Data rate	>23 Mbps	> 200 kbps
Bit error rate	$< 10^{-3}$	$< 10^{-3}$
Security	3–7 mm short link	3–7 mm short link
Frequency band	3–5 GHz	1–12 MHz
Size	<30 mm × 30 mm × 20 mm	<30 mm × 30 mm × 20 mm

2.3 Downlink system: options and proposal

Based on the requirements listed in the previous section, two candidate options are considered for the downlink part of the system. These options will be discussed in the next subsection, after which a motivated choice can be made.

2.3.1 Key options for downlink

BPSK communication system

Figure 2.3 shows a schematic overview for the proposed communication system for the downlink. In the low-frequency range (below 100 MHz), 1–12 MHz is preferred because it is high enough to support the required data rate for the prosthesis with a practical inductive link, and low enough for a low-power sampled receiver. An inductive link enables data transmission at a low carrier frequency of 1–12 MHz to avoid extremely bulky antennas. Employing such a low carrier frequency will allow low-power sampling (digitizing) of the received signal at the receiver, which is at the implant side. Sampling (digitizing) the receiving signal will allow a digital demodulator that employs edge detection to recover the transmitted bits. Using this technique will make use of predominately digital blocks, which allow for low power consumption. The non-coherent digital demodulator can tolerate the phase noise of a low power ring oscillator by increasing its count up value. As a result, power-hungry components such as phase lock loops (PLL) are avoided [66]. At the same time, inductive links can be bandwidth limited to a few Mbps due to the frequency limitations of practical coils. Such order of data rates is still sufficient for the downlink system. With inductive links being near-field and short-range, the communication system is intrinsically secure at its physical layer.
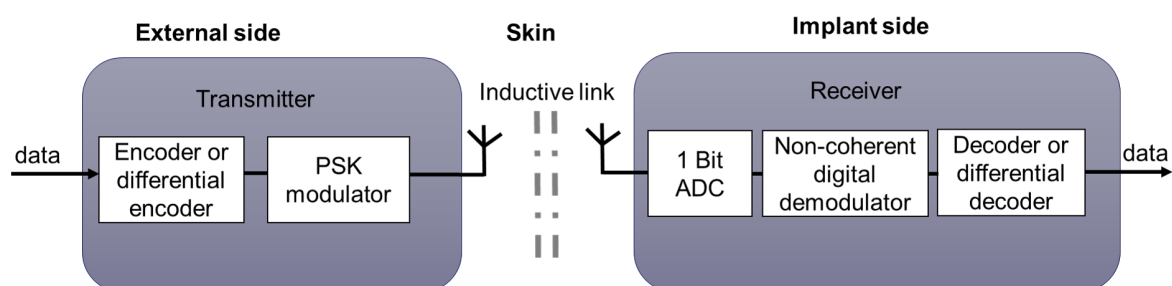
Figure 2.3: A schematic overview of the transmitter and receiver in a BPSK or DPSK system for the downlink.

DPSK communication system

Another key option for the downlink is differential phase shift keying (DPSK). This is a modified version of the previous option by adding differential encoding at the transmitter and differential decoding at the receiver (see the first and last sub-blocks in Figure 2.3). This may

come with a slightly higher power consumption. Also from a theoretical point of view, DPSK tends to have a worse bit error rate performance than BPSK by about 3 dB [78]. However, when used in an inductive link scenario with high power transfer interference, it could develop a robustness to interference as seen in [79]. To achieve this, however, the power carrier frequency will have to be a multiple of the data carrier frequency [79].

2.3.2   Motivation and selection

Table 2.4 compares the pros and cons of DPSK and BPSK communication. BPSK communication promises a low-power solution, sufficient data rate, and good theoretical bit-error-performance. Especially when used with inductive links at low communication frequency and with bandpass sampling at the receiver. At the same time, interference can be taken care of by proper frequency allocation, by filtering or by separate coil design. Interestingly, the BPSK system is flexible because if a differential encoding is added at the transmitter side and a differential decoder is added at the receiver side, it effectively becomes a DPSK system. Furthermore, the differential encoder and decoder are relatively easy to implement by using a D-latch and an exclusive NOR gate connected with feedback in a specific manner [97]. So adding a differential encoder at the transmitter and a differential decoder at output could be done if necessary in more research and design iterations in the future. To summarize, BPSK communication seems the more promising option because of its excellent BER performance, lower-power potential and easy extension to differential encoding. BPSK communication is selected for further research and development as the communication system option for the downlink.

Table 2.4: Comparing BPSK and DPSK communication.

	BPSK	DPSK
Pros	Low-power receiver	Interference cancellation possibility
	Best BER performance	Straightforward non-coherent detection
Cons	No power-carrier cancellation	Poorer BER
	Non-coherent receiver is unconventional	Increase in power consumption

## 2.4   Uplink system: options and proposal

In Section 2.1.3, two major low-power high data rate solutions for the uplink stood out, namely IR-UWB and optical communication. Now considering the system requirements of the visual prosthesis, these options are also considered for the uplink system. These options will be discussed in the next subsection, after which a motivated choice can be made.

2.4.1 Key options for uplink

IR-UWB Communication

Figure 2.4 shows the block diagram of an IR-UWB system suitable for biomedical environments. IR-UWB systems, notably unlicensed UWB systems operating across or within the
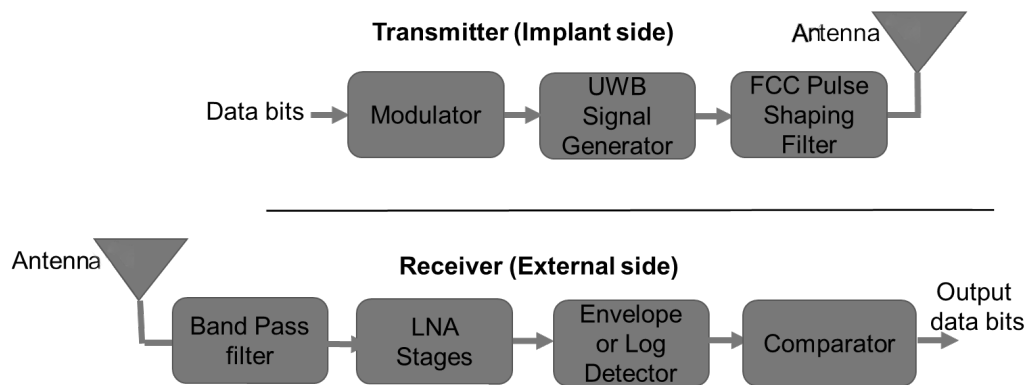
Figure 2.4: A schematic overview of the transmitter and receiver in an IR-UWB system.

frequency band from 3.1—10.6 GHz, are unique systems. Their uniqueness lies in the transmission and reception of only a single signal having pulse waveform at all times, rather than multiple consecutive continuous wave (CW) signals having sinusoidal waveform at different times as in CW-based systems [26]. IR-UWB communication involves transmitting modulated short-duration pulses. The spreading of these short pulses in the frequency domain is over a wide band. This is reflected in the regulations for UWB transmission. For instance, the FCC and Europe permit communication in the 3.1–10.6 GHz band at -41.3 dBm/MHz maximum transmit power [94]. This wide band permits high data rate and the transmitter, which is at the implant side, can be designed to be low-power [73]. The rationale for its low-power potential is explained next.

One of the major advantages of IR-UWB transmitters, as compared to CW transmitters, is the simplicity of their circuits, which do not need complex components as typically employed in CW transmitters, such as frequency synthesizers that contain various circuits like phase-locked-loops (PLLs), voltage-controlled oscillators (VCOs) and mixers [27]. IR-UWB transmitters are thus relatively straightforward to design and implement.

While IR-UWB transmitters come with many pros, IR-UWB receivers can range from straightforward to very complex circuitry depending on the link budget and the data rate target. IR-UWB can be designed to directly convert received radio frequency (RF) signals into a baseband output signal without an intermediate stage using, for instance, envelope detection [28, 29]. The IR-UWB receiver will be on the external side, so it does not have stringent requirements on its power consumption compared to the transmitter at the implant side. Furthermore, with proper link-budget consideration, a low-power and straightforward receiver design still are possible [110, 143].

Optical Communication

Figure 2.5 illustrates the principle of optical biomedical telemetry. A light-emitting element is placed inside the body, and a light-detecting component outside the body tissue receives the light propagated through the body tissue. The feasibility of this approach is also confirmed in [33, 53], which report generic transcutaneous applications.
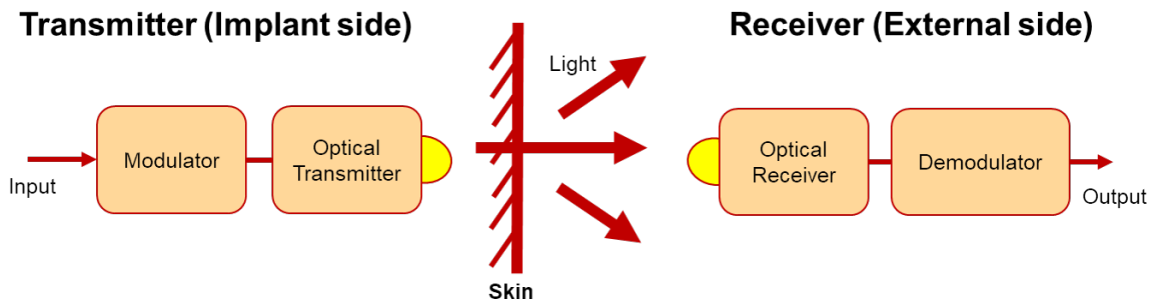
Figure 2.5: Principle of transcutaneous optical telemetry.

Optical wireless communication involves optical communication without optical fibres. Instead, the technique uses a photodiode at the transmitter side and a photodetector at the receiver side. Its infra-red frequencies enable high data rate communications, co-existence with other subsystems and security. Some key advantages driving optical wireless communication as an option are the following [53].

Firstly, wideband signal transmission can be achieved relatively easily. This indicates the possibility of high-speed, large-capacity transmission of information.

Secondly, electromagnetic interference can be controlled more comfortably than with radio telemetry. The light signal of the optical telemetry does not interfere with other instruments and does not receive interference from them. This results intrinsically in shielded and secure communication.

Finally, the legal restriction to use light for communication is not as strict as for radio waves or microwaves. The power limitation for optical communication would be not to heat up the body tissue excessively as the maximum temperature increase in the cortex has to be smaller than 1 °C [88, 89] which corresponds to a maximum power density of 0.8 mW/mm^2 on exposed tissue area [72, 88, 89].

Naturally, there are also disadvantages to optical biotelemetry [53]. One of them is misalignment sensitivity. A transcutaneous optical link can only tolerate less than a few mm misalignments. Another disadvantage is its moderate power consumption. A predominately digital RF IC can be low power <mW, but optical telemetry struggles to reach such levels. Finally, optical frequencies are much higher than RF frequency hence facing over 50 times smaller penetration depth through the skin [34].

2.4.2 Motivation and selection

Table 2.5 compares the pros and cons of IR-UWB and optical wireless communication. The IR-UWB transmitter can be made low-power because UWB signals can be easy to generate at very low power [31]. Compared to the transmitter, the receiver (detection and demodulation) is more challenging (but it is outside the body). It also has the potential for very high data rates without a significant demand on the power consumption of the transmitter, due to its spreading in the frequency domain. In this way, it adequately fits the federal communications commission (FCC) spectral mask restriction. It can have low interference with other systems, by selecting a suitable sub-band of the available 3.1 – 10.6 GHz band.

Table 2.5: Comparing IR-UWB and optical communication.

	IR-UWB	Optical Communication
Pros	Low-power transmitter	Compact
	High data rates	Very secure (infra-red)
	Low external interference	No antennas
Cons	Antenna size	Mis-alignment sensitivity
	Synchronization	Moderate power consumption
	Complex receiver design	High attenuation by the skin

The optical wireless communication can be made compact, and it does not use antennas like the IR-UWB. It is also very secure as infrared frequencies are highly directional and difficult to tap. Its external receiver may not be as complicated as that of IR-UWB. However, due to the directional nature, optical communication is not robust to misalignment (~ 2 mm) [32], and has high attenuation through the skin (1–4 mm penetration depth) [34]. To summarize, IR-UWB seems the more promising option, because of its low misalignment sensitivity and easy future integration with the downlink system. IR-UWB is selected for further research and development as the communication system option for the uplink.

The next chapter will explore the proposed option's system design for the downlink (Chapter 3): BPSK communication system. Chapter 4 details the system design for the uplink: IR-UWB communication. IC design, validation and demonstration are presented in Chapter 5.

Downlink: BPSK communication and inductive link design[1]

3.1 Introduction

In this chapter, we look into the detailed design of the downlink part of the visual prosthesis. Several implanted medical links have been proposed for communication through the body [63–68]. Frequency shift keying (FSK) was investigated in [63]. Differential phase shift keying (DPSK) was used in [64]. In [65, 66], binary phase shift keying (BPSK) was developed. Pulse delay modulation was implemented in [67]. A non-coherent analog BPSK demodulator was presented in [68].

However, for the application to a visual implant, the overall system has to do simultaneous communication and power transfer, and in which power consumption is an issue. The earlier works mentioned above are not directly focused on the visual implant context. Instead, here we take an approach to arrive at a low-power system. The requirements for the downlink part of the implanted visual prosthesis have already been detailed in Section 2.2. Therefore, the requirements of developing the downlink for stimulation include low-power consumption <10 mW, a data rate of 200 kbps, robustness to interference from the power carrier, and link security. As will be detailed in this chapter, these requirements lead to take a low-power system approach which involves using low frequency (<100 MHz), an inductive link for communication, phase shift keying (PSK), a nearly digital receiver, and non-coherent demodulation, as introduced in [70].

The remainder of this chapter is structured as follows. Section 3.2 describes system approach. Section 3.3 describes the proposed transmitter and the implanted receiver. Furthermore, we explain an approach for reducing the clock frequency by skipping periods in the non-coherent demodulation at the receiver. In Section 3.4, we describe the development of

---

[1]This chapter is based on journal publication: "Low-Power Wireless Data Transfer System for Stimulation in an Intracortical Visual Prosthesis" in Sensors 2021 [P1].

the demonstrator at a scaled-down frequency, using off-the-shelf components. In Section 3.5, we present the results of the demonstrator, and in Section 3.6, we discuss the results in the context of future work: scaling for IC integration with the overall wireless-enabled visual prosthesis. Section 3.7 concludes the chapter.

3.2 System Approach

The goal for the downlink part of the prosthesis is to have a low-power, robust communication system meeting the requirements stated in Section 2.2. Here we focus on the receiver side because this will be in the implant and therefore, poses the most challenging design from a power consumption perspective. To minimize power consumption, power-hungry system components such as phase locked loops (PLLs) and high-Q oscillators should be avoided where possible. In addition, high frequencies (above 100 MHz) should be avoided because they usually make devices consume more power and face more signal attenuation through the skin. This has motivated the use of alternatives to classical demodulation techniques which were discussed in Section 2.1.2. As a result, Figure 3.1 shows the proposed downlink system blocks for the external transmitter and the implanted receiver. It contains the following characteristics and features:
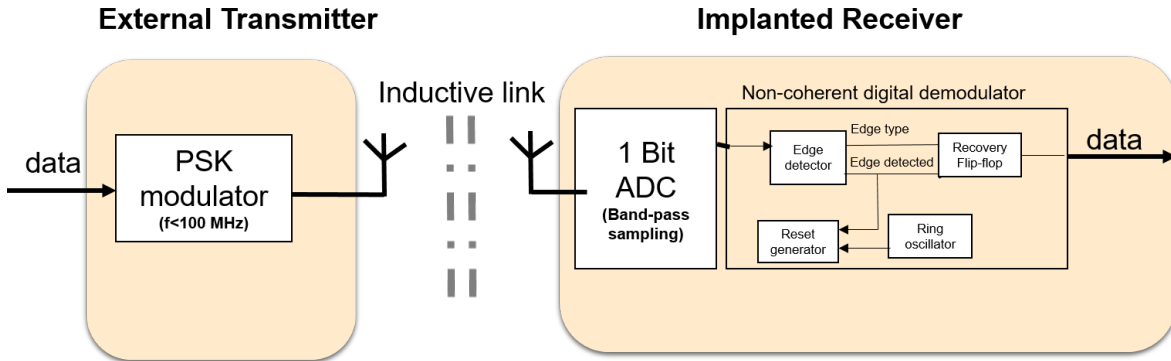
Figure 3.1: System architecture of the communication system for downlink.

- Low frequency: we choose a frequency below 100 MHz. The required downlink data rate is below 10 Mbps. Thus, modulating on carrier frequencies in the 1–12 MHz range can provide sufficient bandwidth. In addition, the electric and magnetic field will face minimal attenuation through the skin [76]. Lower frequencies also imply lower power consumption for the digital components.

- Inductive link: to eliminate the bulky antennas that are needed if low frequencies are used, an inductive link is proposed. The inductive link allows for short transmission ranges in the order of centimeters. This fits well with the application of the visual prosthesis, where transmission through a small layer of tissue (skin), at an implantation

depth of 3 to 7 mm [77] is foreseen (see also Figure 1.4) and where security may be a concern.

• Phase shift keying (PSK): has a better theoretical bit error rate performance than other modulation schemes, such as amplitude shift keying (ASK) and frequency shift keying (FSK), see also Section 2.1.2. Since the PSK modulation scheme is not sensitive to amplitude variations, it can easily cope with misalignment between transmitter and receiver coils, which mainly affects the signal amplitudes. Misalignment will reduce the coupling between the coils, causing a lower amplitude [90]. Its transmitter is of similar complexity as in ASK. It is also spectrally more efficient than FSK which may require wideband inductive links [63].

• Bandpass sampling: at low frequencies (<100 MHz), the entire modulated signal (carrier and information) can be sampled or simply digitized and processed in the analog or digital domain.

• Non-coherent demodulation: using bandpass sampling (i.e. sampling at the RF frequency without prior demodulation) at the receiver side, the entire received signal is sampled (digitized). It is possible to recover the information from the digitized received signal using a non-coherent digital technique. This avoids PLLs and allows for the use of low-power ring oscillators which have relatively large phase noise. The poor phase noise of the ring oscillator is not usually tolerated in classical demodulation techniques. Non-coherent analog demodulation for FSK and PSK generally uses envelope detection as part of the core demodulation process, which has a poorer BER performance than coherent demodulation [78]. However, this degradation in performance does not apply to the non-coherent digital demodulation proposed here as it does not use envelope detection. A possible weakness of the bandpass sampling approach is that it requires proper channel design. To overcome this, a coupled inductive link is used, which provides sufficient channel bandwidth. (Section 3.3.3 further explains the inductive link (channel) design.)

3.3 System Architecture

The communication link for transmitting the stimulation signals to the implanted electrodes (downlink), comprises of the external transmitter, the inductive link, channel and the implanted transceiver. Figure 3.1 shows the entire downlink system with its schematic sub-blocks. Frequencies for inductive powering for minimal skin losses, like the popular 125 kHz ISM band or 6.78 MHz ISM band give some room for interference filtering. The interference filtering, if necessary, can be off-chip within the hollow space of the coil. Typical coil diameters range from 10 mm to 50 mm [35, 40, 67] and in addition, coil self-resonance frequency should be much higher than the operating frequency. These coils sizes facilitate a tolerable misalignment of several mm [90, 130].

3.3.1 External Transmitter

The external transmitter is essentially a binary phase shift keying (BPSK) transmitter. BPSK generally gives a good balance between power consumption and bit error rate performance [80](see also Section 2.3). It comprises of an oscillator for generating the carrier frequency and a mixer for modulating the carrier signal. Since the intended carrier frequency ranges between 1–12 MHz to achieve sufficient data rate, the mixer can be low power, consuming about 1 mW in 180 μm CMOS technology [81]. The BPSK mixer designed is shown in Figure 3.2. The proposed mixer is comparable to the reported mixer in [81], with the exception that the transconductance current is not converted to a voltage level, by omitting the common-mode feedback structure. Two inverters act as switch pairs, switching between signal paths to generate the BPSK signal currents. Next, these BPSK currents of the external transmitter need to be passed to the implanted receiver through a suitable wireless link.
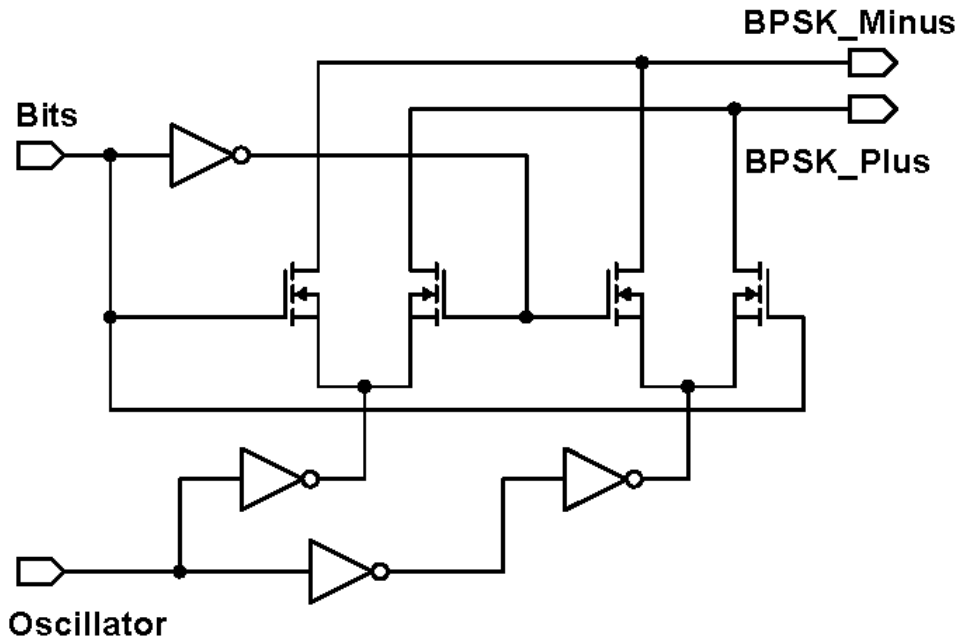
Figure 3.2: Circuit schematic of the binary phase shift keying (BPSK) mixer.

3.3.2 Implanted Receiver

At the receiver side, the entire signal is bandpass sampled (i.e. sampling at the RF frequency without prior demodulation) to allow for digital demodulation. The bandpass sampling is essentially a 1-bit analog to digital converter (1-bit ADC) [68]. This can be implemented using a comparator. After this step, the resulting signal is then non-coherently digitally demodulated. The non-coherent digital demodulator is the central part of the receiver. The 1-bit ADC and the digital demodulator will be described next.

The 1-Bit ADC

From exploratory circuit-model simulations of the inductive link, the received signal voltage level is expected to be in the range of 0.5 to 3 V, a similar range is reported in [47]. This may sometimes be lower than the digital logic level of the digital receiver, for example, if 1.8 V is used. Traditionally, low noise amplifiers are usually used as the first stage of an RF receiver. These may consume up to several milliwatts of power. However, in the context of the 3–7 mm inductive link, we propose a dynamic latch comparator, sometimes also called a 1-bit ADC, as a low-power solution that delivers sufficient signal level during digitization.

The Digital Demodulator

The non-coherent digital demodulator tries to detect if a '0' or a '1' was transmitted by detecting the type of edge it encounters in the digitized received modulated signal. The digitized modulated signal has a falling edge for the '0' and a rising edge for the '1'. While detecting which type of edge is present, the subsystem must take care to avoid the natural transition points between carrier periods so that it is not detected as an edge type. The digital demodulator consists of an edge detector and a reset generator to reset the edge detector before the next carrier period. The edge detector contains a rising edge and falling edge flip-flop. With AND and OR logic gates, the type and timing of the occurring edges are determined. Through a D-flip-flop, the received bits are recovered from the edge type and edge detected. The detected edge is delayed to ensure alignment before entering the recovery D-flip-flop. Section 3.4.3 will give details on the circuit board implementation of the proposed implanted receiver. An IC implementation schematic will be shown in Section 5.3.

3.3.3 Inductive Link Design

The required data rate for the downlink ranges from 0.2 Mbps to 4 Mbps for the wireless enabled visual prosthesis as discussed in Section 2.2. With the proposed system layout of placing the implant side of the wireless module just beneath the skin, the distance from beneath the skin to above the skin is in the range from 3–7 mm [77]. An inductive link is the most suited type of link because of the low attenuation of magnetic fields by the skin tissue and the compactness of the coils [70]. To keep power consumption low, the carrier frequency is chosen to be between 1–12 MHz. Achieving sufficient bandwidth for the desired data rate can be challenging, especially in inductive links. This is generally attempted by reducing the quality factor of the coils which leads to more power dissipation [65]. The transition region of the PSK modulated signal can be distorted if the transmission of the inductive system is not flat enough in the passband. Figure 3.3 illustrates a distortion. The top graph in the figure shows when the received sampled BPSK signal has an ideal transition. The bottom graph in the figure shows when the received sampled BPSK signal has a distorted transition with insufficient bandwidth in the inductive link. For BPSK, the bandwidth required is 2 times the data rate [78]. This determines what is sufficient and insufficient. The region of bandwidth is

defined as the area between the 2 peaks. For instance, 1 Mbps will require 2 MHz bandwidth, which means that for a response like in Figure 3.4 a coupling factor of k=0.1 may be insufficient ($<$ 2 MHz bandwidth), while k=0.3 will be sufficient (3 MHz bandwidth). However, it may not affect the demodulator if the clock is adjusted to operate in the region with the largest available bandwidth in the inductive link.

Creating such a (relatively) flat band can still be done without lowering the quality factor of the coils, by making the transmit and receive coils resonate at the same frequency. If, at the same time, the mutual coupling between the coils is high enough, the resulting coupled response gives two resonance peaks away from the resonance frequency of the individual coils, thereby creating a 'well' between peaks [82]. Extensive treatment of this phenomena is found in [82], and is observed to occur if the coupling factor is high enough. From exploratory simulation/analysis of ideal resonance circuits, If the inductance is high enough (microhenries) and the coupling factor is in range of 0.1-0.4, with the carrier frequency range of 0.1-30 MHz,and when the ohmic resistances of the coils are in the order of a few ohms, the frequency gap between both peaks is empirically given by:

$$\Delta f_{peak2-peak1} \sim k f_{res}, \tag{3.1}$$

where k is the coupling factor between coils and f_{res} is the resonance of one side uncoupled. For example, for a k-factor of 0.3, which is feasible at 5 mm separation distance [47], it follows that at 10 MHz, a flat band of approximately 3 MHz is available. When the coupling factor is larger than 0.4, the symmetry of the response around the tuned frequency will be lost but the system is still operational.

Figure 3.4 shows the ideal channel response for four values of the coupling factor–ideal channel response: 1 V of the signal is coupled between the two resonant sides (ideal inductor 27 μH as coil and capacitor to resonate at 10 MHz at both transmit side and receive side) and the received voltage is plotted against frequency. The well that can be seen has a relatively flat passband to accommodate the data rate bandwidth. For instance at k=0.5 and bandwidth (region between peaks) is about 6 MHz which would support 3 Mbps.

3.3.4 Reducing Receiver Clock Frequency

The role of the reset generator module in the implanted receiver (see Figure 3.1) is to provide a reset signal to reset the edge detector at a time after the detection of the current edge $t = 0$. This needs to be done at a time $0.5T_{PSK} < t < T_{PSK}$ to avoid the transition point between carrier periods, where T_{PSK} is the period of the carrier signal. To achieve this, it uses an asynchronous counter to count from a time of current edge detection $t = 0$ to a desired time as specified above. We determine the frequency of the clock, which is essentially the frequency of the oscillator, as follows. With a count-up number N, the following inequalities must be satisfied. To reset after the transition point between carrier periods, we have:

$$(N-1)T_{OSC} > 0.5T_{PSK}, \tag{3.2}$$
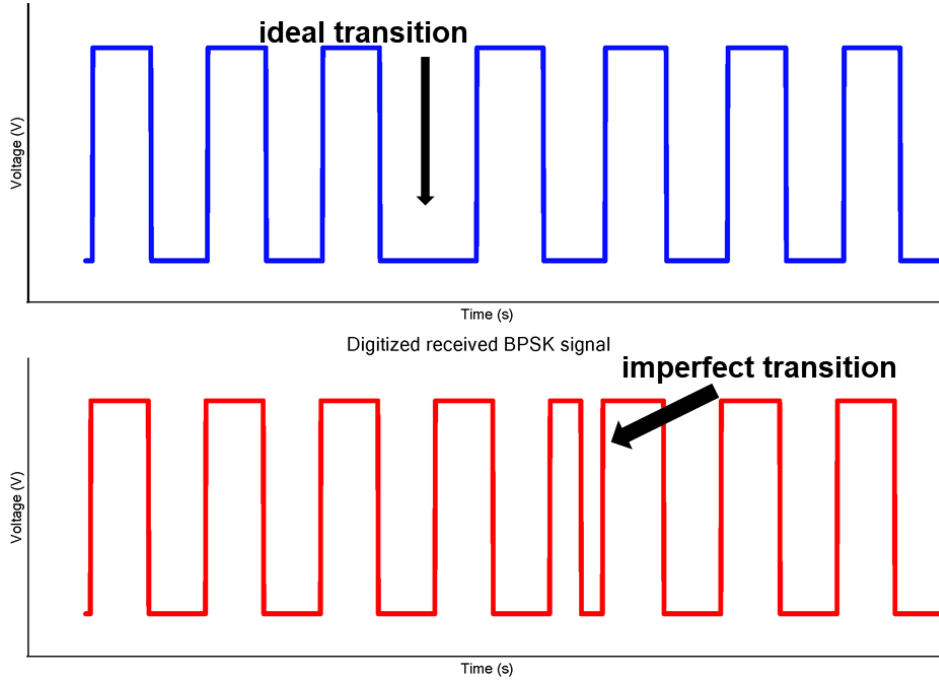
Figure 3.3: Illustrating an imperfect transition on the digitized received BPSK signal due to the inductive link. (a) ideal transition. (b) imperfect transition.

and to ensure that there is no reset after the next edge, we get:

$$NT_{OSC} < T_{PSK}, \tag{3.3}$$

Therefore, the range for the clock frequency is given by:

$$Nf_{PSK} < f_{OSC} < 2(N-1)f_{PSK}, \tag{3.4}$$

where $f_{PSK} = \frac{1}{T_{PSK}}$ is the carrier frequency and f_{OSC} is the oscillator frequency. A practical reset timing constraint relates to the presence of realistic inductive links, in which the phase transition is sometimes not instantaneous. For flexibility in the reset timing, we write in a more general form:

$$\frac{N}{c_{upper}}f_{PSK} < f_{OSC} < \frac{N-1}{c_{lower}}f_{PSK}, \tag{3.5}$$

where c_{upper} and c_{lower} are the set limits (dimensionless, ranging from 0^+ to 1) on the reset timing. It is observed that a higher count-up number N is needed if the range is to be made finer. This implies a higher clock frequency.

The power consumption of the digital demodulator is proportional to the clock frequency. Since the carrier-to data ratio is below one due to bandwidth limitations, in the digitized received signal, there will be repeated bits, since more than one cycle of the carrier-waveform will represent a data symbol. The clock frequency can be reduced by skipping a few periods p during the non-coherent demodulation. The reduction in clock frequency, in turn, will reduce
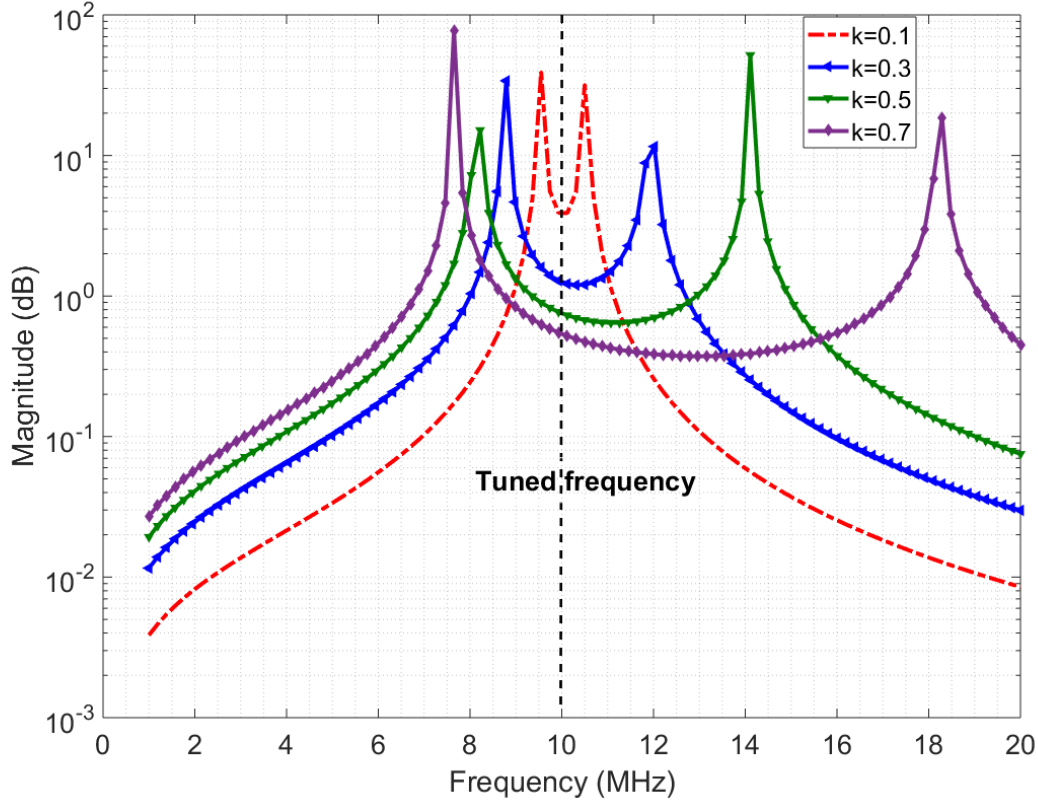
Figure 3.4: Ideal channel response.

power consumption. The carrier-to-frequency ratio is inversely proportional to the number of bits that will be repeated in the digitized received signal. For reducing the receiver clock frequency by skipping p periods, we get modified versions of Equations (3.2) and (3.3):

$$(N-1)T_{OSC} > (c_{lower}+p)T_{PSK}, \tag{3.6}$$
$$NT_{OSC} < (c_{upper}+p)T_{PSK}. \tag{3.7}$$

The resulting clock frequency is given by:

$$\frac{N}{c_{upper}+p}f_{PSK} < f_{OSC} < \frac{N-1}{c_{lower}+p}f_{PSK}. \tag{3.8}$$

For instance, circuit simulation shows that at a data rate of 1.25 Mbps, a carrier frequency of 10 MHz and count-up number of $N = 16$, the clock frequency of the digital demodulator can be reduced from 23 MHz to 5.8 MHz when p=2 periods are skipped. This reduces the power consumption by a factor of 2 for the non-coherent digital demodulator sub-block which is validated by the decrease in clock frequency from 23 MHz to 5.8 MHz as power consumption scales with clock frequency. Although the overall power consumption is technology dependent in general, there is always a reduction in power consumption brought about

by reducing the clock frequency by skipping redundant bits. Figure 3.5 illustrates timing diagram at p=1 of the demodulator. More basic details and illustrations without reducing carrier frequency by skipping bits can be found in [66].
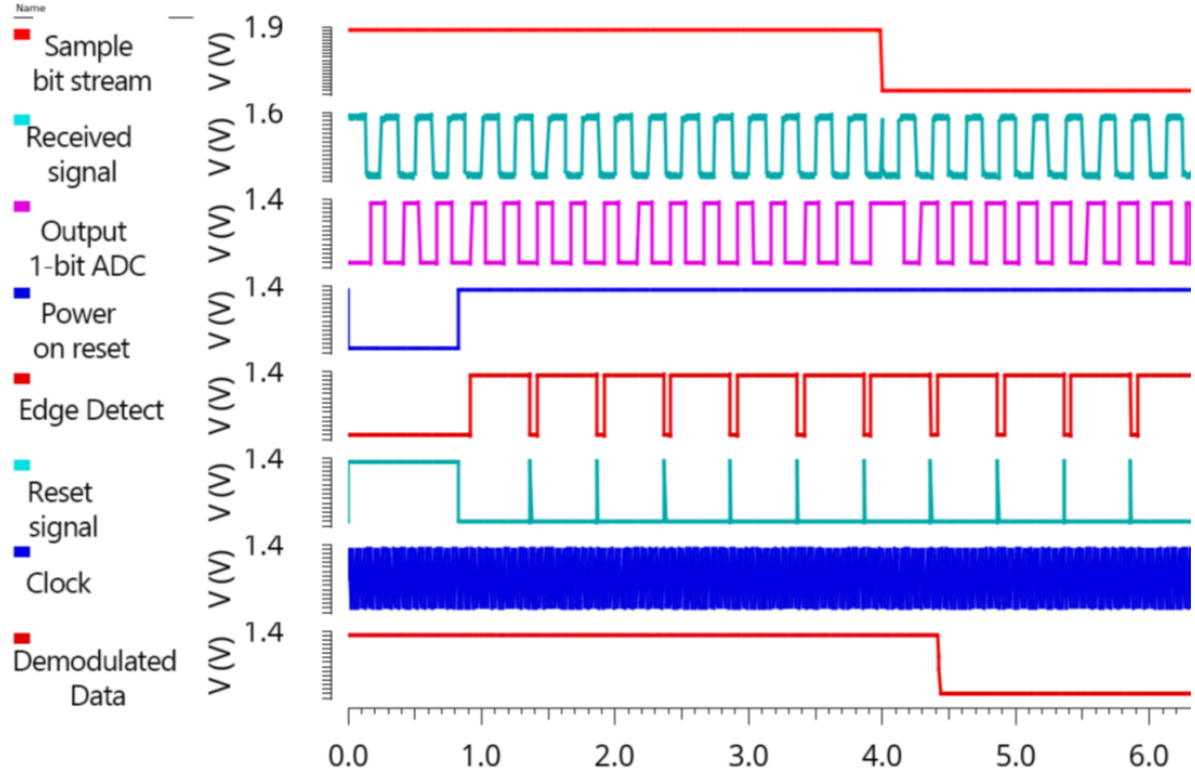
Figure 3.5: Illustrating timing diagram of the receiver at p=1.

3.4 Experimental Demonstrator

For proof of principle of the downlink architecture, the system is built using off-the-shelf components and electronics. A scaled-down carrier frequency of 0.5–2 MHz and data rate of about 200 kbps is used for easy implementation on a breadboard, while still allowing for experimental investigation of key elements of the system, as described in the previous section. The demonstrator is not yet biocompatible. However, once the system has been implemented on an IC (covered Chapter 5), an approach as described in [40] can be used to achieve biocompatibility. In this approach, a transparent window is made at the top of the package for coils which are placed above the PCB housing the electronics, and then the entire package is hermetically sealed [40]. The following subsections present the experimental demonstrator in detail.

3.4.1 External Transmitter

For the experimental demonstrator setup, the external BPSK transmitter is emulated using two single pole single throw (SPST) switches. Figure 3.6 shows the circuit schematic of the external transmitter demonstrator. To achieve BPSK functionality, the inputs into the second switch, which are the carrier signal and data bits, are inverted. The outputs of both switches are connected. Together, the switches act as a switch pair to form the BPSK modulated signals. The DC component is filtered using a high-pass filter. The two SPST switches are in a single component: the DG411LE from Vishay Siliconix Pennsylvania, USA. The inverters are SN74F04 from Texas Instruments Texas, USA. By-pass capacitors of 0.1 μF were used to isolate the power supply of each sub-IC.
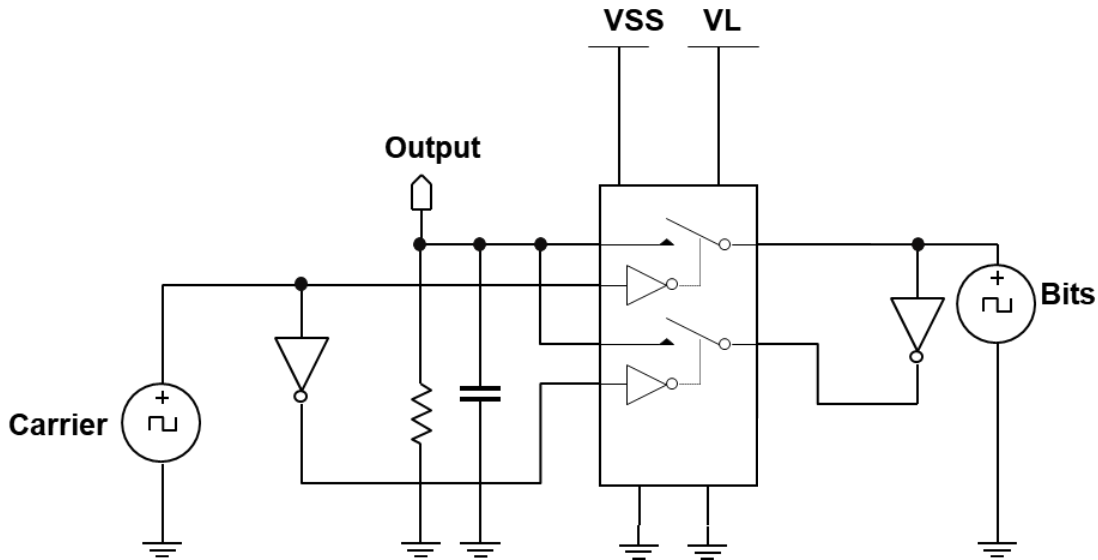
Figure 3.6: Circuit schematic of the emulated BPSK transmitter.

3.4.2 Experimental Inductive Link

We focus on demonstrating the inductive link channel, for which we use off-the-shelf coils of moderate size with ferrite backing. These coils have a self-resonance frequency above 15 MHz, making them suitable for the low-frequency demonstrator. We used a pair of 12 μH coils on a 48 mm by 32 mm ferrite plate for the transmit and receive coils. Alternatively, another pair of 10 μH coils on a 37 mm by 37 mm ferrite plate can be used. Both sets of coils are from Wurth Electronics. Commercial off the shelf coils often comes with ferrite backing to increase the inductance and enhance coupling. Nonetheless, [47] achieved high coupling $> k$=0.3 at 5 mm without ferrite backing. Ceramic capacitors of 2.2 nH are used to tune both the transmit coil and the receive coil to resonate at 1 MHz. Zener diodes are used to limit the maximum voltage to protect the comparator. Figure 3.7 shows the circuit schematic of this implementation.
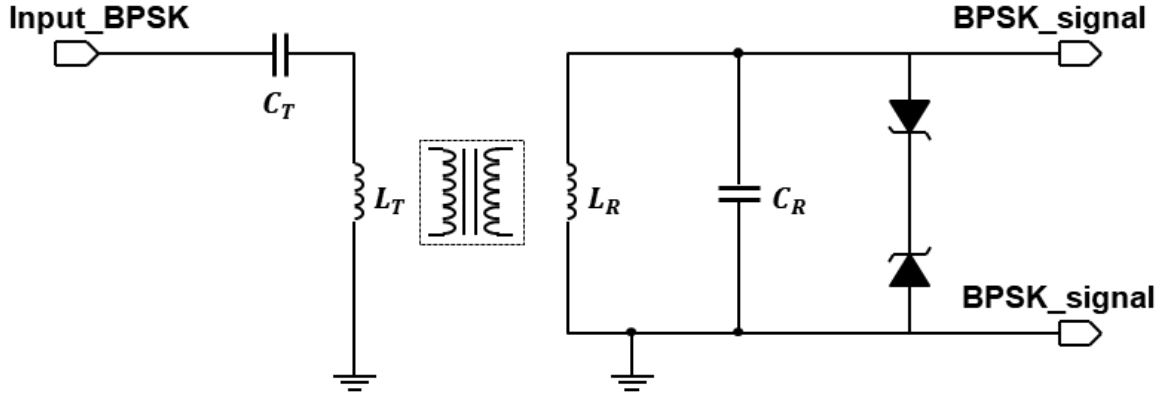
Figure 3.7: Inductive link schematic.

3.4.3 Implanted Receiver

Figure 3.8 shows the schematic of the circuit board implementation of the proposed implanted receiver. The ADCMP600BRJZR2 comparator from Analog Devices acted as the 1-bit ADC. The 74F74N dual D flip-flops along with the 74F08 AND gate and the 74F32 OR gate are used to construct the edge detector are from Analog Devices. The 74F04 NOT gate is inserted before the clock input to make it a negative edge. For the reset generator, the 74F161 4-bit counter is used from Analog Devices. In recovering the actual bits from the edge detector, two 74F74N flip-flops are used, one for alignment and the other for the recovery of the bits. By-pass capacitors of 0.1 μF are used (not depicted in Figure 3.8) to isolate the power supply of each IC. Figure 3.9 shows a picture of the implementation on a breadboard.

3.5 Results

With the demonstrator described in Section 3.4, the coupled coils are tested on open-loop voltage to determine their coupling factor k, which has an impact on the channel response. Next, the channel response is characterized by transmitting a sine wave and sweeping its frequency. Finally, data transfer is validated by sending the bits to the receiver, where they are recovered. The following sub-sections present these results, respectively.

3.5.1 Open-Loop Voltage on the Inductive Link

To determine the coupling factor between the transmit and receive coils when they are separated a certain distance, an open-loop voltage test was carried out. The coupling factor is found by determining the output voltage of the receiver coil divided by the input voltage of the receiver coil without any tuning capacitor. The input voltage has a source resistance of around 50 Ω. While estimating the coupling factor, the source resistance was corrected for because open-loop voltage calculation assumes no source resistance. Layers of foam of about
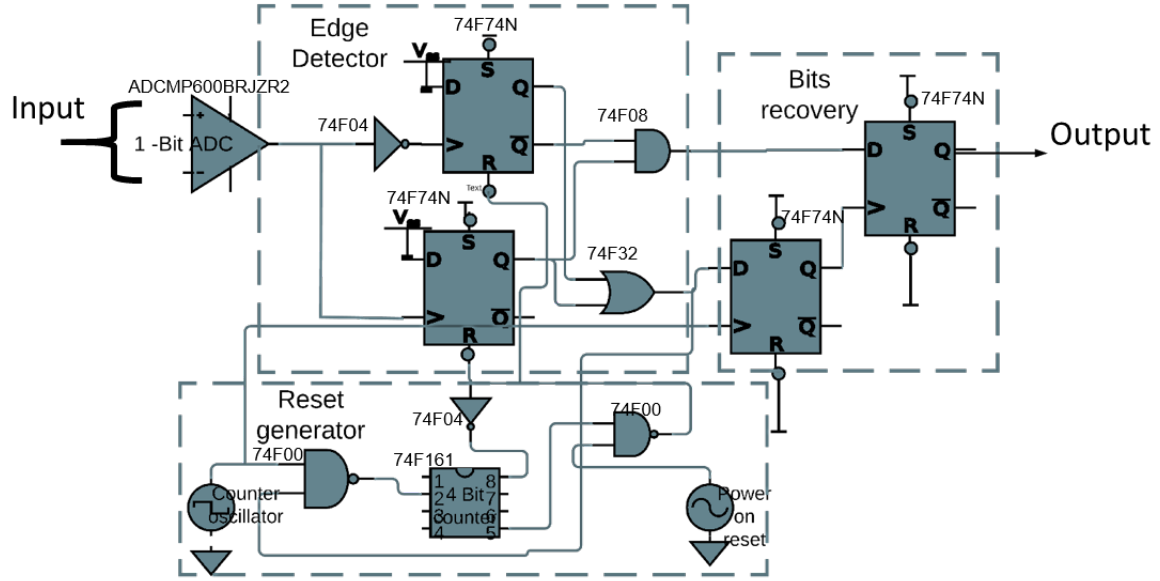
Figure 3.8: Downlink receiver demonstrator: schematic.

2.5 mm/layer were used to create various separation distances between the transmit and receive coils to mimic different skin thicknesses as in Figure 1.4. Below 100 MHz, the effect of skin on magnetic fields is negligible [76], so results with foam are expected to be representative for those with skin tissue. On the other hand, transmission through skin tissue may heat the tissue due to the specific absorption rate (SAR) and the implanted electronics may generate heat as well. Considerations for this will be given in Section 5.6.2.

Table 3.1 shows the received voltage for 2 sets of coils at an input amplitude of 5 V. At 7.5 mm separation distance, the coupling-factor was slightly above 0.3 which would still result in 3 MHz bandwidth at k=0.3 according to Fig. 3.4 which is sufficient for 1.5 Mbps communication through the skin (bandwidth required is twice the data rate for BPSK [78]).

Table 3.1: Open-loop voltage test to estimate the coupling factor.

12 μH coil [48 mm by 32 mm Ferrite plate]		
	Open-loop voltage	k-factor
1 layer of foam [2.5 mm] 5 V input @ 1 MHz	3.30 V	0.80
3 layers of foam [7.5 mm] 5 V input @ 1 MHz	1.90 V	0.46

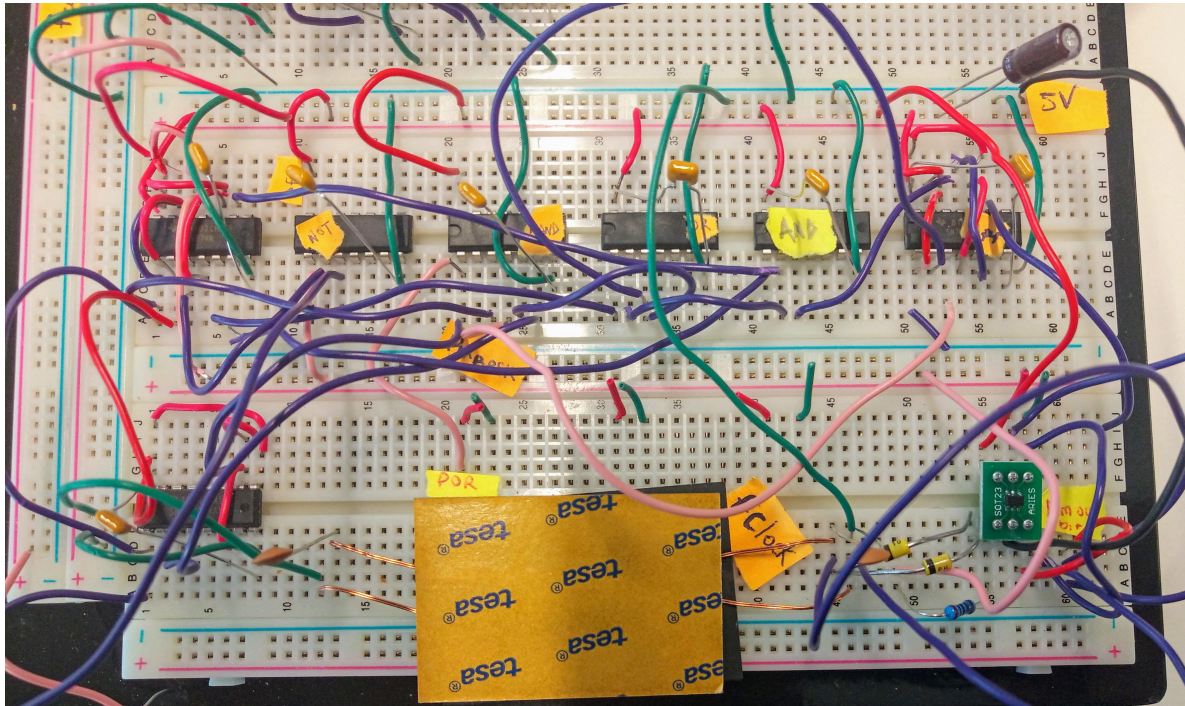| 10 μH coil [37 mm by 37 mm Ferrite plate]		
	Open-loop voltage	k-factor
1 layer of foam [2.5 mm] 5 V input @ 1 MHz	3.30 V	0.80
3 layers of foam [7.5 mm] 5 V input @ 1 MHz	1.27 V	0.31

Figure 3.9: Downlink receiver demonstrator: realization.

3.5.2 Inductive Link Response

In estimating the channel response, an input single sine wave is swept in frequency, and the amplitude voltage at the receiver coil is recorded. However, one significant deviation is that the source is not resistance-free (unlike as in Figure 3.4), but has a 50 Ω impedance which decreases the quality factor and the amplitude at the resonance peaks. As a result, the two peaks of the coupled response as described in Section 3.3.3 blend together. Figure 3.10 shows the simulated response with a 50 Ω source impedance and measured results of the 12 μH coils for two separation distances (1 and 3 layers of foam). The deviation (< 125 kHz) between the simulated and measured plots is due to measurement errors, deviation in component values and impedance differences. Figure 3.11 shows the channel response on the 10 μH coils at 3 different layers (2.5 mm thick foam). Also here, the 50 Ω impedance decreases the quality factor, causing the two resonance peaks to blend. In addition, a smaller separation distance (less layers of foam) results in more bandwidth because of the higher coupling factor, which is similar to the ideal response in Figure 3.4. The similarity in bandwidth behavior between Figures 3.4, 3.10, and 3.11 indicates the feasibility of inductively coupled coils for the wireless link. In addition, the approach allows for scaling up to 12 MHz for the IC-implementation (4 MHz will be demonstrated in Chapter 5, 13.56 MHz was attempted in [67] for data transfer). This will be covered in Chapter 5. The relevant part of the behavior is the frequency band in between the peaks, as it indicates the bandwidth for the data transfer available as explained in Section 3.3.3.
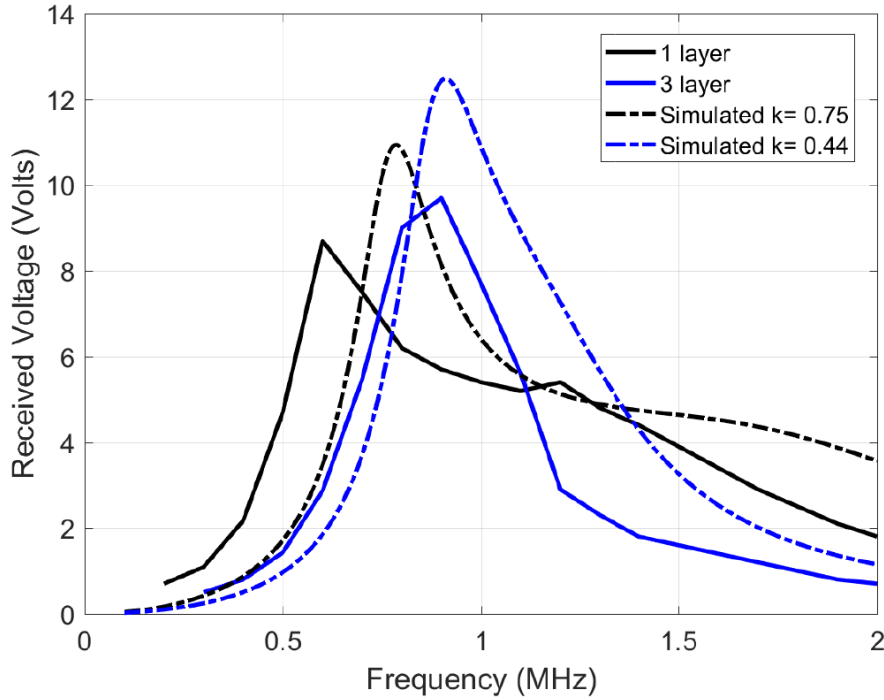
Figure 3.10: Channel response of the 12 μH transmit and receive coils, tuned individually to 1 MHz using 2.2 nF capacitors.

3.5.3   System with Inductive Link

The complete downlink system demonstrator is tested on the breadboard setup. A carrier frequency of 1 MHz is used and a bitrate of 125 kHz. The clock of the digital receiver was set to $10 * f_{psk}$ which is 10 MHz. In this case, a count-up number $N = 8$ was used, which also satisfies the range constraint in Equation (3.8). Figure 3.12 shows the measured signal results. The transmitted bits had some carrier patterns due to imperfect isolation between sub-blocks. On the digitized received signal, phase changes due to bit type changes in PSK modulation can be seen in areas with a longer period. These are indicated in the figure. The digitized signal waveform also indicates that the desired bandwidth was achieved. The reset signal is also shown in Figure 3.12, every rise in the reset signal indicates a reset triggering by the reset generator for digital demodulation. The recovered bits are in agreement with the transmitted bits indicating successful demodulation with a typical harmless time lag arising from the demodulation process.

3.6   Discussion

A scaled-down carrier frequency of 1 MHz and data rate of about 125 kbps are used for implementation on circuit board for proof of principle. The data rate is sufficient for testing since the 125 kbps data rate is close to the lower bound of the requirements of the data rate for the final system. The system will be scaled up to operate at 4 MHz and at a higher data
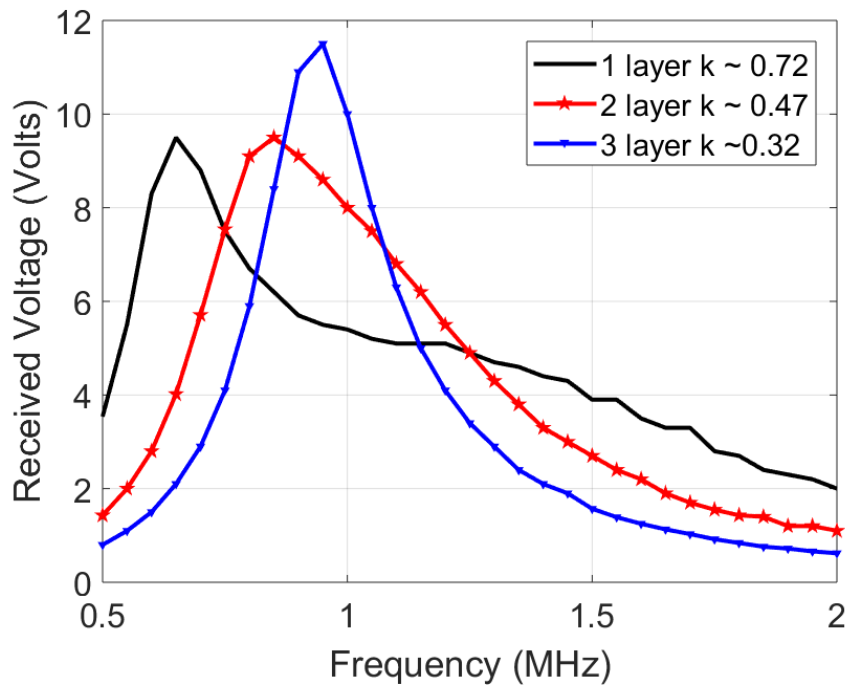
Figure 3.11: Channel response of the 10 μH transmit and receive coils, tuned individually to 1 MHz using 2.2 nF capacitors.

rate up to 1 Mbps as will be shown with the IC implementation, described in Chapter 5. It is important to stress that the power consumption of the receiver scales linearly with frequency due to its predominantly digital circuits. Consuming below 1 mW at 4 MHz on IC simulation clearly indicates that tuning to a 6.78 or 13.56 MHz ISM band is well possible.

3.7 Conclusions

The BPSK modulated downlink system for delivering stimulation data to a visual prosthesis was experimentally demonstrated on a proof-of-principle breadboard implementation. Commercial off-the-shelf coils were used, showing a bandwidth of 0.5 MHz, which is sufficient to achieve a data rate of 125 kbps. Power consumption at the implanted receiver could be reduced by lowering the clock frequency by skipping redundant bits in the digitized received signal. The system meets the specified requirements.

Although the system was clearly demonstrated on a scaled-down version on a circuit board, the experimental results show everything is in order from a system point of view for a more compact, integrated design, together with the uplink system which will be explored in Chapter 5. The results of the sub-milliwatt and compact IC version will be presented there. This will wirelessly enable the visual prosthesis in a low-power and robust way.
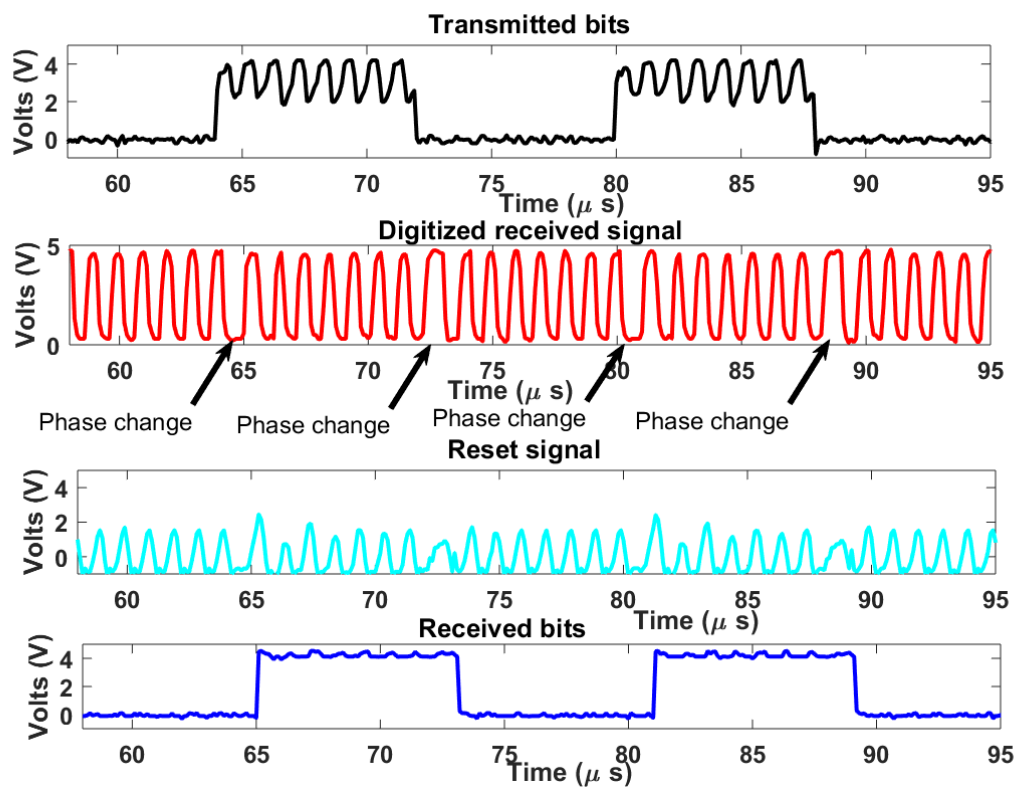
Figure 3.12: Measured signal results.

Uplink: IR-UWB communication design[1]

4.1 Introduction

The wireless system required for an intracortical visual prosthesis also involves communication from the implanted electrode (uplink) for neural recording, apart from the downlink and wireless power transfer. The neural recording (uplink) is needed for calibration and monitoring. The uplink is the focus of this chapter. Figure 4.1 shows the wireless system layout, highlighting the uplink.

Developing a low-power implanted transmitter to get the recorded neural signal out of the brain (uplink) is quite challenging due to the high data rate required. The requirements for the uplink part of the implanted visual prosthesis have already been detailed in Section 2.2 of Chapter 2. It is even more complicated in the presence of nearly simultaneous reception of stimulation signal and wireless power transfer. In [35, 73, 91, 92] several generic medical telemetry systems were reported. In [92] optical communication was attempted for the uplink. However, this faces a challenge of misalignment sensitivity. Impulse radio ultrawideband (IR-UWB) was used in [73] showing a promising result. A high data rate was achieved in [35] using an IR-UWB transmitter. However, none of these telemetry systems is in the context of the 1024-count implanted electrode visual prosthesis, where sending stimulation information to the implanted electrode is taking place concurrently.

This chapter describes the communication link system requirements for sending recorded neural information out of the brain. Some background on IR-UWB will be presented, and then the uplink system approach is described. Following this, the system architecture will be explored. A proposed transmitter, a tunable on-off keying (OOK) IR-UWB transmitter for low-power, will be designed and simulated at a circuit level (For IC layout and fabrication see Chapter 5). The proposed transmitter will address the potential miniaturisation and power consumption constraints. The feasibility of a moderate power consumption non-coherent ex-

---

[1]This chapter is partly based on publication [P5].

ternal receiver will also be explored in the system architecture. Next, transmission loss and link budget analysis will be investigated. A transmit antenna and a receive antenna, one below and the other above the skin, respectively, will be designed in electromagnetic simulation software to validate the feasibility and to quantify the path loss for the link budget. Furthermore, the link budget of the proposed system will be analysed to demonstrate its feasibility. After describing the results obtained with the designed system, the chapter will be brought to a conclusion.
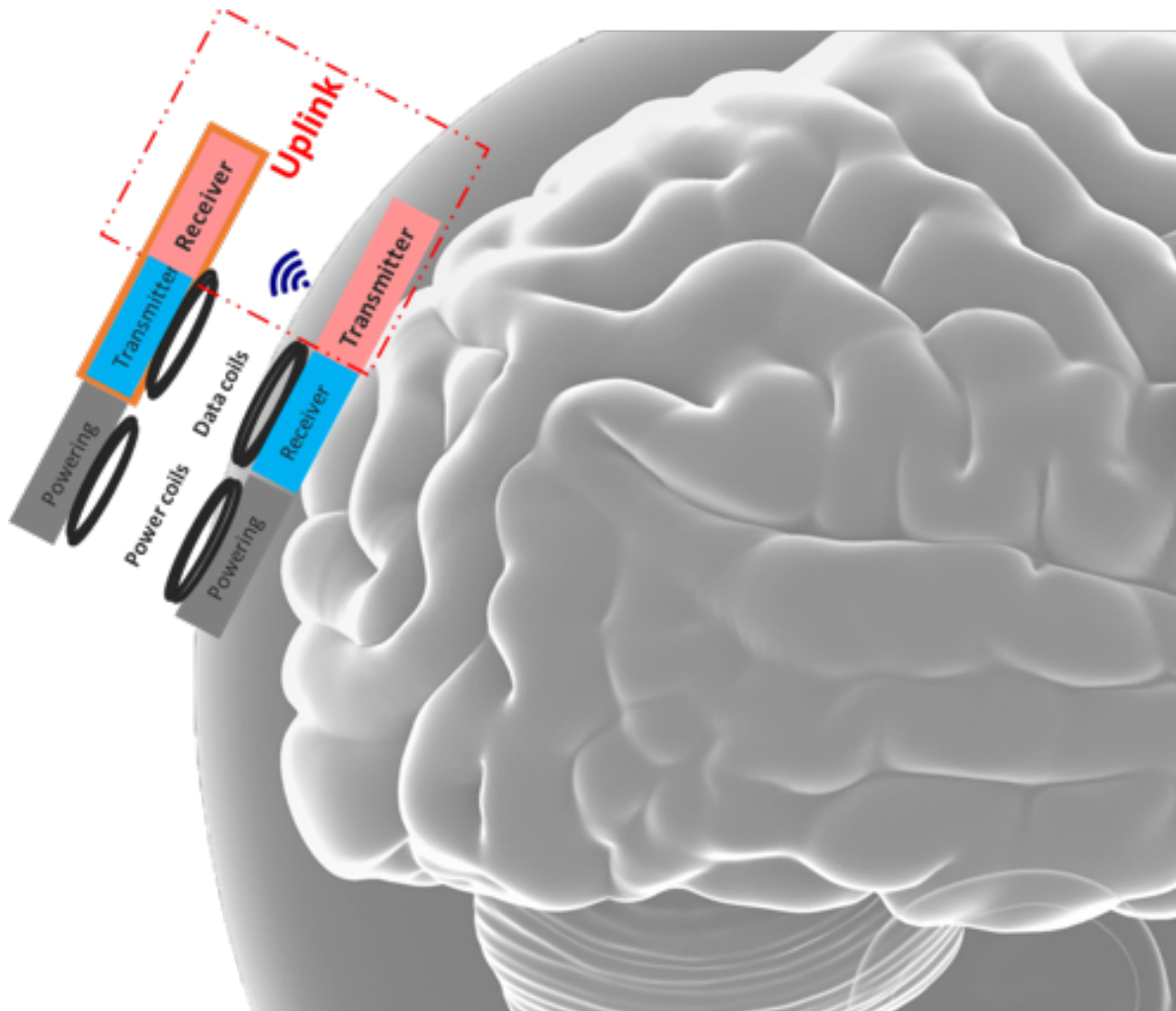
Figure 4.1: Layout of the wireless system of the intracortical visual prosthesis.

4.2   Background on IR-UWB

4.2.1   IR-UWB basics

Over the unlicensed frequency range of 3.1–10.6 GHz, the FCC [94] has defined UWB signals as those that occupy greater than 500-MHz bandwidth or larger than 20% fractional bandwidth as defined by:

$$Fractional\ Bandwidth = \frac{2(f_U - f_L)}{f_U + f_L} \geq 20\%, \tag{4.1}$$

where f_U and f_L are the upper and lower frequency limits, respectively, of the 10-dB bandwidth of the signal spectrum. The FCC and Europe also requires that the power emission levels of the UWB signals within the UWB spectrum of 3.1–10.6 GHz must be low enough. The low power emission levels avoid interference with other existing communication systems, technologies and services operating in the same frequency band, such as Wireless Fidelity (WiFi). In this way, UWB can co-exist with the other systems. From a regulatory point of view, the FCC and Europe requires that the maximum allowed power spectral density (PSD) not exceed -41.3 dBm/MHz for the 3.1–10.6 GHz frequency range [94]. Other services could be operating under different rules that share the same bandwidth with the UWB frequency range. This low RF transmit power requirement causes these unlicensed UWB systems to work mainly within short ranges, making them suitable to employ miniature CMOS RFICs. Their RF power capability and dc power consumption are relatively small [26]. In UWB pulse systems, the transmitting pulse contains energy, or information, over a much wider frequency band as compared to narrow-band signals.

4.2.2   Basic Modulation Topologies

Several modulation techniques can be used to generate UWB signals, which modulate the information bits directly into very short UWB pulses [98]. Since there is no intermediate frequency (IF) processing in systems employing such signals, these systems are often called "base-band" or "impulse radio systems". Typical modulations in UWB pulse systems can be divided into the mono-phase and bi-phase techniques. The three most popular mono-phase UWB modulation approaches are pulse position modulation (PPM), pulse amplitude modulation (PAM), and on-off keying (OOK). In these techniques, the data signal "1" is distinguished from the data signal "0" either by the size of the pulse signal or by its time of arrival. Apart from that, all the pulses essentially have a similar same shape. Figure 4.2 illustrates the waveform for these different modulation options. In addition, bi-phase shift keying (BPSK) is a bi-phase case, see also Fig. 4.2. This modulation transmits a single bit of data with each pulse, with the positive pulse representing "1" and the negative pulse signifying "0".

For the uplink communication from the wireless implant, OOK modulation is considered the best candidate, because of its straightforward implementation which can lead to very low power consumption and less complex design. For instance, OOK modulation can be implemented with a D-latch which is a digital circuit leading to a potential predominantly digital architecture. In OOK modulation, information bits "1" and "0" are represented with the full-amplitude and zero-amplitude of the UWB pulse, which are obtained by turning the UWB pulse on and off, respectively.

4.3 System Approach

The requirements for the intracortical visual prosthesis and specific requirements for the wireless link for getting the recorded neural signal out of the brain were described in Section 2.2 of Chapter 2. From the system requirements summarized in Table 4.1, it has become clear that the transmitter should be a low-power implementation, that achieves a high data rate at the implant side. For this reason, the IR-UWB transmitter can be designed as a radio fre-

Table 4.1: Summary of system requirements for the uplink transmitter.

Requirement	Target
Power conusumption	<10 mW
Data rate	>23 Mbps
Bit error rate	$< 10^{-3}$
Security	3–7 mm short link
Frequency band	3–5 GHz
Size	<30 mm $\times$ 30 mm

quency integrated circuit (RFIC) rather than with discrete microwave components [31]. The transmitter can be implemented in RFIC using CMOS technology. Since the transmit power of IR-UWB is low due to the FCC restriction, a simple CMOS IC is sufficient. Furthermore, an IC implementation allows for integration with the downlink implanted receiver. The RFIC fabrication and validation will be discussed further in Chapter 5.

Another important approach in the system design for the implanted transmitter is to use predominately digital components to enforce low power consumption and high-speed circuitry. For instance, the modulator can be implemented by using a D-Latch and the pulse forming by using inverters and a NOR- gate, which are digital circuits.

Finally, with the transmission loss modelling and link budget analysis, an external receiver can be explored in future work. Power consumption in the external part of the system is less critical.
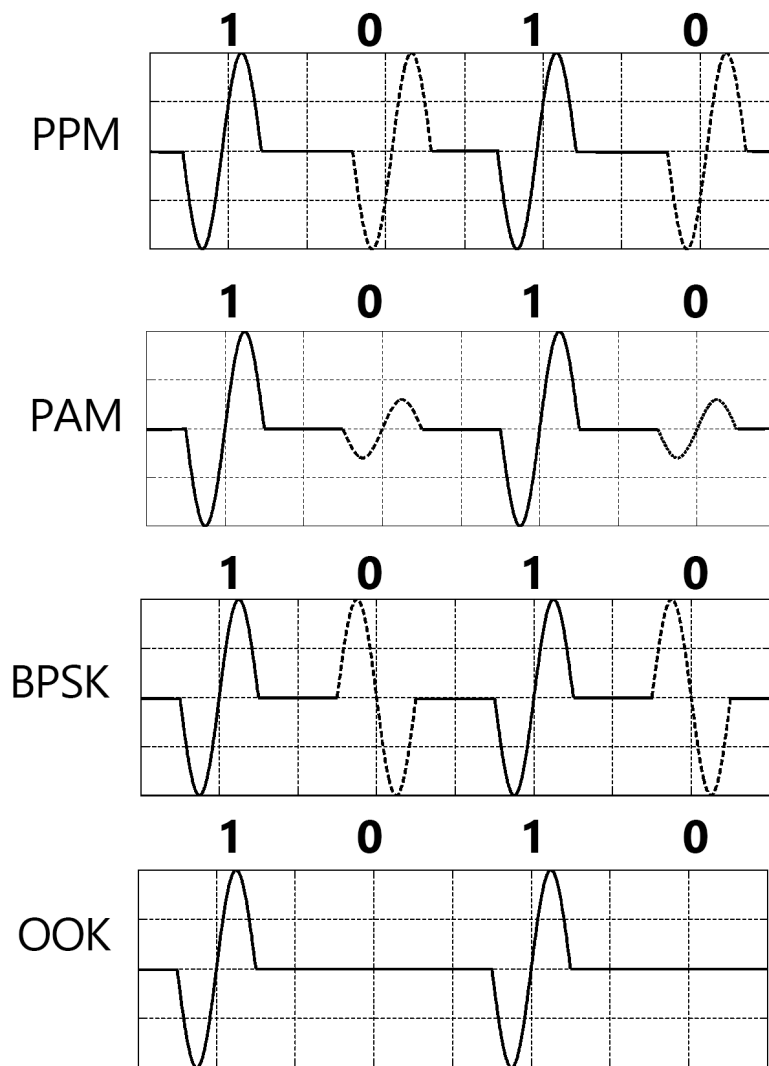
Figure 4.2: Illustration of the various modulation options in waveform: PPM - pulse position modulation, PAM - pulse amplitude modulation, BPSK - bi-phase shift keying and OOK - on-off keying.

4.4 System architecture

4.4.1 Implanted transmitter

Figure 4.3 shows the overall circuit diagram of the proposed CMOS IC IR-UWB transmitter. The IR-UWB transmitter comprises mainly of the modulator and the pulse generator. The design of the transmit antenna, which will be connected to the chip is also an important

aspect and will be discussed in Section 4.5. The modulator can be implemented in CMOS technology by a D-Latch [99]. The data bits and the off-chip clock source are fed as the control signal and D-input of the latch, respectively. The resulting signal is fed to the pulse generator.
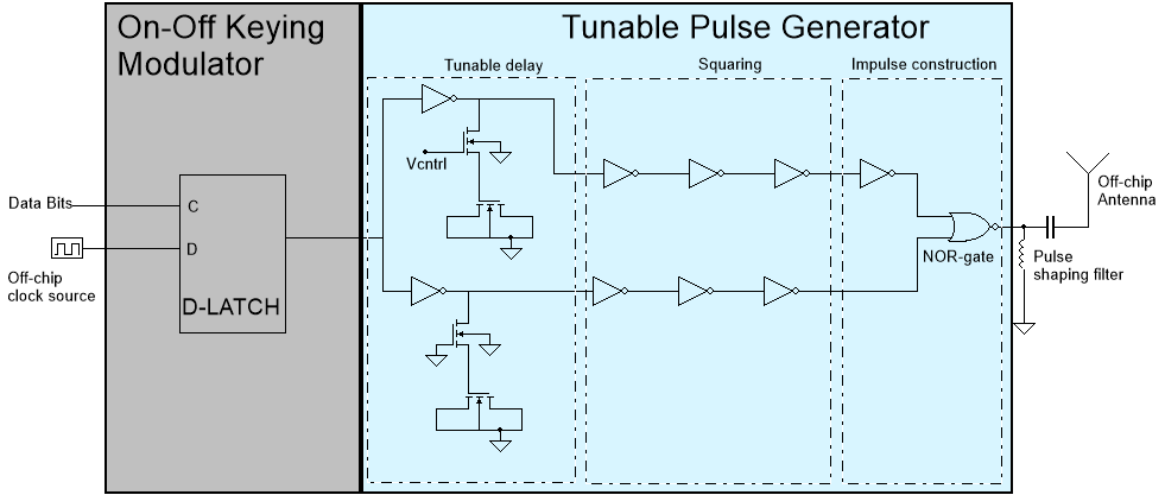
Figure 4.3: Circuit schematic of the proposed IR-UWB Transmitter.

Implementing the pulse generator in CMOS technology can be done by a tunable delay element, followed by pulse squaring, a NOR-logic gate for pulse forming, and, finally, pulse shaping filters, which can be implemented off-chip. For tunable delay elements, a voltage controlled shunt-capacitor as in [26] is proposed. The tunable delay elements allows for adjusting the pulse width. For proper pulse forming using NOR-logic gates, the squareness of the signals coming from the tunable delay lines is crucial, and this is done by using three inverters on both the reference line and the delay line for symmetry. Further details on the implementation will be given when the combined IC implementation is described in Section 5.3.

4.4.2 Proof of principle external receiver

Although the research focus is more on the implanted side of the visual prosthesis, a proof of principle external IR-UWB receiver will benefit the complete system design in the future. Such an IR-UWB receiver could be coherent, which means that it requires synchronization and other power-hungry parts, such as phase locked loops in most architectures [108, 109]. It could also be non-coherent, thereby avoiding clock synchronization issues and a matching local oscillator [29, 110–112]. From a power consumption point of view, and also for design simplicity, we propose to use a non-coherent design. Figure 4.4 shows two typical architectures of implementing a non-coherent receiver for OOK IR-UWB. The key difference is using an RF detector diode [29], or an RF log detector [110]. A log-detector requires fewer sublocks and is more straightforward to implement with off-the-shelf components. Therefore, it was selected for the proof of principle.
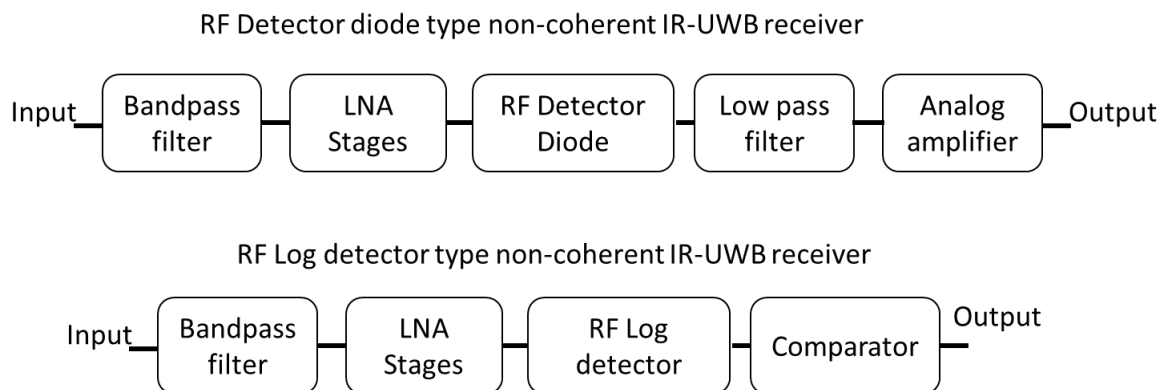
Figure 4.5 shows a non-coherent IR-UWB receiver demonstrator using a log detector built from off the shelf components. The VBFZ3590S+ from Mini Circuits was used as a bandpass filter [113]. The AD5541 from Analog Devices was used as an LNA [114]. The AD8318 from Analog Devices was used as a log detector [115], while the ADCMP600 from Analog Devices was used as the comparator [116].

4.5 Transmission loss and link budget analysis

4.5.1 Antenna design

In the IR-UWB system, the frequency band of 3–5 GHz is targeted, the lower band of the 3.1–10.6 GHz available spectrum, because of lower attenuation through the skin than in the upper band. Considering the biological environment around the antennas and the tissues between the implanted (transmit) and external (receive) antenna is important in the antenna design. Figure 4.6 shows the layer stack used to represent the tissues around and between the antennas for transcutaneous communication. The transmit antenna is located just beneath the skin and is backed by the skull bone, dura, cerebrospinal fluid (CSF) and brain matter. In reality, the layers will have a curved shape, due to the human skull. This will have an influence on the antenna performance. It is beyond the scope of the thesis to determine the exact effect, because this would have to be tailored for every patient. Instead, we aim to derive a decent estimate based on the layer stack in Fig. 4.6 and account for non-modeled effects (like the exact shaping) by creating margin in the link budget. The relative permittivity and conductivity of these tissues used were obtained from the Gabriel database [100–102], for the 3–5 GHz band of interest. Table 4.2 shows the thicknesses and material properties at two frequencies for the tissues in the layer stack.

Electromagnetic simulations are carried out in SIMULIA Studio Suite [117]. The human tissue layer stack environment is 60 mm by 60 mm in the *xy*-plane, which is terminated by free space in all directions. The time-domain solver in SIMULIA was used with a hexahedral mesh. The time-domain solver is optimal for wideband signals. The mesh is convenient for

Figure 4.4: Two possible system architectures for a non-coherent IR-UWB receiver.
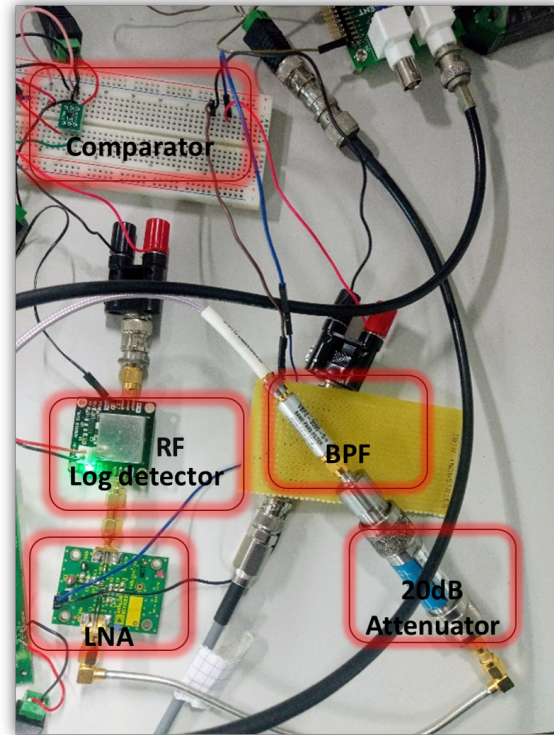
Figure 4.5: A proof of principle non-coherent IR-UWB receiver.

the layered structure. A total amount of 145,222 mesh cells is used, with at least 7 cells per wavelength, and the boundary conditions are chosen such that the reflections at the edges only minimally affect the antennas. The simulation setup was checked for convergence. An 80 mm by 80 mm sized stack environment show less than 0.05 dB difference in S-parameter values.

Several UWB antennas for body area communication could be designed [103–105]. However, we take a more straightforward approach to the antenna design by using a co-planar fed antenna with a monopole patch at its end-radiator [106, 107]. Co-planar feeding generally results in larger impedance bandwidth while allowing for some design tuning freedom using the feed gap.

Table 4.2: Layer stack up, thickness and dieletric properties of body tissues.

Layer	Thickness	Permittivity ε_r at 3 GHz, 5 GHz	Conductivity (S/m) at 3 GHz, 5 GHz
Skin	3–7 mm	42.1 , 39.6	1.95 , 3.57
Fat	2 mm	5.2 , 5.0	0.13 , 0.24
Bone	5 mm	11.1 , 10.0	0.51 , 0.96
Dura	1 mm	41.3 , 38.9	2.01 , 3.58
CSF	1 mm	65.4 , 62.0	4.00 , 6.60
Brain matter	2 mm	48.1 , 45.1	2.22 , 4.10
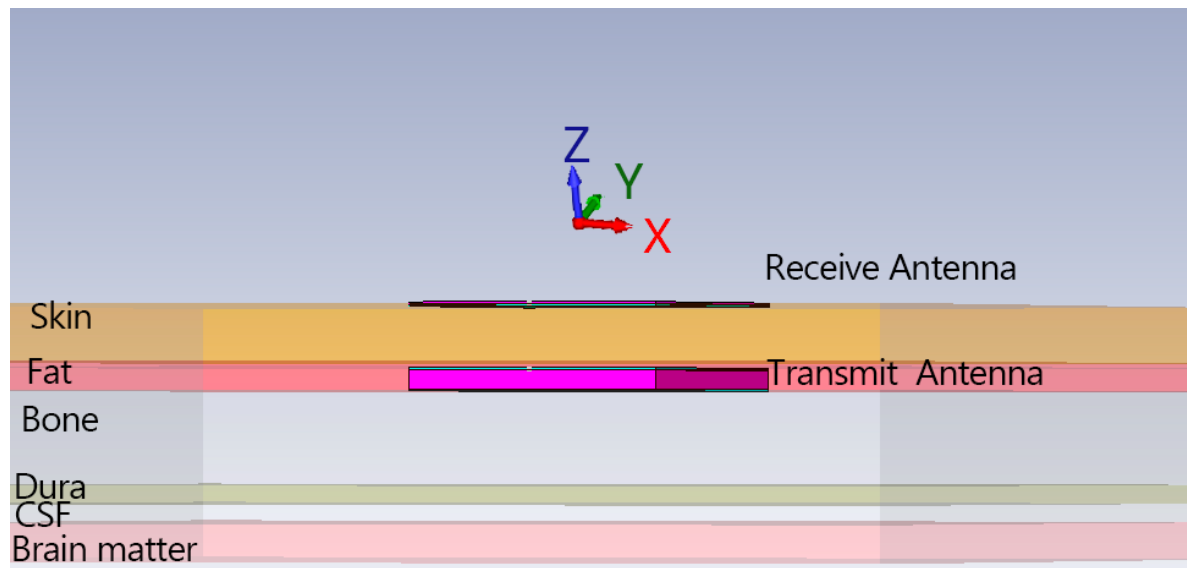
Figure 4.6: Layer stack of tissue for electromagnetic modeling and simulation.

Figure 4.7 shows the final dimensions of transmitting and receiver antennas designed with the biological tissues modelled. The U-shaped transmission line connecting the two ground patches of the co-planar feed is used to model the excitation by an edge-mount SMA connector. The size of the radiator of a typical monopole antenna is a quarter of its wavelength ($\lambda/4$), which is 18.75 mm at 4 GHz. However, we need to take the direct environment of the antennas into account, which is the tissue as shown in the layer stack in Figure 4.6. The proximity of the tissue changes the effective wavelength for the antenna, especially for the receive antenna as it will operate close to the skin, as seen in Figure 4.2. The effective wavelength $\lambda/\sqrt{\varepsilon_r}$ for the receive antenna is shorter than of the transmit antenna because the relative permittivity ε_r of skin is much higher than fat. Therefore, the resulting dimensions of the receive antenna are smaller than that of the transmit antenna. The co-planar fed monopole antenna was on 14 mm by 18 mm substrate for both transmitting and receiving antennas.

The antenna substrate thickness of the receive antenna is 0.1 mm and 1 mm for the receive antenna. The 1 mm thickness of the transmit antenna gives less transmission loss than using 0.1 mm since there is an increase in the effective distance (direct contact) between its top metal layer and the bone tissue. The relative permittivity of the antenna substrate is 2.2. An insulator coating (Kapton polymide which is bio-compatible with a relative permittivity of 3.4) of 0.1 mm was placed over the transmit antenna to avoid direct contact between conductors and tissue. The back side of the substrate of both antennas has an insulator coating of 0.1 mm.

Figure 4.8 shows the reflection coefficients (S11) for both transmit and receive antennas for two different skin thicknesses. At 3 mm skin within 3–5 GHz band, the reflection coefficients range between -10.6 dB and -24.2 dB for the transmit antenna and -7.3 dB and -12.4 dB for the receive antenna. At 7 mm skin within 3–5 GHz band, the reflection coefficients range between -12.2 dB and -41.5 dB for the transmit antenna and -7.3 dB and -12.4 dB for
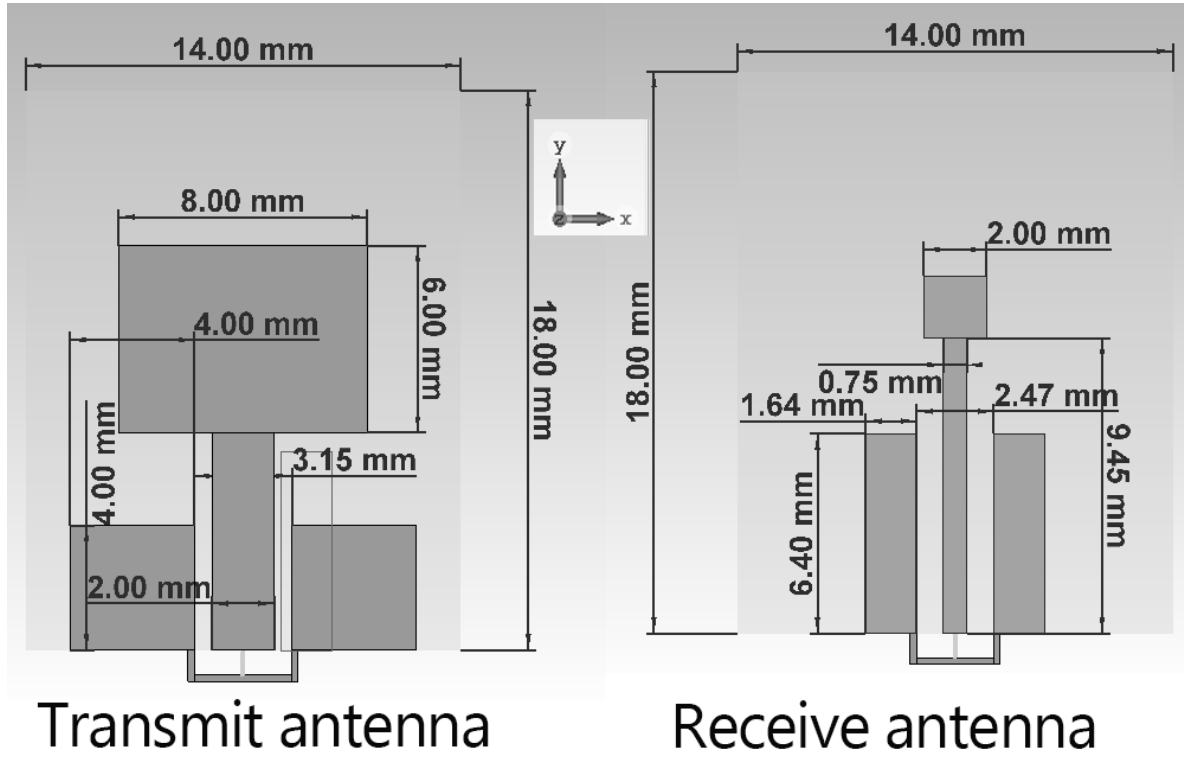
Figure 4.7: Transmit and receive antenna for IR-UWB.

the receive antenna. Therefore, the S11 is under -10 dB in the 3–5 GHz band for the transmit antenna and under -7 dB for the receive antenna. The antenna simulation result is from a first design effort. Further design optimization was not done, since the focus in this chapter is on the IR-UWB system design. It is recommended to improve the S11 for the receive antenna further.

4.5.2 Path loss simulation

An important research aspect of the IR-UWB system design for the uplink is understanding what happens in the path from the transmit antenna beneath the skin to the receiver antenna outside the skin. The transmission (path) loss through 3–7 mm transcutaneous distance is the S21-parameter for the transmit-receive antenna pair in the presence of the biological tissues as detailed in the layer stack in Figure 4.6. Figure 4.9 shows the S21 results of the transmit antenna and the receive antenna in the presence of the biological tissues at 3 mm and 7 mm skin thickness. At 3 mm skin within the 3–5 GHz band, the S21 ranges between -12.8 dB and -19.3 dB. At 7 mm skin within the 3–5 GHz band, the S21 ranges between -16.7 dB and -25.4 dB. As a result, increasing the skin thickness from 3 mm to 7 mm, gives around 5 dB increase in transmission loss in the 3–5 GHz band.

Furthermore, various misalignment scenarios have been investigated, in which there is a horizontal misalignment of 5 or 10 mm between the antennas, either in *x*- or *y*-direction with coordinate system indicated in Figures 4.2 and 4.7. Figure 4.10 shows the S21 for the various
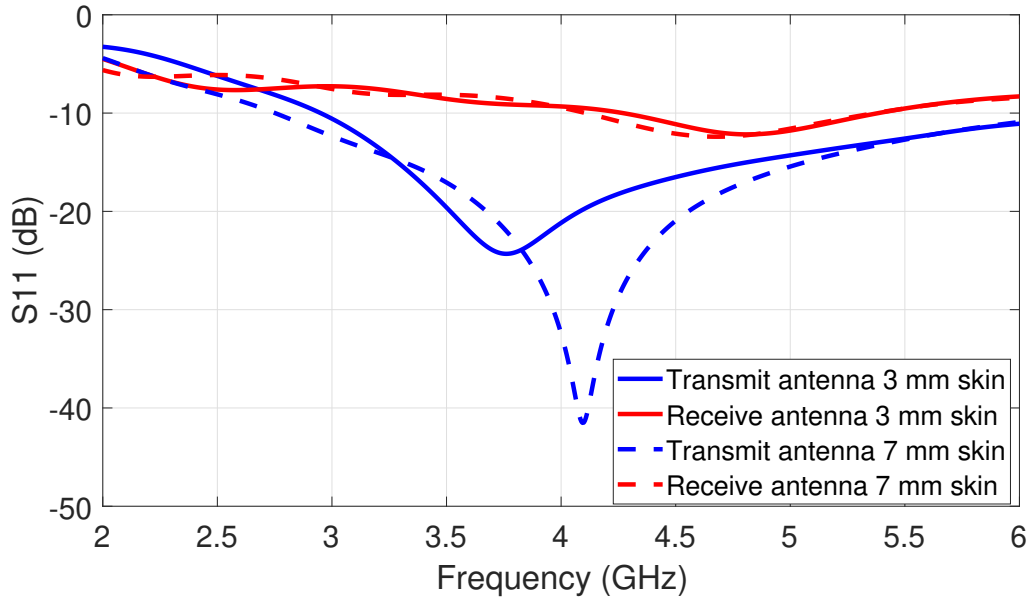
Figure 4.8: S11 of the transmit and receive antennas at 3 mm and 7 mm skin thickness.

misalignment cases. It can be observed that a 5 mm offset leads to about 2 dB more loss, and a 10 mm offset leads up to 11 dB more loss. Therefore, we can approximate the link losses within a 5 mm offset to about 20 dB. To be on the safe side and to account for effects that have not been included in the model (such as tissue property variability), a value of 30 dB is used as a worst-case transmission loss (S21). This value is then used in the link-budget calculation in the next subsection.

4.5.3 Link budget analysis

For the uplink solution based on IR-UWB, it is important to demonstrate its feasibility at system level by analysing the worst-case link budget in the context of the visual prosthesis.

Table 4.3 shows the link budget of the system at worst case, which is estimated based on the path loss simulations described in the previous section as well as on literature. Selecting the lower part of the IR-UWB band (3–5 GHz) is optimal because the wideband design complexity is reduced and 7–10 dB less attenuation than at 8–10 GHz [123], through the skin is present. The thermal noise of a receiver matched to an antenna is -174 dBm/Hz [97]. With a bandwidth of 2 GHz for the IR-UWB signals, the noise floor (N_{floor}) is -81 dBm. Low noise amplifiers (LNA) of IR-UWB have a noise figure typically in the range of 4–10 dB at these frequencies [96]. Taking the noise figure (NF) of the LNA to be 10 dB, and using the formula for noise figure of cascaded stages [97], it is highly unlikely that the noise figure of the entire receiver will exceed 15 dB.

The typical normalized signal to noise ratio (E_b/N_0) required by on-off keying modulation to reach a bit error rate of 10^{-7} with non-coherent demodulation is 15 dB [78]. Assuming the data rate equals the bandwidth, which is easy to reach with IR-UWB, the signal to noise ratio
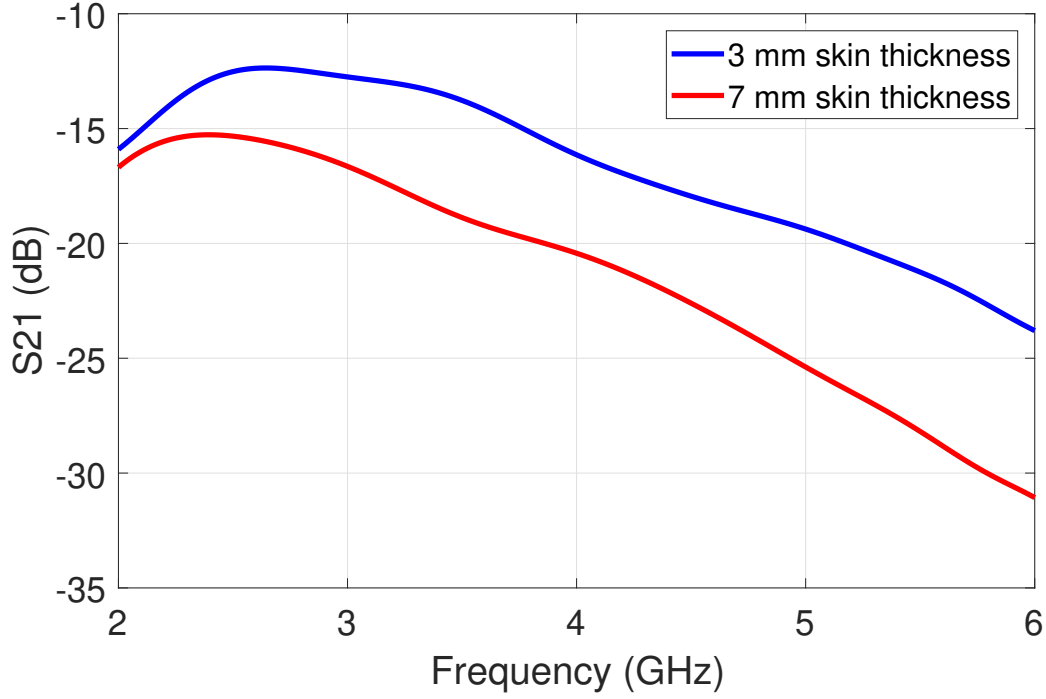
Figure 4.9: Transmission loss at 3 mm and 7 mm skin thicknesses.

(SNR) required is not more than 20 dB, taking into account a reasonable 5 dB buffer. With this in view, the estimated receiver sensitivity S in dBm is given by:

$$S = \text{SNR(dB)} + \text{NF(dB)} + N_{\text{floor}}(\text{dBm}) = 20 + 15 + (-81) = -46 \text{ dBm}. \tag{4.2}$$

With the maximum allowable transmit power of -41.3 dBm/MHz set by the FCC, the maximum total transmission power equals P_{TX} = -8.3 (or -9 dBm if rounded down) for the 3–5 GHz band. Therefore, the maximum allowable link losses PL_{MAX}, tolerable by the system, are $PL_{\text{MAX}} = P_{\text{TX}} - S = -9 - (-46) = 37$ dB. While this maximum allowable path loss of 37 dB can be quite small for free space path of over a few meters, in the context of the visual prosthesis, it is primarily sought to communicate from beneath the skin to just above the surface of the head which is about 5 mm [77].

Losses through 3–7 mm of skin are found to be well below the estimated 37 dB for PL_{MAX}. From our path loss simulations in the previous section and from results reported in [95], the worst-case transmission is 30 dB at 5 GHz. Therefore, from this estimation, it can be concluded that the link will be closed with an excess of 6 dB. Therefore, the application of IR-UWB seems practical and realizable for the intended application.
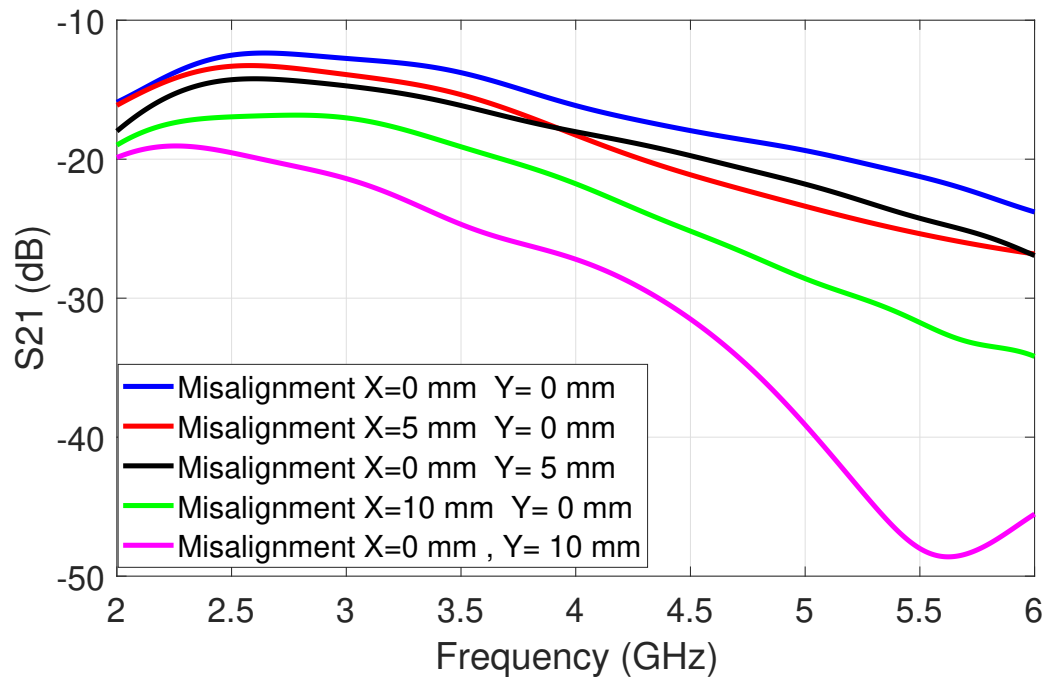
Figure 4.10: Transmission loss and antenna misalignment at 3 mm skin thickness.

Table 4.3: IR-UWB link budget analysis.

Thermal Noise at 2 GHz bandwidth	-81 dBm
Esitmated Noise figure of receiver	15 dB
Typical SNR required	20 dB
Estimated receiver sensitivity	-46 dBm
Maximum transmit power @ 2GHz bandwidth	-9 dBm
Loss tolerable	37 dB
Estimated S21 @ 3–5 GHz through skin	30 dB
Margin (excess)	6 dB

4.6 Results

4.6.1 Simulation results for transmitter

The IR-UWB transmitter as described in Section 4.4.1 is designed and simulated in Cadence software [118], using 180 nm technology at the circuit level. The supply voltage is 1.8 V. An external off-chip oscillator is assumed with an ideal clock source. An ideal parallel inductor with a capacitor in series models the pulse shaping filter. Their parasitic resistances, however, will cause some minor losses in the system. With a pulse repetition frequency of 1 GHz, which makes a 250 Mbps data rate easily possible, the transmitter (modulator and pulse generator) consumed 2.8 mW. This gross data frequency of 250 MHz demonstrates a 250 Mbps data rate potential to be recovered at the receiver. However, the realized data rate may be lower

depending on the type/performance of the external receiver. Although power consumption is not a priority for the part of the system outside the human head, a non-coherent receiver is a straightforward, fail-safe solution.

4.6.2 Results for external receiver

Figure 4.11 shows a snapshot of the output waveform of the proof-of-principle external receiver. The output waveform is not sampled optimally due to the frequency limitation of the Analog Discovery 2 [140] acting as the oscilloscope and the ADCMP600 comparator final sub-block. The proof of principle IR-UWB receiver was able to receive signals only up to 33 Mbps due to the frequency limitation performance of the off-the-shelf comparator and the log-detector. In a future final system, the frequency limitation will even be further reduced when implemented on an IC. Nevertheless, the 33 Mbps is already above the required 23 Mbps data rate for the uplink. This high data rate realized in the demonstrator based on off-the-shelf components holds the promise that even higher data rates could be achieved in the external receiver once miniaturized into high-frequency performance technology.
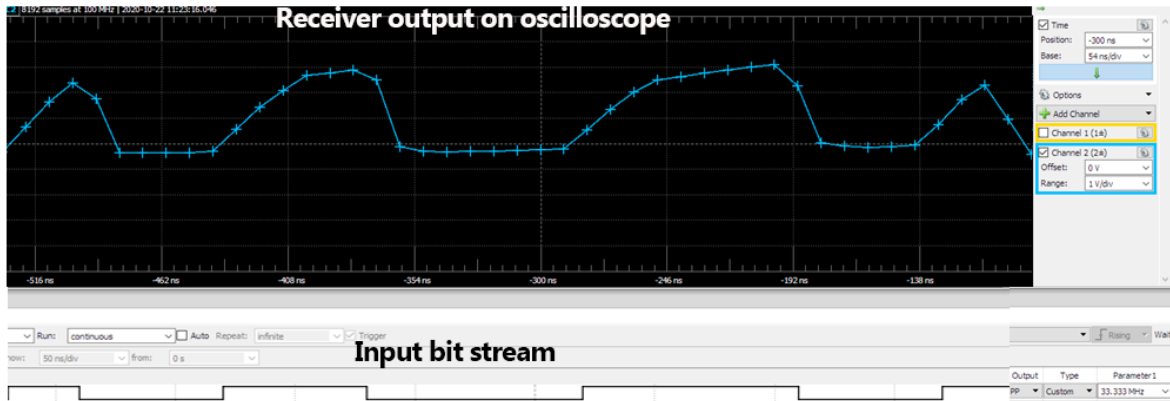
Figure 4.11: Recorded output of proof-of-principle receiver at 33 Mbps.

4.7 Conclusion

In this chapter, the system approach for IR-UWB communication for the wireless link for neural recording (uplink) was presented. The implanted transmitter is the most important component in the system. It was designed and simulated on CMOS IC showing potential low power consumption (under 3 mW). A proof-of-principle receiver was developed using commercial off-the-shelf components. Coplanar-fed monopole antennas were designed, and electromagnetic simulations with body tissues were carried out, showing typical path losses of 20 to 30 dB. The worst-case link budget of the IR-UWB demonstrates its system-level feasibility with excess margin.

The implanted transmitter can be designed together on the same IC with the implanted receiver for the downlink system. This will be covered in the next chapter. The design of a non-coherent receiver on IC, as well as an optimized design of the antennas is also an exciting area of research. The uplink system promises to deliver a high data rate for neural recording in the intracortical visual prosthesis.

IC design, validation and demonstration[1]

5.1 Introduction

Wireless connection between the implanted electrode and the external processor is desired to facilitate mobility and to avoid infections during long-term use [40]. On the implant side, this wireless connection involves uplink (for recording), downlink (for stimulation) and wireless power transfer. This work focuses on the implanted transceiver IC, which is the transmitter for sending out of the head (uplink) and the receiver for receiving stimulation data (downlink). Figure 5.1 illustrates our solution. In this chapter, we focus on the implanted transceiver IC design and analyze its link budget in the context of a complete system.

Generic biomedical telemetries have been proposed for the implanted transmitter for recording and also for an implanted receiver for stimulation. However, in this work, we combine them into a single implanted transceiver for bi-directional communication in an intracortical visual prosthesis. In [33] optical communication was attempted for the uplink. However, this faces a challenge of alignment sensitivity. Impulse radio ultrawideband (IR-UWB) was used in [73] showing a promising result. A high data rate was achieved in [35] using an IR-UWB transmitter.

In our work, for the recording, we use IR-UWB for the uplink because of its low-power and high data rate potential at its transmitter, which will be at the implant side. For our implanted transmitter, we applied current control to make the impulse generator tunable for pulse width. A straightforward on-off keying modulation (OOK) scheme is implemented, based on a simple D-latch to achieve low-power consumption. Furthermore, a current-controlled variable oscillator is proposed to tune the number of pulses per bit. The transmitter is built using predominantly digital components to strive towards low power consumption while delivering a high data rate (a minimum of 23 Mbps is required see Section 2.2). The potential of

---

[1]This chapter is based on journal publication: "Sub-milliwatt Transceiver IC for transcutaneous communication of an Intracortical Visual Prosthesis" in Electronics, Published December 2021 [P2].
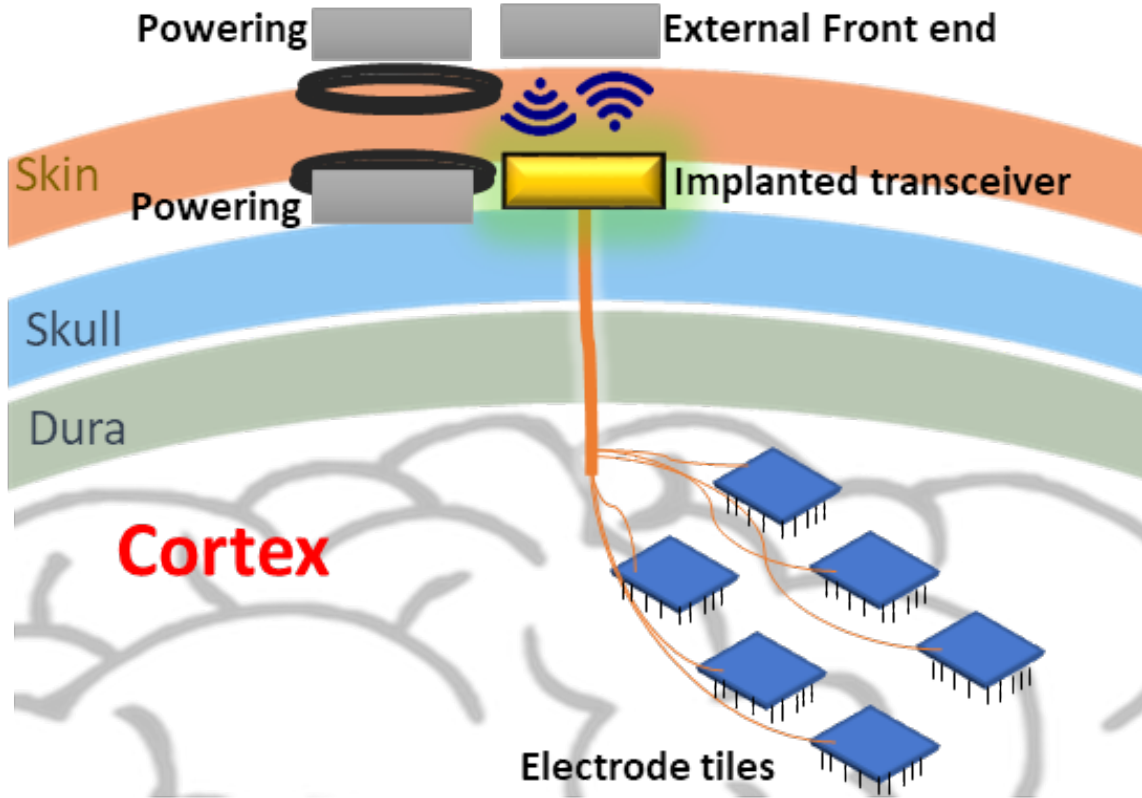
Figure 5.1: System layout of the wireless enabled visual prosthesis.

digital-based designs is discussed in [128, 129], which is beneficial to low-power transceivers.

For the downlink receiver, an analog differential phase-shift keying (DPSK) receiver was used in [79]. Pulse delay modulation (PDM) was used in [67] and an Amplitude Shift Keying (ASK) to Frequency Shift Keying (FSK) conversion receiver in [83], both for low power consumption. However, for our implanted receiver we took an approach of a non-coherent digital receiver, with low-carrier frequency (4 MHz) using an inductive link. Implanted receiver's low-power and sufficient data rate due to its predominantly digital components and low frequency motivate its selection. The receiver is above the minimum data rate requirement of 200 kbps for the downlink.

In this work we describe the design of our fabricated implanted transceiver (excluding coils and antenna) on IC, based on CMOS 180 nm technology. Our idea is to: 1) reduce power consumption to less than a milliwatt using predominantly digital components. 2) provide tunability in the spectrum of the pulsed signals in the IR-UWB transmitter using current control for its oscillator and impulse generator; 3) make the implanted receiver's operating frequency point adjustable with current control to accommodate different frequency bands for an inductive link.

The remainder of the chapter is structured as follows. Section 5.2 highlights key overall system requirements and considerations. Section 5.3 describes the implanted transceiver (IR-UWB transmitter and non-coherent BPSK receiver) design and integration into IC. Section

5.4 provides more information about the measurement setup. Section 5.5 shows the measure results of the fabricated chip and a link budget discussion on how it will fit in the entire system. Section 5.6 discuss medical safety concerns and shows a comparison with recent works from literature. Section 5.7 concludes the chapter.

5.2   System Requirements and Considerations

For the implanted transceiver, which comprises of the transmitter for uplink (sending out data from the implanted side) and its receiver for downlink (receiving stimulation data), the following essential system requirements are considered:

1. Power consumption: Based on power consumption reported in [72, 73], the projected power consumption of the implant side of the 1024 electrode visual prosthesis without a wireless interface is in the order of 100 mW. Considering the wireless power transfer, and possible battery constraints at the implant side, it is desired that the wireless system adds minimal extra power consumption to the power budget at the implant side. This implies that only a low-power solution for the implanted transceiver will create a viable system. The external transceiver above the skin will be allowed to consume more power. Our proposed non-coherent BPSK receiver will fulfill this due to its simple architecture and predominantly digital components. For the uplink, on-off keying (OOK) is used for the IR-UWB transmitter because of its simple architecture making for a low-power transmitter.

2. Transmission data rate: It is required to transmit a minimum of 23 Mbps for compressed data with electrode recordings (see Appendix A). The receiver is required to handle a minimum of 200 kbps of stimulation data (See Section 2.2). IR-UWB for the uplink has the potential to deliver high data rate for short distances. Using an inductively-coupled link with BPSK at low frequency will provide sufficient data rate, while yielding a low-power solution.

3. Bit-error-rate (BER): the uplink and downlink system should give a BER of at least 10^{-3} over the full communication chain with an external side. BPSK is used for the downlink because it has a better theoretical bit error rate performance than other modulation schemes, such as amplitude shift keying and frequency shift keying [78]. The BER target is checked by using the IC results in the overall link budget. The focus of this work is on a low-power implanted side transceiver IC. Any need for improved BER could be taken care of by adjusting the link budget through the coil design with the external side. The case of the uplink, for example, where the IR-UWB receiver is external, reported receivers [110, 143] at similar sensitivities already meet the BER target of 10^{-3}, Similarly for the downlink case, where the transmitter is external, the transmit voltage can be scaled easily to meet the implanted receiver sensitivity of 50 mV (related to the offset voltage of the 1- bit ADC i.e. comparator [119]). In addition,

straightforward coil design can already realize the required channel bandwidth which a minimum of 400 kHz (bandwidth required is twice the data rate for BPSK [78], which is a minimum of 200 kbps for the downlink).

4. Security: with the increasing risk of communication security breaches, the wireless link needs to be secure (safe from other external sources/receivers), especially at the physical level. Therefore, short range transcutaneous communication is proposed from beneath the skin to the receiver just outside the head. The expected transmission path through skin is expected to be in the range of 3–7 mm [77]. In daily use situations, this comes down to a system that cannot be influenced or read from sources as close as 0.2 m to the implant.

5. Co-existence with other sub-systems: in the overall wireless system of the visual prosthesis, the downlink and wireless powering are also present. The wireless link should be able to cope with other sub-systems in terms of frequency spectrum use, interference, and cross talk. Using the 3–5 GHz band for the uplink and the 1–12 MHz band for downlink provides sufficient frequency spacing to avoid interference. In addition, we propose to use coupled inductive link. Furthermore, the lower 3-5 GHz band of the 3-10 GHz for UWB is preferred due to lower attenuation through the skin [123]. In principle, pulse based system like IR-UWB are carrierless and our target frequency band is 3-5 GHz as opposed to a carrier frequency which is about 1–12 MHz for the BPSK communication in the downlink. Interference will be minimal due to its localization and near-field nature.

5.3 Implanted Transceiver

5.3.1 IR-UWB Transmitter

To achieve the low power consumption, the IR-UWB transmitter can be designed as a radio frequency integrated circuit (RFIC) rather than with discrete microwave components [31]. The IR-UWB transmitter can be implemented as an RFIC using CMOS technology. Since the transmit power of IR-UWB is low due to the FCC restriction [94], a simple CMOS IC is sufficient. This renders the CMOS RFIC transmitter to consume little power and it allows for integration with the downlink implanted receiver in the same IC.

   Figure 5.2 shows the overall circuit diagram of the proposed CMOS IC IR-UWB transmitter. The IR-UWB transmitter comprises mainly of the modulator, the impulse generator and a current-controlled oscillator. The design of the transmit antenna, which will be connected to the chip, should be compact and wideband. Although this is also an important aspect for the overall system, it is outside the scope of this chapter. To attain low power consumption and reduce complexity, an on-off keying modulation (OOK) scheme is used. It modulates the short pulses (impulse signals) that come from the impulse generator. The modulator can

be implemented in CMOS technology by a simple D-Latch [99], making it a digital component. The data bits and the current-controlled oscillator clock are fed as the control signal and D-input of the latch, respectively. The resulting signal is fed to the impulse generator, see Fig. 5.2.
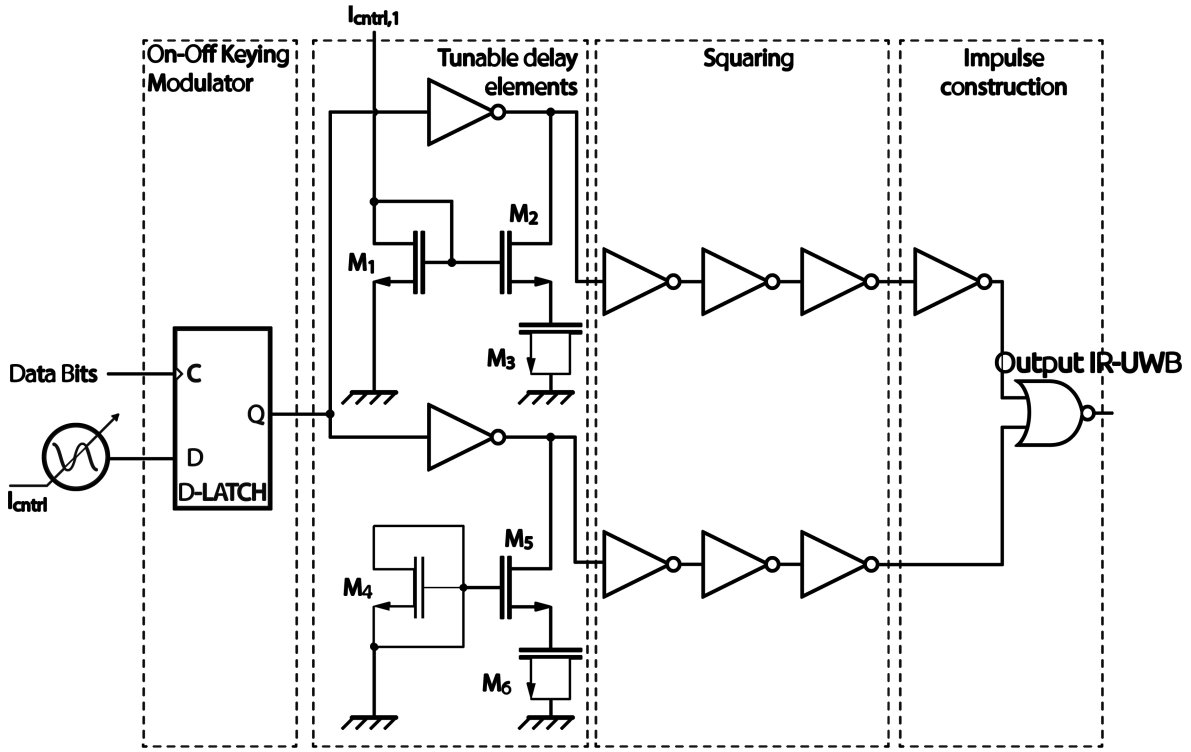
Figure 5.2: Schematic of the IR-UWB transmitter.

Implementing the impulse generator in CMOS technology can be done with a tunable delay element, followed by squaring of both the signal and its delayed version, and then a NOR-logic gate to form the pulses.

The oscillator used for pulse generation in the pulse generator is a 5-stage current-starved single-ended ring oscillator as reported in [124]. Figure 5.3 shows the circuit schematic of the 5-stage current-starved single-ended ring oscillator. The difference compared to [124], however, is that 5 stages was used in our work, and an extra transistor for current control makes it differ from [124].

For tunable delay elements, a current-controlled shunt-capacitor (M2 and M3 form the current-controlled shunt capacitor) as is proposed in [26]. Tuning is realised via transistors M1, M2, and M3, while transistors M4, M5 and M6 are used for balance, see Fig. 5.2. Transistor M1 transforms the control current into voltage and biases M2. By changing the input current, the resistance of M2 is tuned. This changes the capacitive loading of M3 on the first stage of the inverter chain and hence change in the delay of the signal [26]. The tunable delay elements add flexibility and help shaping the spectrum of the impulse signals as first explored in [125], our differs with an extra transistor to make it current-controlled rather than voltage-
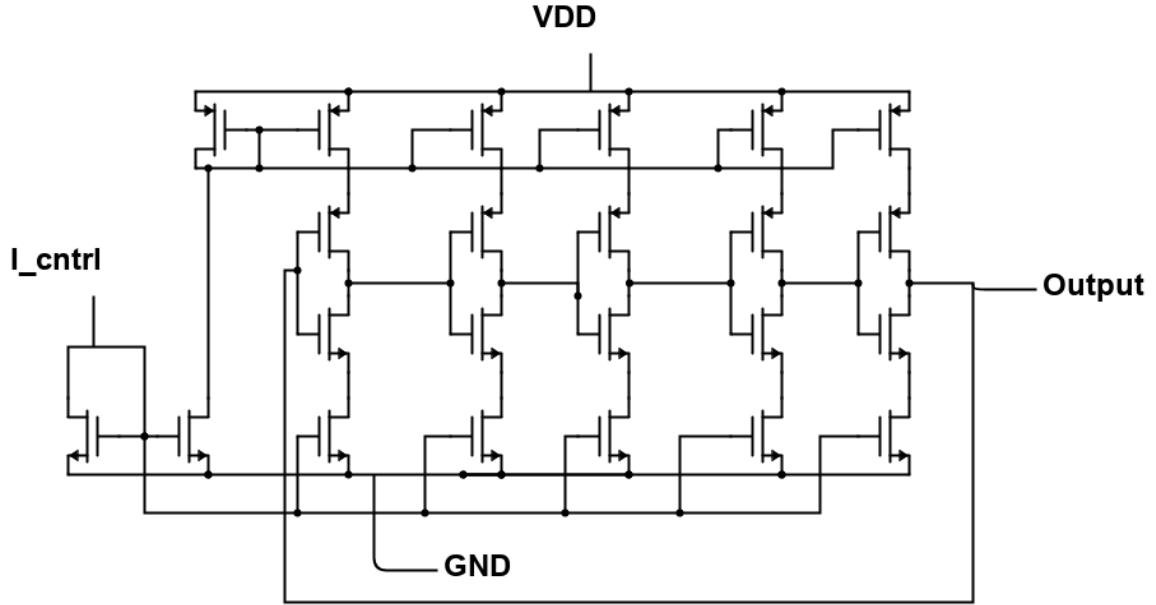
Figure 5.3: Schematic diagram of the 5-stage current-starved single-ended ring oscillator for receiver and transmitter.

controlled. For proper impulse forming using a NOR-logic gate, the squareness of the signals coming from the tunable delay lines is crucial, and this is done by using three inverters on both the reference line and the delay line for symmetry. This combination of logic circuits ensures a low-power implementation for forming the pulses as, for instance, detailed in [26]. Figure 5.4 shows the IC layout design of the IR-UWB transmitter. From the figure it can be seen that the NOR gate which is the impulse construction block is made large enough to drive an antenna that could be connected to it in future work.The NOR gate at the final block in the transmitter has NMOS and PMOS transistors with widths of 90 um and 180 um, respectively (using 18 fingers), i.e. more than 400 times the minimum width of 0.22 um. Large transistor sizes improve the drive capability of the last stage especially when logic gates are used [126].

Finally, pulse shaping filters are needed, which can be implemented off-chip by a band-pass filter. In addition, the transmission characteristics of biological tissue (skin) will have to be experimentally quantified over the frequency range of 3-5 GHz for a final design of the antenna (which is out of the scope of this thesis). In open air, far-field transmission, pulse shaping filters are relevant to make the system satisfy the FCC mask. However, in our context, with transmission through 3-7 mm of skin, already 20-25 dB loss is seen, which causes the radiated power at the surface of the head to be already far below the FCC mask (3–10 GHz spectral mask of -41.3 dBm/MHz). This is based on our transmitter delivering -27 dBm and the aforementioned attenuation through skin. In spite of these losses, the link budget can still be met.
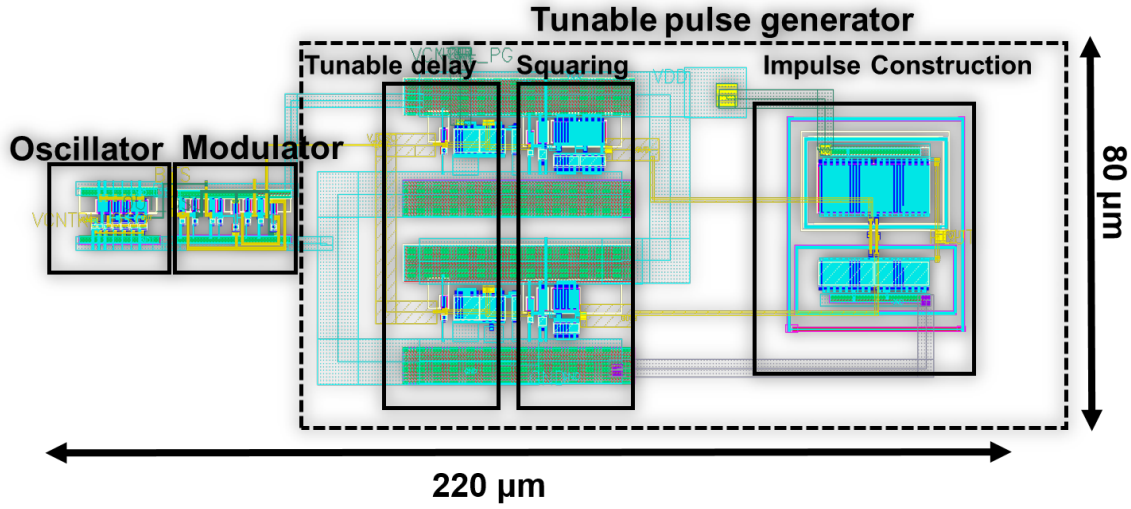
Figure 5.4: Layout of the IR-UWB transmitter.

5.3.2 Non-coherent BPSK Receiver

Similarly to the transmitter design for uplink, the requirements for downlink can be met by taking a system approach aimed at designing a low-power implementation. This involves using low frequency (<100 MHz), an inductive link, phase shift keying (PSK), and a nearly digital receiver with non-coherent demodulation after sampling and by means of edge detection , as introduced in [70]. The sampling of the received signal makes it possible for a non-coherent demodulation in the BPSK signal by using only edge detection as described in [66]. We say the receiver is nearly digital because of the use of predominately digital components.

Figure 5.5 shows the block diagram of the receiver. At the receiver side, the entire signal is sampled. The sampling is essentially done using a comparator, sometimes also called a 1-bit analog to digital converter (ADC). This comparator is a dynamic comparator as in [127]. Its threshold, which is the input common-mode voltage, can be set by Vcntrl comparator as shown in Figure 5.5 (Set CM sub-block) and the sensitivity is found to be below 50 mV (in simulations). The comparator shares the same clock with the non-coherent digital demodulator. Figure 5.6 shows the circuit schematic of the 1-bit ADC which is based on [127]. After this 1-bit ADC stage, the resulting signal is non-coherently digitally demodulated. The non-coherent digital demodulator is the central part of the receiver, and it will be detailed next.

Figure 5.7 shows the schematic of the non-coherent-digital demodulator. The non-coherent digital demodulator detects if a '0' or a '1' was transmitted by detecting the type of edge it encounters in the digitized received modulated signal. Note that the digitized modulated signal has a falling edge for the '0' and a rising edge for the '1'. While detecting which type of edge is present, the sub-system must take care to avoid the transition points between carrier periods so that these are not detected as edge types. This will be explained next. The
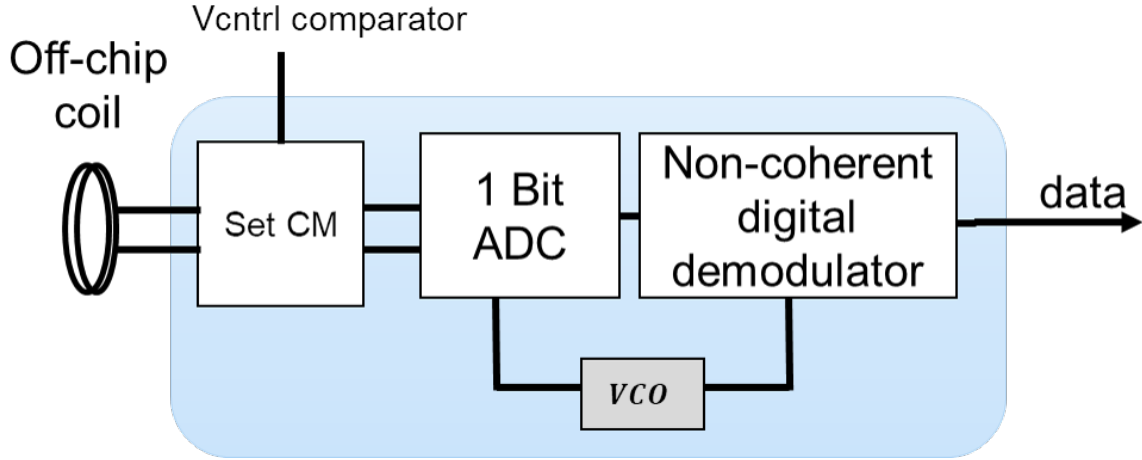
Figure 5.5: Schematic diagram of the BPSK receiver (set CM – set common-mode). Note: IC excludes the coil.
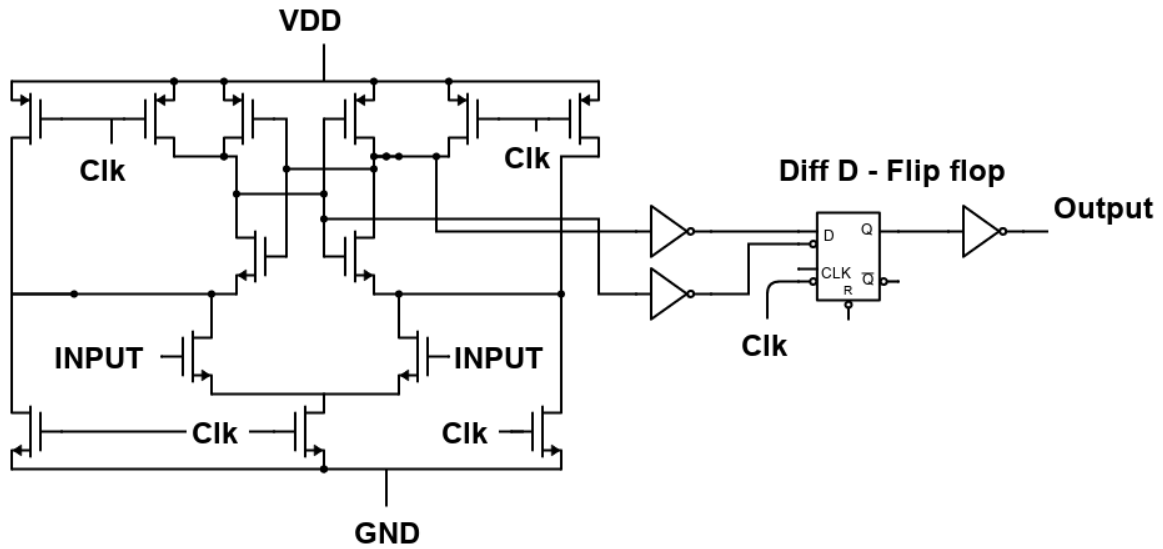
Figure 5.6: Schematic diagram of the 1-bit ADC.

sub-system comprises mainly of an edge detector, a reset generator, and an oscillator. A similar concept was presented in [66], but in our case, the data rate to carrier frequency ratio is not 100% due to practical bandwidth limitations and losses in inductive links. Inductive coils that are designed for transmission and reception create a bandwidth over which the BPSK signal is communicated. This is band-limited by design. Literature reports values for the data rate to carrier frequency ratio ranging from as low as 5% [38] up to 40% [47]. We aim to also be within this range as delivering sufficient data rate is the main priority and because the carrier frequency can be scaled appropriately.

The edge detector uses a rising edge D-type flip-flop and a falling edge D-type flip-flop to detect if an edge occurs and which type of edge it is, using an OR logic gate and an AND logic gate, respectively. These logic gates will take the outputs of the flip-flops as their input.
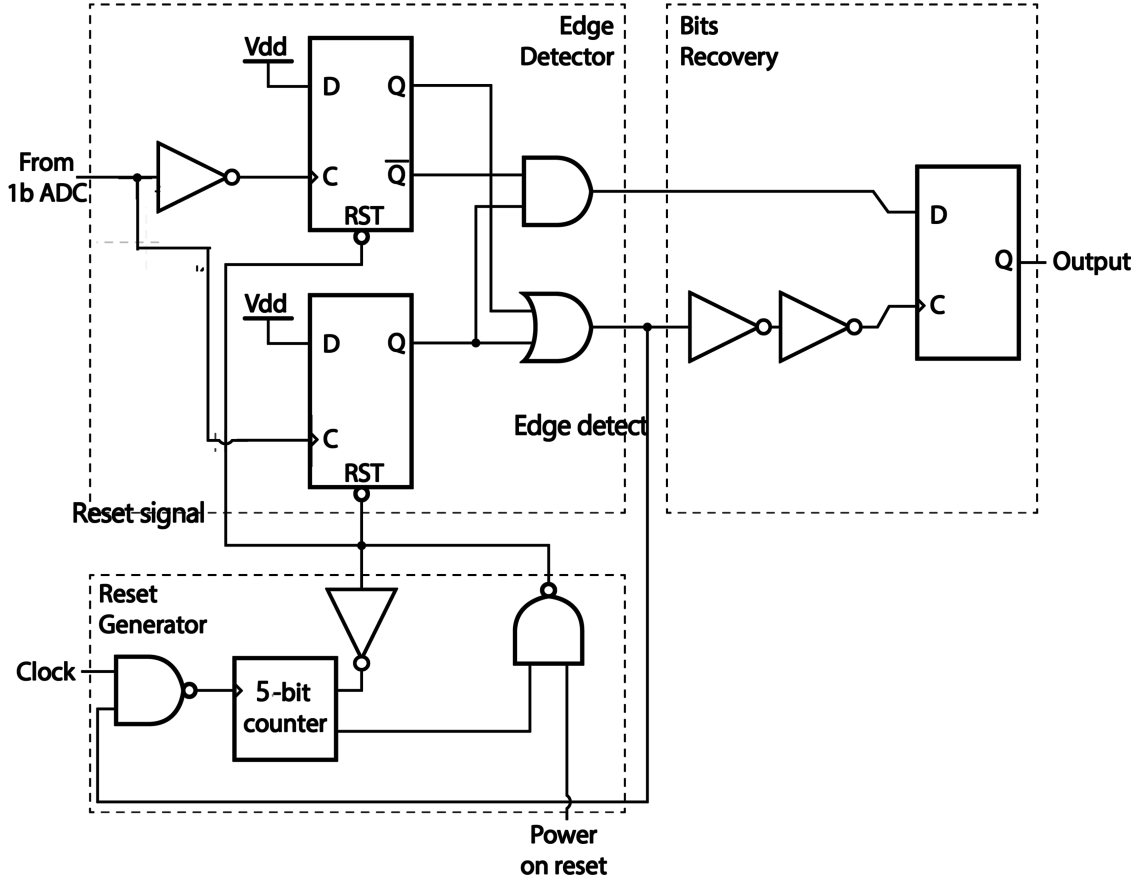
Figure 5.7: Schematic of non-coherent digital demodulator (a sub-block of Fig. 5.5).

The inputs of both flip-flops are a logical '1' while the received digitized modulated signal is fed as its clock input. This configuration yields the desired effect of edge detection in a power-efficient way. The asynchronous clear input of the flip-flops is connected to the reset generator. Asynchronous clearing implies that the flip-flops are cleared decoupled from clock ticks. This is done to reset the flip-flops to avoid detecting the transition point between carrier periods.

The role of the reset generator module is to provide a reset signal to reset the edge detector at a time after an edge detection at $t = 0$, between $t = 0.5T_{PSK}$ and $t = T_{PSK}$. Here, T_{PSK} is the period of the carrier frequency.To achieve this, it counts, using an asynchronous counter. We determine the frequency of the clock, which is essentially the frequency of the oscillator, as follows.

Let N be the count-up number $(0, 1, \ldots, N)$. The following inequalities must be satisfied. To reset after the transition point between carrier periods, we have

$$(N-1)T_{OSC} > 0.5T_{PSK}. \tag{5.1}$$

To ensure that there is no reset after the next edge, we set

$$NT_{OSC} < T_{PSK}. \tag{5.2}$$

Combining (5.1) and (5.2), we arrive at

$$\frac{1}{2(N-1)}T_{PSK} < T_{OSC} < \frac{1}{N}T_{PSK}. \tag{5.3}$$

Taking reciprocals, the range of the frequency of the oscillator to avoid transition between carrier symbols then results:

$$Nf_{PSK} < f_{OSC} < 2(N-1)f_{PSK}. \tag{5.4}$$

A low count-up number of N, for example $N = 3$, yields an oscillator frequency range of $3f_{PSK} < f_{OSC} < 4f_{PSK}$. This already strongly relaxes the jitter or quality factor requirement of the oscillator. Thus, a low-power current-controlled oscillator can be used. Figure 5.8 shows the layout of the receiver on IC. A count-up number of $N = 16$ was used to improve flexibility of adjusting timing range, which corresponds to the most-significant bit of the 5-bit counter in the reset generator.Similar to the IR-UWB transmitter, the oscillator used for clock is in the receiver is another 5-stage current-starved single-ended ring oscillator as in Figure 5.3.

5.4 Measurement Setup

5.4.1 Test IC

The IR-UWB transmitter and the BPSK receiver were fabricated on the same die; 1.66 mm by 1.66 mm of the CMOS 180 nm semiconductor technology process. It is a mature and robust technology which is important for medical applications. Figure 5.9 shows the silicon die. The active areas of the IR-UWB transmitter and BPSK receiver are 220 μm by 80 μm and 170 μm by 160 μm, respectively. Decoupling capacitors were placed to fill the empty area in the die and to improve the signal performance. The die was package in a Quad flat no leads package with 32 pins (QFN32), 5 mm by 5 mm. Care was taken to minimize the bond-wire distance for the IR-UWB transmitter by moving it closer to the package pins. This minimize high-frequency distortion. Bond wires have a typical inductance of about 1nH/mm. The typical values were taken into account in simulations. The measured result of the output of the IR-UWB, as seen in Figure 5.12, is not distorted. The package is already 5 mm by 5 mm, which indicates the maximum limit on the distance of the bond wires, which connects a 1.66 mm by 1.66 mm die within the package.

5.4.2 Demonstrator board

To test the chip, a printed circuit board (PCB) was fabricated and the packaged chip was mounted on the PCB. The picture inset in Figure 5.10 shows the manufactured PCB. The board is 84 mm by 95 mm. For alternative test paths and for circuit debugging purposes,
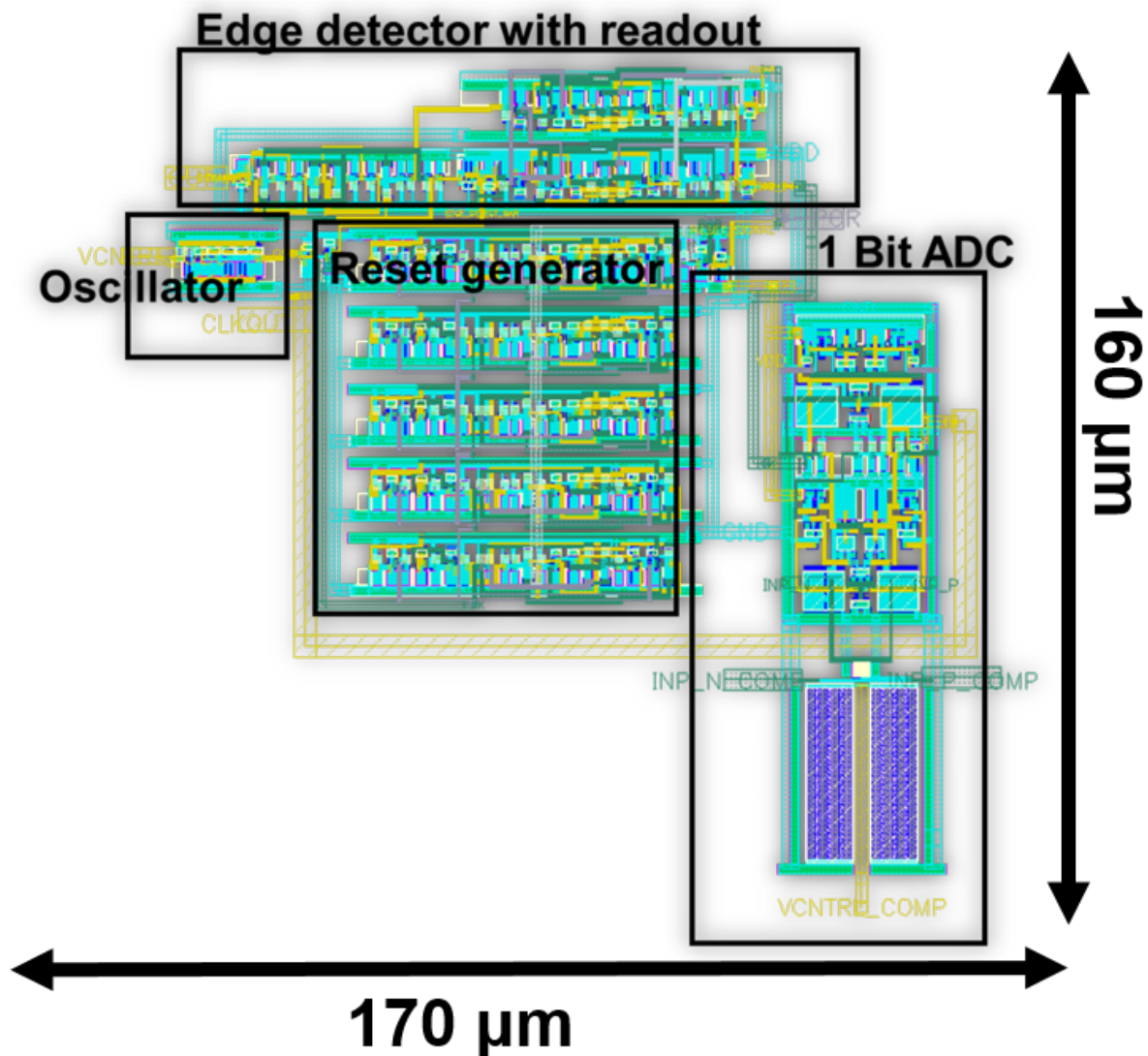
Figure 5.8: Layout of the BPSK receiver.

more SMA connectors were included on the PCB. Two possible pathways are made for current control: direct current supply and a potentiometer connected to the voltage supply. These controls are used for the oscillator of the BPSK receiver, the oscillator of the IR-UWB transmitter, and the pulse delay. The IR-UWB transmitter output SMA connector was placed very close to the chip as it is the highest frequency on the PCB.

5.4.3 Experimental test setup

Figure 5.10 shows the block diagram of experimental test setup for the IR-UWB transmitter. The IR-UWB transmitter was tested using the Analog Discovery 2 [140] to generate a bit-stream to be transmitted. Analog Discovery 2 is a 100MS/s USB oscilloscope, logic analyzer, variable power supply and multi-function instrument that allows users to measure, visualize,
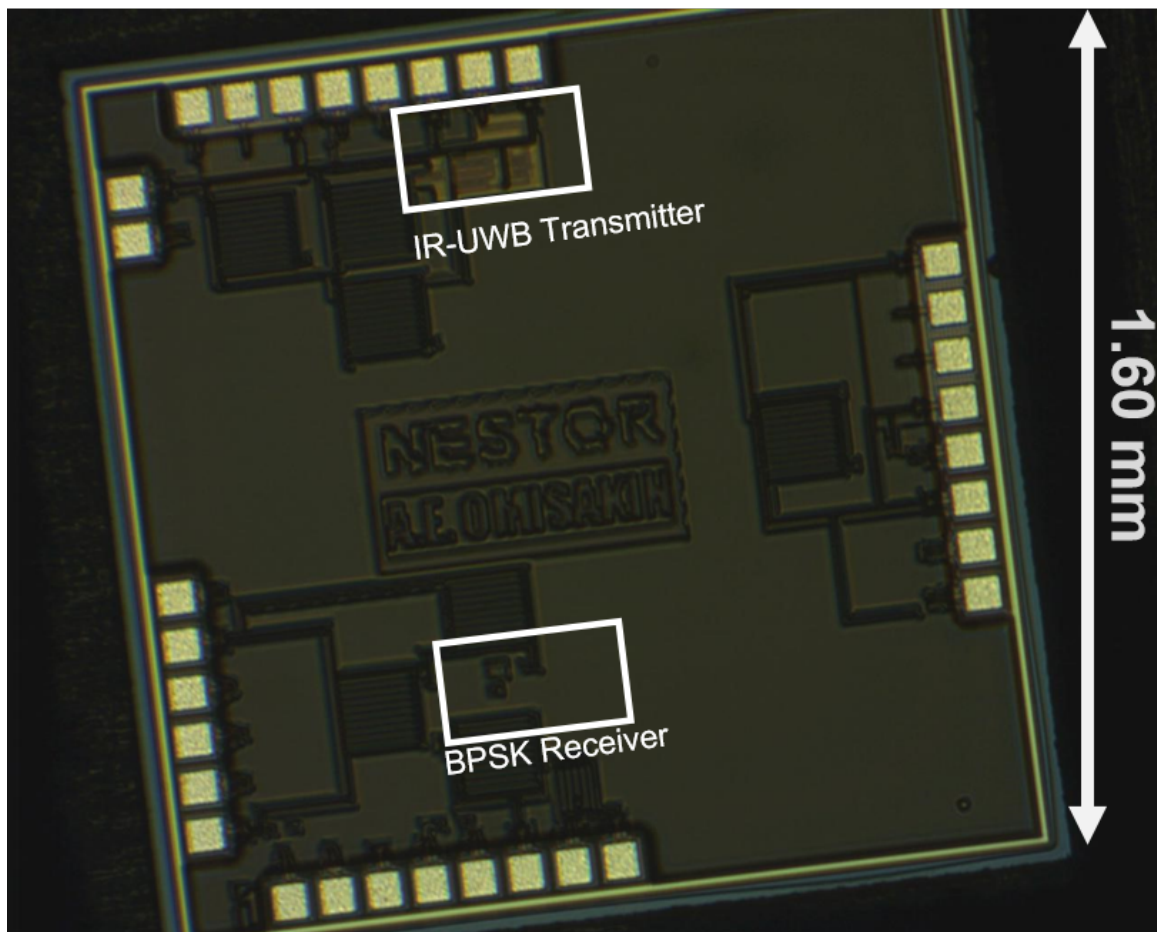
Figure 5.9: Micro-graph of the fabricated transceiver IC.

generate, record, and control mixed-signal circuits [140]. Current sources were used to control the oscillator and impulse generator. The LeCroy WaveMaster 830 Zi oscilloscope [141], was used to measure the output of the transmitter signal in time-domain waveform as well as its spectrum.

Figure 5.11 shows the block diagram of experimental test setup for the IR-UWB transmitter. The BPSK receiver was measured using the Analog Discovery 2 as pattern generator and as an oscilloscope for the low-frequency <100 MHz measurement. A voltage supply was used for powering the circuit and power-on-reset (POR). A current supply was used for oscillator control. Another voltage supply for control voltage for the comparator. A BPSK transmitter was used to generate the modulated signal on a 4 MHz carrier with a 1 Mbps data rate.
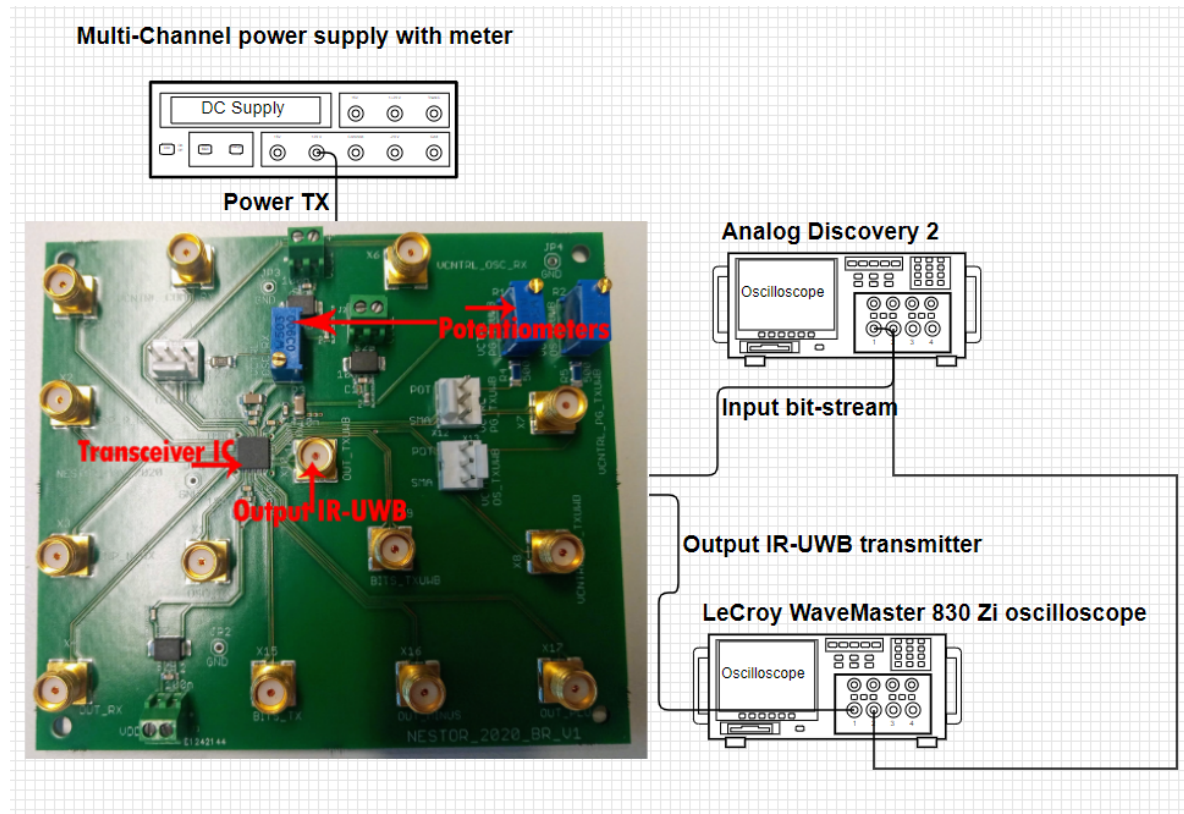
Figure 5.10: Block diagram of experimental test setup for the IR-UWB transmitter with the demonstrator board as picture, the rest of the setup as a diagram.

5.5 Results

In this section, we will show the relevant measurement results for the IC, for both the uplink and downlink subsystems. Furthermore, to show the performance of the subsystem in the context of the overall system requirements, link budgets for the two subsystems are also given.

5.5.1 IR-UWB Transmitter

IC measurement results

Figure 5.12 shows the transmitter output (bottom panel) on a bit-stream and shows the input 50 Mbps data stream from the Analog Discovery 2 acting as a pattern generator (top panel). The measured transmitted bits appear to be distorted due to the bandwidth limitation of the pattern generator. The distortion is also due to the interface where the input bit signal is tapped into the oscilloscope. Both distortion mechanisms do not influence actual performance because they are related to measurement imperfections only. A '1' logic level corresponds to no pulse on the output, while a '0' logic level corresponds to a pulse at the output. This demonstrates the on-off keying modulation. Although not depicted, the output voltage levels of the measured and simulated signals agree to within ±5%.
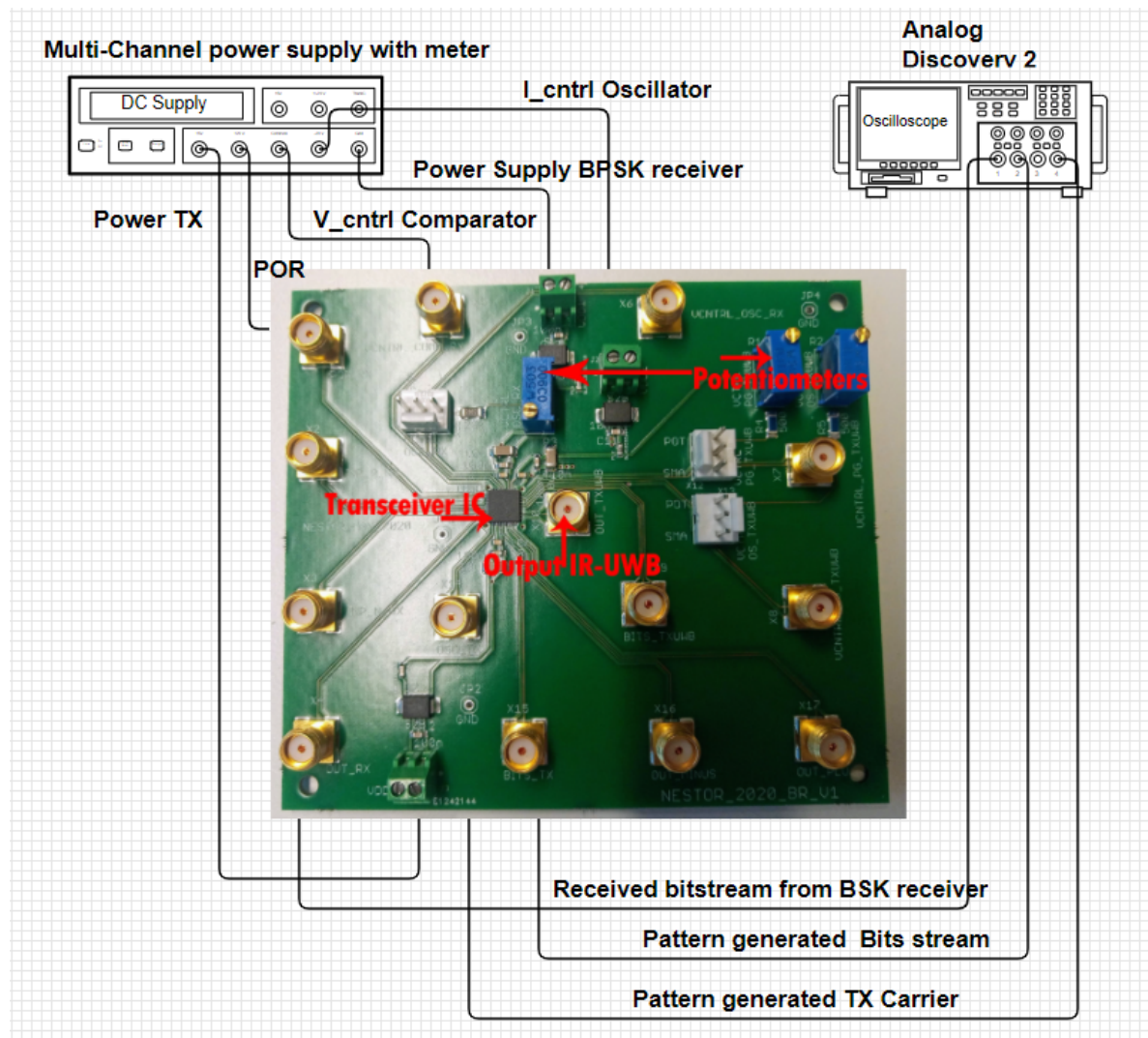
Figure 5.11: Block diagram of experimental test setup for the BPSK receiver.

Figure 5.13 shows the spectrum (FFT of the time signal) of the transmitter output and also with an external bandpass filter for the 3–5 GHz band. To show the additional effect of a bandpass filter, the VBFZ-3590-S+ from Mini-circuits USA, which is a bulky off-chip BPF is included in a measurement. The measured output spectrum falls below the FCC spectral mask limits. The transmitter waveform will further meet the IR-UWB standard in a full system scenario due to the skin attenuation.

Figure 5.14 shows the measured power consumption of the transmitter versus supply voltage. This is not the optimized result yet, to be able to compare with post-layout simulation. A 1 kΩ resistance from a potentiometer in series with the supply voltage was used to generate current for the oscillator's current control. Another 1 kΩ resistance from a potentiometer in series with the supply voltage was used to generate current for the impulse generator's current control. The measured and simulated power consumption agree to within ±5% and show the same trend. Figure 5.15 shows the corresponding simulated RF output power versus voltage
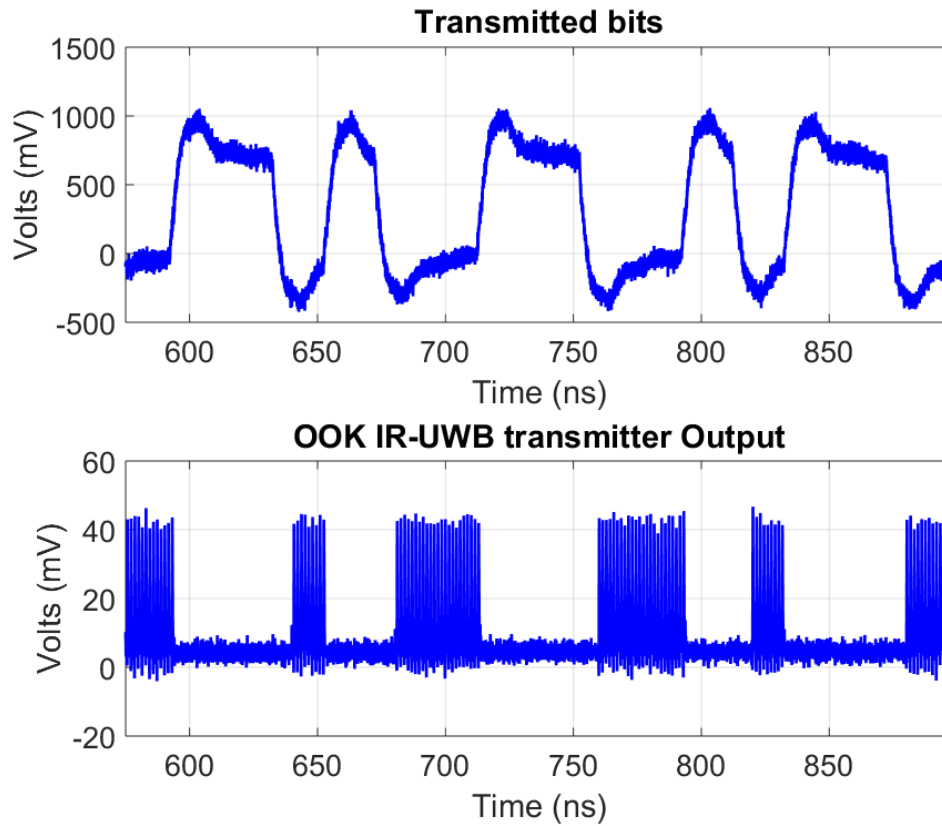
Figure 5.12: Measured time domain waveform of the IR-UWB transmitter at 50 Mbps bit stream, 1.3 V supply voltage. The top panel shows the input bit-stream. The bottom panel shows the output of the transmitter IC, which is the modulated data. The measurement has been done without antennas, for convenience.

supply for the unoptimized IR-UWB Transmitter at 50 Mbps data rate vs supply voltage, with fixed 1 kΩ resistance for current control. Finally, it can be observed from Figure 5.14 how the power consumption scales with the supply voltage to emphasize the predominantly digital architecture. This gives a promise for even better performance with more advanced CMOS technologies(such as 16 nm, 28 nm and 40 nm semiconductor processes), which operates at lower power supply voltages. The results in Figure 5.14 are for comparison only (simulation with measurement) and are not optimized yet. The optimization was done as follows.

The current from both current supplies (to control the oscillator and pulse generator) were adjusted to find optimal pulses per bit and power-output level. At 1.3 V supply voltage, using 100 μA and 10 μA for impulse generator and oscillator control respectively, the transmitter consumed 0.15–0.3 mW. The output waveform for this setting, already shown in Figure 5.12, has an RMS output power at the transmitter of -27 dBm. To obtain insight into what parts of the system consume most power, the simulated power breakdown of the transmitter is as follows: 75% is consumed in the pulse generator, 20% in the oscillator, and 5% in the modulator.
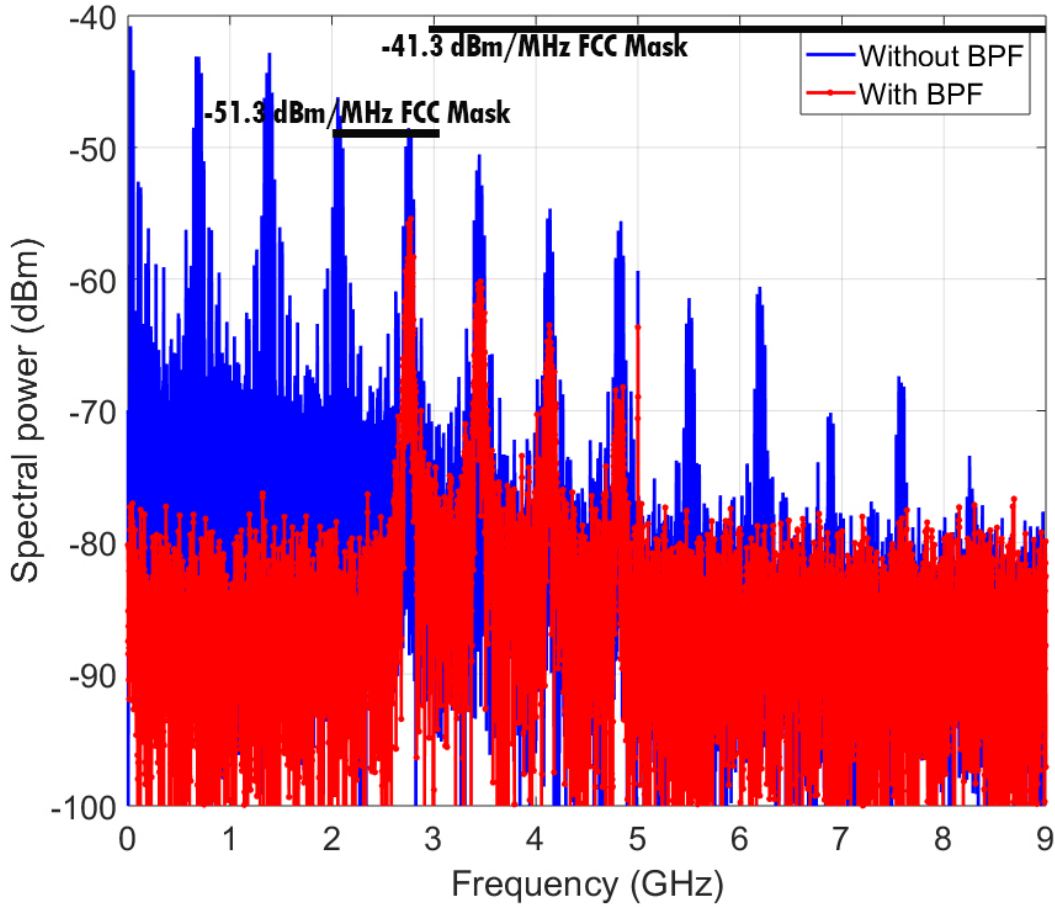
Figure 5.13: Spectrum of IR-UWB transmitter before and after bandpass filter at 1.3 V supply voltage. The FCC spectral mask is also shown.The spectrum is computed in the oscilloscope as the FFT of the measured time signal.

Link budget for uplink

It is important to analyze how the transmitter would fit in the complete chain, with a transmit/receive antenna pair, communication through 3–7 mm of skin, and an external receiver. For this purpose, we look at the link budget. Our IR-UWB transmitter delivers -27 dBm. The FCC regulations impose approximately a -9 dBm limit for a 2 GHz bandwidth in the UWB 3–10 GHz spectral mask of -41.3 dBm/MHz. For the -27 dBm output, the consumed power is 0.15–0.3 mW on 1.3 V supply. From simulation results reported in Section 4.5, the S21/link loss through 3 mm skin is found to be approximately 20 dB from electromagnetic simulations (the worst-case scenario at 7 mm skin thickness gives an extra 5 dB loss around the target 3-5 GHz band), which means that -47 dBm will reach the LNA of the external receiver or -52 dBm at 7 mm skin thickness. A received power level of -47 dBm reaching the LNA of the external side is feasible from the calculation above. A similar antenna skin interface design was shown in [123], which agrees with our simulated loss. The simulation was carried out
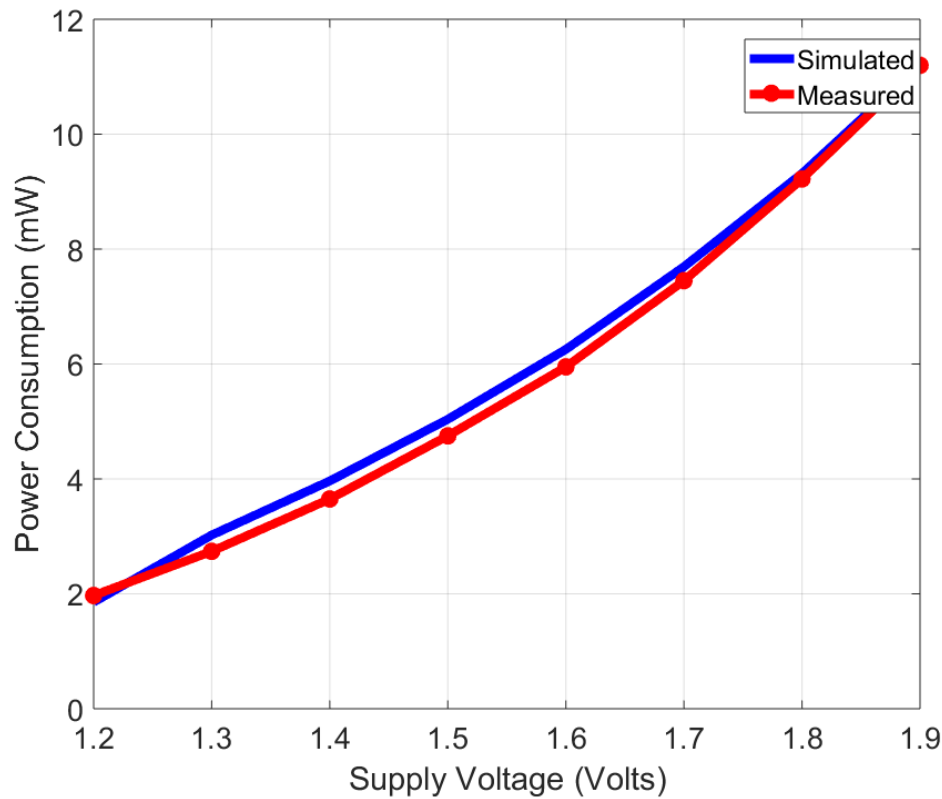
Figure 5.14: Power-consumption versus voltage supply for the unoptimized IR-UWB Transmitter at 50 Mbps data rate with fixed 1 kΩ resistance for current control.

in SIMULIA Studio Suite with antenna dimensions of 12 mm by 12 mm, thickness of 1 mm and insulator coating of 1 mm. Reported UWB receiver IC sensitivities are about -70 dBm to -65 dBm [110, 142, 143], which implies that we have an excess margin of 18–23 dB in closing the link for our application at 3–7 mm assuming a -70 dBm sensitivity of the external receiver. The excess margin is also considered sufficient to account for any mismatch at the antenna, under varying operating conditions. BER performance assumes that, at this sensitivity, the $< 10^{-3}$ target is reached [110, 143], otherwise the sensitivity is lowered, taking into account the 18–23 dB excess margin. In Chapter 4, Table 4.3 shows a link budget analysis from a theoretical perspective. The new link budget discussed here, based on state-of-the-art receivers, is also working despite the lower transmitter power because it should be possible to compensate with a better receiver sensitivity of state-of-the-art receivers. Finally, error detection and protection methods such as linear and convolutional codes could further increase the link margin which is already in excess.
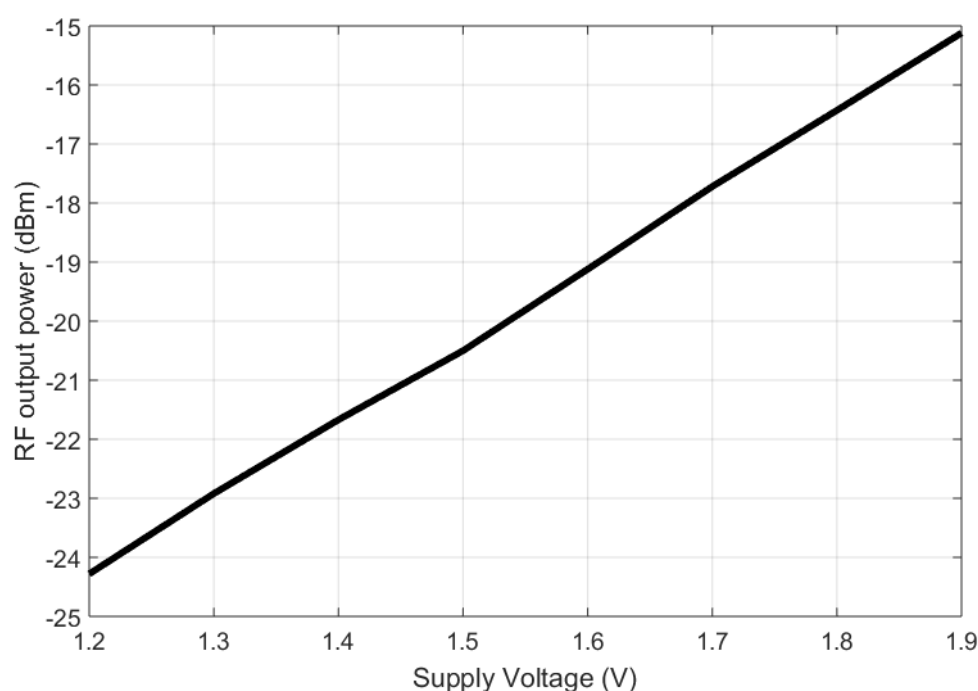
Figure 5.15: RF power versus voltage supply for the unoptimized IR-UWB Transmitter at 50 Mbps data rate vs supply voltage, with fixed 1 kΩ resistance for current control.

5.5.2   Non-coherent BPSK Receiver

IC measurement results

We connect directly without coils delivering 200 mV (this is realistic see Figure 3.10 and 3.11) modulated signal level into the receiver to examine its power consumption. Figure 5.16 shows the transmitted input bits and the recovered output for the receiver. These are recorded using the following settings: 1.3 V supply, a Vcntrl comparator setting of 0.6 V (the input common-mode voltage level), and a current source for oscillator controlled at 9.3 μA. To better illustrate internal signal of the receiver, Figure 5.17 shows the internal timing diagram from simulation, in which the demodulation of the received signal can be observed. The BPSK receiver consumed 0.2 mW while demodulating 1 Mbps data rate which was on a 4 MHz carrier. Figure 5.18 shows the measured power consumption of the receiver versus supply voltage at a 1 MHz repeated square wave cycle. The purpose of Figure 5.18 is to show the dependence of the power consumption on the carrier frequency and the supply voltage. A fixed repeated data square wave cycle of 1 MHz has two times the rate of a 1 Mbps bit-stream and should have a higher power consumption than the reported 0.2 mW at 1 Mbps. The decrease in power consumption as the supply voltage is lowered can be observed. The higher power consumption at a 5 MHz carrier demonstrates the predominately digital architecture. To indicate how much power parts of the system consume, the simulated power breakdown of the receiver is as follows: 35% is consumed in the 1-bit ADC, 35% in the digital demodulator, and 30% in the oscillator (clock).
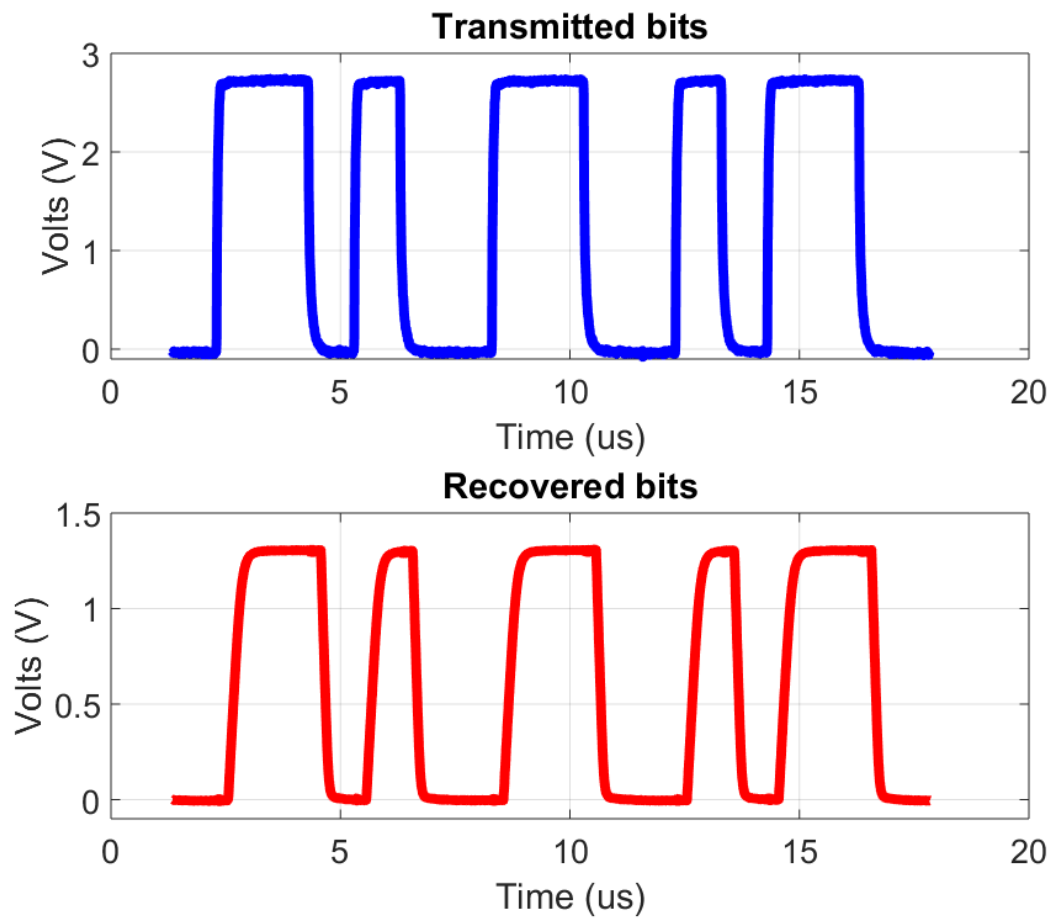
Figure 5.16: BPSK receiver recovered bits on 1 Mbps on 4 MHz carrier.

Link budget for downlink

Similarly to the uplink case, it is important to analyze in a link budget how the receiver would fit with the transmit/receive coils, while taking into account 3–7 mm transcutaneous communication with the transmitter on the outside. The BPSK receiver sensitivity is about 10–50 mV, determined by its comparator, the first stage. Furthermore, from our coil and transmitter simulation, a voltage level of 200–2500 mV could reach the receiver, depending on the coil design and distance. Typical coil sizes range from 10 mm to 50 mm in diameter depending on the size desired(e.g. depending on the position on the skull). The coupled inductive link from the coils acts as a low-power voltage transformer, boosting the voltage around the resonance frequency it is designed for. Typical coil diameters range from 10 mm to 50 mm [35,40,67], sometimes dictated by constraints on the size of the device. In addition, coil self-resonance frequency should be much higher than the operating frequency. These coils sizes facilitate a tolerable misalignment of several mm [90]. However, here we connect directly without coils to deliver 200 mV level into the receiver. From a sensitivity of 50 mV and a possible coil output of 200–2500 mV (this is realistic see Figure 3.10 and 3.11), the link
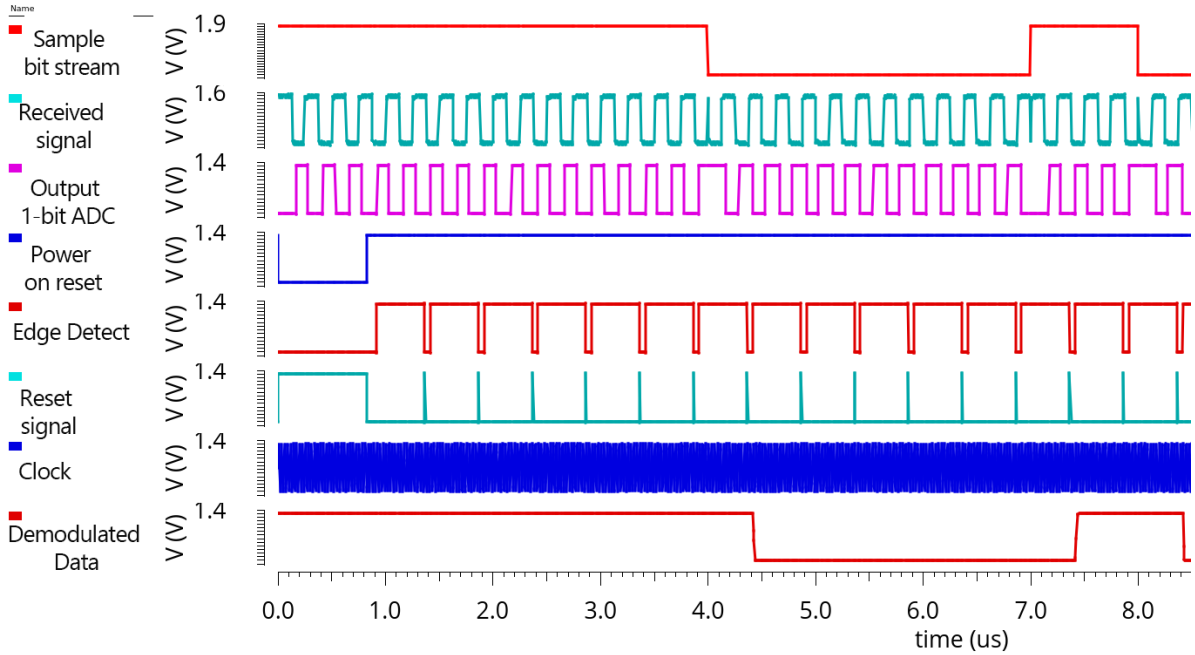
Figure 5.17: Simulated waveforms and timing diagram of the BPSK receiver.

will be closed with a 12–26 dB excess margin for downlink when the coupled coil response has the desired bandwidth of about 2 MHz as investigated in 3.3.3. BER performance assumes that the $<10^{-3}$ target is reached; otherwise, the receiver power level can be adjusted from the external transmitter and coil design, considering the 12–26 dB excess margin. Finally, also here, error detection and protection methods such as linear and convolutional codes could further increase the link margin.

5.6   Discussion

5.6.1   Comparison with the state of the art

Next, we benchmark our work with the state of the art in literature. Table 5.1 compares our implanted transmitter with recently published general transmitter ICs. In terms of data rate, our transmitter performs similar, or better. Power consumption is better than reported in [144–146] with the standard 180 nm CMOS technology available for IC design in our lab, but worse than reported in [130] and [131]. The latter two [130, 131], however, use 0-200 MHz and body coupled communication, respectively. In terms of frequency separation, the systems in [130] and [131] are not suitable to meet the co-existence requirements for our overall system application. This is mainly due to differences in applications and intended ranges. However this stresses the need for the low-power approach that we followed for the intracortical visual prosthesis.

Table 5.2 compares with other high data rate state-of-the-art medical implants. We
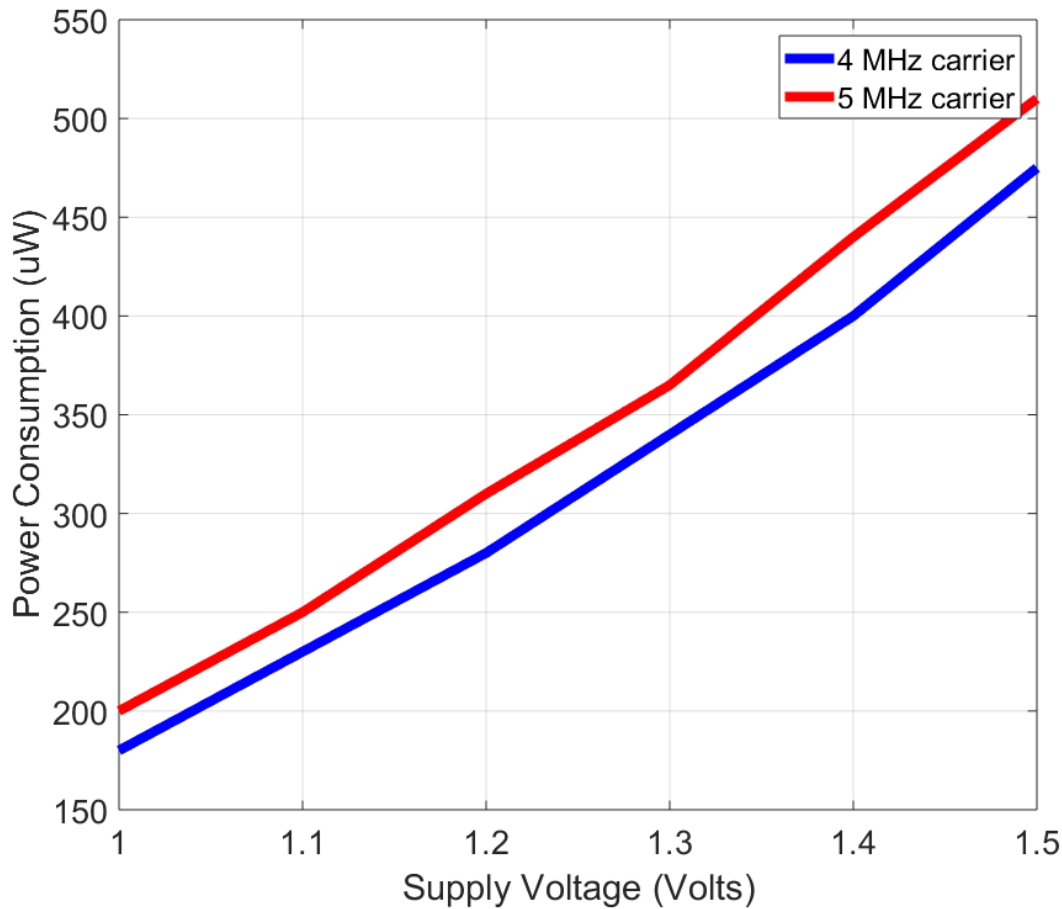
Figure 5.18: Measured power consumption of the receiver vs supply voltage at 1 MHz repeated data square wave cycle.

achieved a lower power consumption than most transmitters, and only slightly higher than reported in [135]. We have a lower data rate, however, which is still sufficient for our current application. This shows that our IR-UWB transmitter approach to use predominantly digital components and simple architecture is effective.In [132–134], a much lower data rate of < 30 Mbps was reported, which is not well-suited for our data rate requirements for the uplink. In [135], a higher data rate is shown at slightly lower power consumption, but the higher frequency band of 6.8-9 GHz reportedly used will face about 10 dB more attenuation through the skin tissue [123].

Table 5.3 compares the implanted receiver with recently published general receiver ICs. While we have a comparable data rate, we achieve much lower power consumption, except for the results reported in [130] which is not designed for skin tissue interaction, its frequency spectrum of 0-200 MHz may not co-exist in frequency band with other parts (possibly uplink and power transfer) of the system. This is due to our short-range and coupled-coil link, which relaxes the need for very sensitive receiver, which would have raised the power consumption.

Table 5.4 compares our receiver with other medical implants. Our receiver is of compa-

rable data rate with much lower power consumption. Our power consumption is better than in the first five columns and only worse than in [138]. However, the data rate of 0.01 Mbps reported in [138] is low and 20 times below the minimum data rate requirement of 0.2 Mbps for the intracortical visual prosthesis. This shows that our non-coherent digital demodulator is effective in low-power consumption compared to traditional receivers.

Table 5.1: Comparison with recently published IC-transmitters[1].

	[144]	[145]	[146]	[130]	[131]	This work
Data rate	1 Mbps	1 Mbps	11 Mbps	50 Mbps	30 Mbps	50 Mbps
Power cons.	3.7 mW	0.42 mW	4 mW	0.0237 mW	0.093 mW	**0.3 mW**
Frequency	2.4 GHz	3–5 GHz	401–428 MHz	0-200 MHz	Broadband	3–5 GHz
Modulation[1]	BLE	UWB	QPSK	TTC	HBC	UWB
Technology	28 nm	180 nm	130 nm	180 nm	180 nm	180 nm
Supply Volt	1 V	1.8 V	1 V	1 V	1 V	1.3 V

[1] Transmit power is not shown as data is mostly not available. Not relevant for the context as link-budget and external front-end compensate for power margin needs.
[2] HBC - Human body communication, TTC - Transmission time control.

Table 5.2: Comparison with other medical implant transmitters[1].

	[33]	[73]	[35]	[135]	[134]	[133]	This work
Data rate	100 Mbps	90 Mbps	500 Mbps	100 Mbps	30 Mbps	0.14 Mbps	50 Mbps
Power cons.	2.1 mW	1.6 mW	5.4 mW	0.26 mW	30 mW	0.085 mW	**0.3 mW**
Freq	Light	3–5 GHz	3–7 GHz	6.8-9 GHz	Sub-GHz	3-5 GHz	3–5 GHz
Mod	-	UWB	UWB	UWB	UWB	UWB	UWB
Tech	-	350 nm	130 nm	180 nm	350 nm	90 nm	180 nm
Supply Volt	-	1.65 V	1.8 V	1.5 V	3.3 V	-	1.3 V

[1] Transmit power is not shown as data is mostly not available. Not relevant for the context as link-budget and external front-end compensate for power margin needs.

Table 5.3: Comparison with recently published IC-receivers[1].

	[92]	[147]	[149]	[136]	[137]	[130]	This work
Data rate	1.3 Mbps	10 Mbps	11 Mbps	1 Mbps	1 Mbps	50 Mbps	1 Mbps
Power cons.	5.2 mW	3.2 mW	2.4 mW	0.9 mW	1.5 mW	0.041 mW	**0.2 mW**
Freq	18–23 MHz	40–120 MHz	2.4 GHz	2.4 GHz	2.4 GHz	0-200 MHz	4 MHz
Mod[2]	BPSK	Double FSK	BLE	BLE	BLE	DDM	BPSK
Tech	130 nm	180 nm	40 nm	28 nm	28 nm	180 nm	180 nm
Supply Volt	1.2 V	1 V	1 V	0.7 V	0.7 V	1 V	1.3 V

[1] Receiver sensitivity is not shown as data is mostly not available. Not relevant for the context as link-budget and external front-end compensate for power margin needs.
[2] DDM - Differential detection method, BLE- Bluetooth Low Energy.

Table 5.4: Comparison with other medical implant receivers[1].

	[79]	[38]	[67]	[83]	[139]	[138]	This work
Data rate	2 Mbps	100 kbps	13.56 Mbps	8 Mbps	2 Mbps	0.01 Mbps	1 Mbps
Power cons.	6.2 mW	-	2.2 mW	0.6 mW	1.1 mW	0.092 mW	**0.2 mW**
Frequency	20 MHz	5 MHz	13.56 MHz	902–928 MHz	20-120 MHz	413-419 MHz	4 MHz
Mod[2]	DPSK	-	PDM	FSK-ASK	P-OFDM	OOK	BPSK
Tech	350 nm	-	350 nm	130 nm	65 nm	180 nm	180 nm
Supply Volt	-	1 V	1 V	3 V	1.1 V	1.5 V	1.3 V

[1] Receiver sensitivity is not shown as data is mostly not available. Not relevant for the context as link-budget and external front-end compensate for power margin needs.

[2] P-OFDM - Pseudo orthogonal frequency-division multiplexing.

5.6.2 Medical safety

It is essential to investigate the system's safety concerning the SAR limits and tissue heating. In related work [75], a power of 1000 mW was transmitted, and SAR simulations were performed. This resulted in 10 g averaged SAR levels of a maximum of 1.92 W/kg. This value is below the specified 2 W/kg safety level. The wireless power transfer system for the visual cortex is foreseen to transfer up to 100 mW [152]. In addition, data communication through the skin will take place at a total power consumption of the IC below 1 mW. This concerns both downlink and uplink, with the inductive link and UWB antenna, respectively. With the low power levels for data communication, the coils and antennas will only transmit a fraction of that in [75], and the transmission is therefore considered to be far below the SAR limit.

The implanted transceiver can also dissipate power, causing the tissue directly surrounding it to heat up. The maximum temperature increase in the cortex has to be smaller than 1 °C [88, 89], which corresponds to a maximum power density of 0.8 mW/mm^2 of exposed tissue area [72, 88, 89]. Our measured implanted transceiver IC consumes 0.5 mW in a 25 mm^2 QFN package, which brings the power density to 0.02 mW/mm^2, which is well below the safety limit. In [151], research into electromagnetic and thermal effects on IR-UWB on the human head was reported in the 3.5-4.5 GHz frequency band. This work also confirmed that the power levels for our IC are well within the control of thermal regulatory mechanisms of the human body.

5.7 Conclusion

A sub-milliwatt transceiver IC for the implant side of an intracortical visual prosthesis is designed, fabricated and measured. It delivers 1 Mbps for the downlink (for stimulation) and 50 Mbps for the uplink (for recording), using a non-coherent BPSK demodulator and an IR-UWB transmitter, respectively. Its predominately digital components and adjustability lead to the low power consumption of 0.2 mW for the BPSK receiver and 0.3 mW for the IR-UWB transmitter at 1.3 V supply on 180 nm CMOS technology. Based on our transceiver IC in the implant, the system link budget analysis for both uplink and downlink show achievable figures: there is 18–23 dB excess margin for uplink, and 12–26 dB for downlink. These figures

show that the link can be closed with an excess margin for the antenna/coil pair to communicate through 3–7 mm skin, which is the transcutaneous interface between the implant side and outer side, while achieving good BER performance as a result of closing the link with excess margin.

In the future, should it be required that power consumption is even further reduced, scaling to more advanced processes that use lower supply voltages will be a solution due to the predominately digital architecture. With the current IC satisfying the requirements for the system, the next step would be to consider the integrated system, including both wireless power transfer and data communication and fabricated coils and antennas. This will allow for complete characterization of the system and the performance of all components and the interplay between them in terms of co-existence and robustness.

Conclusions and Recommendations

6.1 Conclusions

An intracortical visual prosthesis is vital in giving blind patients some form of rudimentary vision. Amongst others, the required technology involves an external camera, pocket processor, and a number of electrode arrays (Utah arrays) to be implanted on the visual cortex. In addition, wireless communication and wireless power transfer is required between the implanted electrode arrays with their implanted electronics and the outside world. In our work, we focused on investigating communication techniques that fit the uplink and the downlink systems requirements, carrying out system-level feasibility studies on the proposed option, miniaturizing the implanted side's core parts, and keeping the overall solution low power. The system will enable free movement and will avoid infections since transcutaneous wires will be eliminated.

The wireless system layout we proposed was based on placing the central transceiver beneath the skin, with the electrode arrays tethered to it. This results in a scalable solution because it avoids multiple transceivers, and it avoids excessive attenuation or path loss to deeper placed devices, which would require communication through the skull. However, the main challenge during operation is the possible micro-motion of the implanted connecting wires, which can be partly alleviated with better packaging and implantation using slack wires to mitigate mechanical stress.

Various generic communications techniques related to medical systems were discussed in Chapter 2. Based on the demand for low-power, as well as high data rates on the implanted side, key options were selected for the receiver for the downlink part and for the transmitter for the uplink part. For the downlink, BPSK communication with an inductive link was selected. Its potential for a digital receiver with bandpass sampling and the well-known reliability of BPSK modulation make it a viable option. With the required data rate of 200 kbps for downlink, the BPSK system is a feasible option, showing clear potential of reaching the data rate needed at a power consumption of less than ten mW.

For uplink, IR-UWB with OOK modulation was selected for the required uplink data rate of 23 Mbps. Suitability is based on its low-power transmitter architecture, its very high data rate potential due to its broad spectrum bandwidth, and the low external interference. IR-UWB's known weakness of short range, due to the FCC restriction on transmit power, does not hamper the short-range transcutaneous communication link. Antenna sizing and receiver design is challenging but can be compromised due to potential excess link margin for the context of our application. As a result of this, IR-UWB is a feasible option.

The proposed communication system for downlink was analyzed in detail and designed in Chapter 3. A BPSK communication system with an inductive link was presented, featuring a unique non-coherent receiver. The receiver is unique in that it uses predominately digital components and has low-power potential. It was shown that its power consumption could be further reduced by skipping redundant bits arising from bandpass sampling of the received signal by adjusting the clock frequency. The inductive link that involves the transmit coil, receive coil and separation distance was analyzed and designed. When both transmit and receive coil are matched to resonate at the same frequency under moderate coupling, the coupled link creates a 'well'-shaped transmission response, providing sufficient bandwidth for reliable BPSK communication. The experimental demonstrator developed is a scaled-down version of the design, demonstrating a 1 MHz carrier frequency and a data rate of 125 kbps. The demonstrator is a good representation of the scaled-up version because the frequency characteristics in the 1–12 MHz band remain the same. The experimental demonstration provides proof of principle for a future system that consumes under one milliwatt at the receiver side in an integrated circuit (IC) simulation. Due to its digital architecture, the system is easily adjustable to an ISM frequency band, with its power consumption scaling linearly with the carrier frequency. The demonstrator uses off-the-shelf coils, which already gave sufficient bandwidth.

In Chapter 4, the selected uplink communication system was investigated. For the intra-cortical visual prosthesis, IR-UWB with OOK modulation was chosen for low power consumption, and the 3–5 GHz band to avoid excessive signal attenuation through the skin. Preliminary integrated circuit simulation for the transmitter at the implant side showed low-power and high data rate potential. A proof-of-principle external receiver was investigated. The data rate of 33 Mbps demonstrated by the proof-of-principle external receiver already assures that a future receiver IC version will easily meet the required data rate of 23 Mbps for the uplink. The electromagnetic simulation of the transmission (path) loss was carried out using co-planar fed planar monopole designed as transmit and receive antennas with the body tissue environment, mimicking 3–7 mm transcutaneous communication. The transmission (path) loss or signal attenuation is found to be in the range of 20–30 dB, which renders the link feasible for use. The return loss of the antennas is not yet optimal, but this first design effort for the 3–5 GHz band is already promising. The return loss can be improved in further iterations, for instance, by exploring more shapes and dimensions for the monopole radiator. From the link budget analysis, while taking into account the thermal noise bandwidth, the maximum allowable transmit power by the FCC, the BER, and the link path loss, the system is shown to

have 6 dB excess margin, proving the feasibility of the proposed solution.

In Chapter 5, we have focused on the miniaturization of the core parts on the implant side of the bi-directional communication system. This gives a closer look at the future reality on the demonstration of low power consumption and sufficient data rate capability. Therefore, a transceiver IC for the implant side of an intracortical visual prosthesis has been designed, fabricated and measured. The design has been done in 180 nm CMOS technology, for low production cost and as the fundamental step in evaluating performance. Measurements on the IC show promising results. The OOK IR-UWB Transmitter in the IC delivered 50 Mbps for the uplink, consuming 0.3 mW at 1.3 V supply. The BPSK receiver for the downlink delivered 1 Mbps consuming 0.2 mW. The drastic reduction in power consumption as the operating supply voltage was lowered infers its predominately digital components. With this IC validation, it can be concluded that the implant side is miniaturized (core electronics in 5 mm by 5 mm chip package excluding antenna/coil), low-power (under one milliwatt), and delivers the required data rate for uplink and downlink.

Based on our transceiver IC in the implant, the system link budget analysis for both uplink and downlink shows promising figures: 18–23 dB excess margin for uplink, and 12–26 dB for downlink. The large excess margin can be used for a more robust system by ensuring even lower bit error rate and by providing the IC design of the future external side of the system more design margin. The excess margin also gives sufficient design freedom to close the link with an antenna/coil pair to communicate through 3–7 mm skin. The implant-side transceiver IC demonstrates that there is a clear path to a compact, low-power, high data rate wireless-enabled visual prosthesis at both circuit and system level.

6.2 Recommendations

Based on the work presented in this thesis, several recommendations can be made. In Chapter 3, the downlink system using the BPSK communication system was designed with an inductive link in mind. A low-power receiver for the implant side was demonstrated on a scaled-down version with commercial off-the-shelf coils. Custom coil design, meeting desired specifications on size, self-resonant frequency, and inductance is an area for further research and optimization. For instance, coils without ferrite backing, or more compact coils ($<$ 30 mm) with high self-resonance frequency ($\gg$ 12 MHz). In addition, to bring the technology further to implementation in humans, transmit/receive coil fabrication, packaging for biocompatibility, and alignment is to be considered.

The uplink using IR-UWB was designed in chapter 4, with its link budget and electromagnetic simulation of the transcutaneous interface demonstrating its feasibility. Improved antenna design with better return loss, realization of the antenna with standard and biocompatible materials is recommended. Furthermore, external receiver IC fabrication and packaging for biocompatibility would need to be addressed in bringing the technology further to implementation in humans.

The system's heart, which is the implanted transceiver, was miniaturized and fabricated on 180 nm CMOS in Chapter 5. It is recommended to scale to more advanced processes that use lower supply voltages to further reduce power consumption due to the predominately digital architecture. Furthermore, in bringing the technology further to implementation in humans, it is recommended, and required even with the medical device regulations, to perform a complete system validation with actual (or phantom) body tissues to validate the integration of the system into a functional intracortical prosthesis after complete system optimization. A functional intracortical prosthesis will include wireless powering. The wireless power transfer sub-system will need to be combined with our data transfer system by the frequency band, multiplexing in the time domain, physical separation, or a combination, and thoroughly tested for robustness and co-existence. In addition, integrating the electrode arrays with the wireless system is also needed. This integration will involve tethered wires as the proposed wireless system layout places the central transceiver beneath the skin. Tethered to the transceiver are the electrode arrays. After successfully integrating the wireless powering and electrodes, a recommendation is to re-validate the system to ensure proper integration.

6.3 Outlook

Looking beyond an intracortical visual prosthesis, the investigation leading up to BPSK communication with inductive links for downlink and IR-UWB communication for the uplink could find some relevance for other body communication applications as well, like for instance hearing implants [153]. For instance, our transcutaneous approach through 3–7 mm of skin could form a suitable starting point for the contexts of implants for hearing, epilepsy, and paralysis, each with specific demands [154]. Our data rates of 1 Mbps for stimulation and 50 Mbps for recording purposes could be tailored to meet such demands by extending tethered wires and multiplexing the recording on stimulation information from the electrodes pertaining to the individual applications.

While our work's current context is at 1024 electrodes, futuristic projects such as the IN-TENSE project could desire up to 60,000 electrodes [154]. Such a high electrode count could require re-thinking the whole wireless system design. However, our early investigations in Chapter 2 may give some pointers as to what routes may be feasible. One area that calls for concern is the number of wires involved if our tethered wires to an implanted receiver beneath the skin approach taken in this thesis will be feasible? The large amount of tethered wires required may lead to a more distributed approach, as in Figure 1.2 with multiple transceivers. However, our proposed BPSK communication with inductive link and the IR-UWB communication for each independent transceiver could still be very relevant because of their high data rate capability. The advancement of wireless enablement of ultra-high-density electrode counts implants bi-directionally communicating presents new exciting research opportunites [37].

Data compression for neural recording

## A.1 Derivation of Data compression for neural recording

In this appendix, the data rate for neural recording with data compression defined for the NESTOR project is estimated.

Some considerations that relate to the data rate and data compression are the following:

1. As point of departure we assume that we want to transmit the essential information for 1000 channels and, in addition, transmit full bandwidth information (25 kHz) for a few channels (e.g. 10 channels) so that we can check data quality. The condensed but essential information (CEI), (see Figure A.1) can be captured by a) LFP, local field potential, sampled at 500 Hz at 12 bit resolution b) SUA, single unit activity, typically detected as threshold crossings, sampled with 1kHz, 1 bit resolution. c) MUAE, the envelope of the bandpass filtered signal, sampled at 1 kHz with 12 bit resolution The resulting compression results in a data stream of 19 kbit/s per CEI channel. For 1000 channels it amounts to 19 Mbit/s.

   For the few channels for which full bandwidth information is transmitted, the resolution is 16bit, 25 kHz, which amounts to 0.4 Mbit/s. If we transmit information about 10 selected channels this amounts to 4 Mbit/s.

2. Channels for recording the CEI and full bandwidth can be flexibly selected out of 106 recording channels. The channels for stimulation can be flexibly selected out of 105 stimulation channels.

3. Detecting single units requires determination of a threshold. It would be useful if this threshold could be set by the controller, i.e. from outside the patient.

4. A minimal amount of information transfer is required for selecting the channels for CEI and full bandwidth and also for setting the thresholds for detecting spikes at the CEI channels.
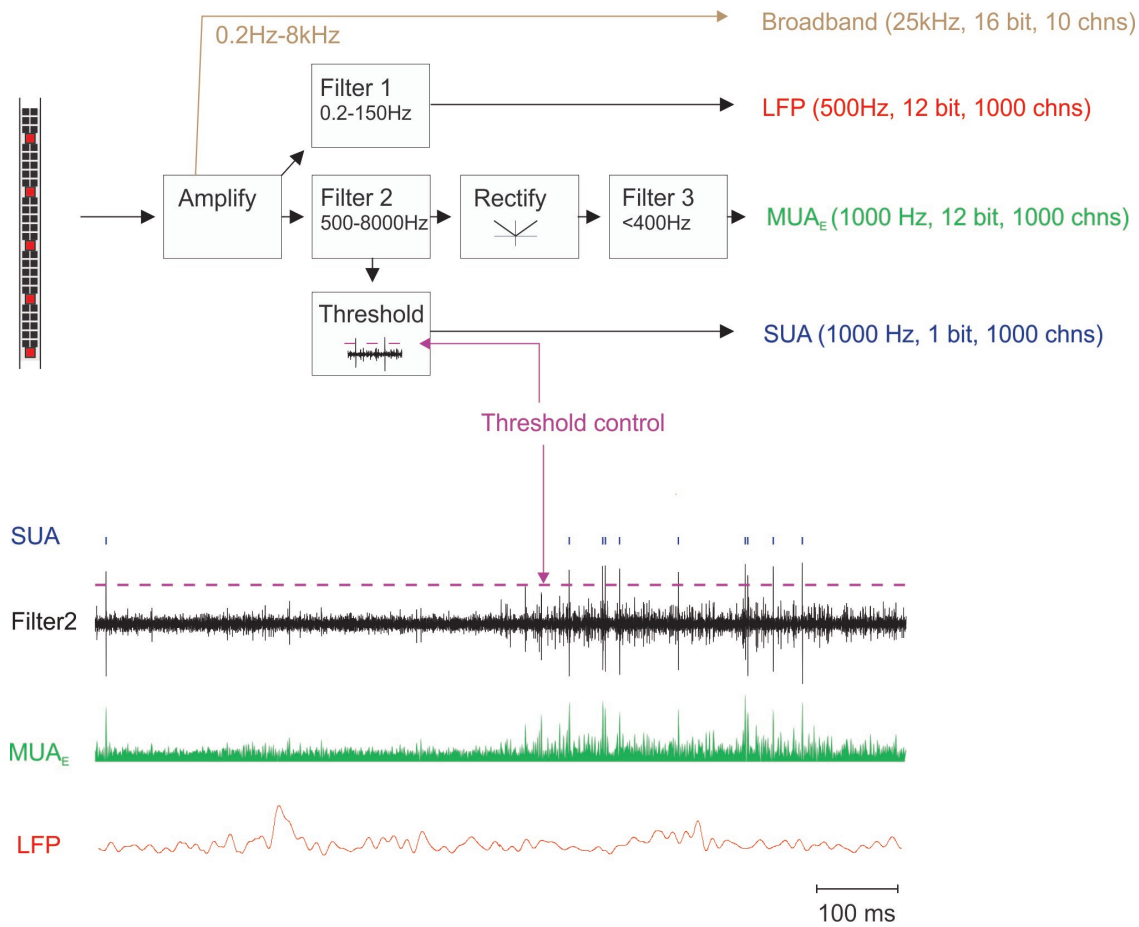
Figure A.1: Condensed, but essential information (CEI). The signal from 1000 selected electrodes is first amplified, then filtered between 0.2–150Hz (Filter 1) to measure LFP and between 500–8000Hz (Filter 2) for detecting the band that contains information about neuronal firing. The output of filter 2 is used for the detection of spikes with a threshold, and it is also rectified (negative becomes positive) and then low-pass filtered (<400Hz) to produce MUAE, the envelope of the signal. At the same time, we will transmit high bandwidth information from 10 channels, which will allow us to compare this signal to the compressed data. These channels will allow us to check signal and compression quality.

Based on the abovementioned considerations, the total bandwidth required for 1000 read is estimated at 23 Mbit/s: 19 Mbit/s for 1000 CEI read channels, and 4 Mbit/s for 10 full bandwidth read channels.

List of Publications

Journal publications

[P1] **A. E. Omisakin**, R. M. C. Mestrom, M. J. Bentum, "Low-Power Wireless Data Transfer System for Stimulation in an Intracortical Visual Prosthesis," in *Sensors, Special Issue: Implantable Systems for Biomedical Applications*, vol. 21, no. 3, pp. 735-751, January 2021.

[P2] **A. E. Omisakin**, R. M. C. Mestrom, G. Radulov, M. J. Bentum, "Sub-milliwatt Transceiver IC for transcutaneous communication of an Intracortical Visual Prosthesis," in *Electronics, Special Issue: Analog/RF Integrated Circuits and System Design for Neural Interface Applications,* vol. 11, no. 1, Published: 22 December 2021.

Conference publications

[P3] **A. E. Omisakin**, R. M. C. Mestrom, M. J. Bentum, "Low-Power Communication for an Implanted Intracortical Visual Prosthesis," *13th IEEE European Conference on Antennas and Propagation EuCAP*, Krakow, Poland, 2019, pp. 1-4.

[P4] **A. E. Omisakin**, R. M. C. Mestrom, M. J. Bentum, "Low-Power BPSK Inductive Data Link for an Implanted Intracortical Visual Prosthesis," *41st IEEE Conference on Engineering in Medicine and Biology EMBC*, Berlin, Germany, 2019, pp. 1-5.

[P5] **A. E. Omisakin**, R. M. C. Mestrom, M. J. Bentum, "System Design of a Low-power Wireless Link for Neural Recording in a Visual Prosthesis," *IEEE AFRICON*, Accra, Ghana, 2019, pp. 1-4.

Other publications

[P6] **A. E. Omisakin**, R. M. C. Mestrom, M. J. Bentum, "Bi-directional Wireless Communication for an Implanted Cortical Visual Prosthesis," *IEEE Eindhoven poster contest 2017*, Eindhoven, Netherlands, 2017, poster presented.

[P7] **A. E. Omisakin**, R. M. C. Mestrom, M. J. Bentum, "Bi-directional Wireless Data transfer for an Implanted Cortical Visual Prosthesis," *URSI Beneleux 2018*, Delft, Netherlands, January 2018, poster presented.

Bibliography

[1] G. S. Brindley, P. E. Donaldson, M. A. Falconer, and D. N. Rushton, "The extent of the region of occipital cortex that when stimulated gives phosphenes fixed in the visual field," *The Journal of physiology*, 225(2), pp. 57-58. 1972.

[2] W. H. Dobelle and M. G. Mladejovsky, "Phosphenes produced by electrical stimulation of human occipital cortex, and their application to the development of a prosthesis for the blind," *The Journal of physiology*, 243(2), 553-576. 1974.

[3] G. S. Brindley, "Effects of electrical stimulation of the visual cortex," *Human neurobiology*, 1(4), 281-283. 1982.

[4] J. Moss, T. Ryder, T. Z. Aziz, M. B. Graeber, P. G. Bain, "Electron microscopy of tissue adherent to explanted electrodes in dystonia and Parkinson's disease," *Brain*, vol. 127, no. 12, pp. 2755–2763, 2004.

[5] D. G. Sayenko, C. Angeli, S. J. Harkema, V. R. Edgerton, and Y. P. Gerasimenko, "Neuromodulation of evoked muscle potentials induced by epidural spinal-cord stimulation in paralyzed individuals," *Journal of Neurophysiology* , vol. 111, no. 5, pp. 1088–1099, 2014.

[6] J. B. Zimmermann and A. Jackson, "Closed-loop control of spinal cord stimulation to restore hand function after paralysis," *Frontiers in Neuroscience*, vol. 8, p. 87, 2014.

[7] E. M. Maynard, "Visual prostheses," *Annual review of biomedical engineering*, vol. 3, pp. 145-168, 2001.

[8] R. R. A. Bourne, S. R. Flaxman, T. Braithwaite, M. V. Cicinelli, A. Das, J. B. Jonas, J. Keeffe, J. H. Kempen, J. Leasher, *et al*. "Magnitude, temporal trends, and projections of the global prevalence of blindness and distance and near vision impairment: A systematic review and meta-analysis". *Lancet Glob. Health* , 5, pp. 888-897, 2017.

[9] D. Pascolini and S. P. Mariotti, "Global estimates of visual impairment: 2010," *British Journal of Ophthalmology*, vol. 96, no. 5, pp. 614-618, 2012. [Online]. Available: http://bjo.bmj.com/content/96/5/614

[10] G. G. Celesia and M. G. Brigell "Cortical visual processing," *Electroencephalography and clinical neurophysiology* . Supplement, 50,pp. 202-209,1999.

[11] W. H. Dobelle, D. O. Quest, J. L. Antunes, T. S. Roberts, and J. P. Girvin, "Artificial vision for the blind by electrical stimulation of the visual cortex," *Neurosurgery*, 1979 Oct;5(4):521-7.

[12] W. H. Dobelle, M. G. Mladejovsky, J. R. Evans, T. S. Roberts, and J. P. Girvin," "Braille" reading by a blind volunteer by visual cortex stimulation," 1976, *Nature* 259:111–112.

[13] N. S. Peachey and A. Y. Chow, "Subretinal implantation of semiconductor-based photodiodes: Progress and challenges", *Journal of Rehabilitation Research and Development*, vol. 36, no. 4, Oct. 1999.

[14] E. Zrenner and A. Stett, "Can subretinal microphotodiodes successfully replace degenerated photoreceptors?," *Vision Research*, vol. 39, no. 15, pp. 2555-2567, Jul. 1999.

[15] J. Wyatt and J. Rizzo, "Ocular implants for the blind," *in IEEE Spectrum*, vol. 33, no. 5, pp. 47-53, May 1996.

[16] R. J. Greenberg, T. J. Velte, M. S. Humayun, G. N. Scarlatis, and E. J. de Juan, "A computational model of electrical stimulation of the retinal ganglion cell.," *IEEE Transanctions on Biomedical Engineering*, vol. 46, no. 5, pp. 505-514, May 1999.

[17] J. D. Weiland, M. S. Humayun, G. Dagnelie, E. J. de Juan, R. J. Greenberg, and N. T. Iliff, "Understanding the origin of visual percepts elicited by electrical stimulation of the human retina.," *Graefe's Arch. Clin. Exp. Ophthalmol. = Albr. von Graefes Arch. fur Klin. und Exp. Ophthalmol.*, vol. 237, no. 12, pp. 1007-1013, Dec. 1999.

[18] G. G. Naples, J. T. Mortimer, A. Scheiner and J. D. Sweeney, "A spiral nerve cuff electrode for peripheral nerve stimulation," *IEEE Transactions on Biomedical Engineering*, vol. 35, no. 11, pp. 905-916, 1988.

[19] J. S. Walterm, P.Griffith, J.Sweeney, V. Scarpine, M. Bidnar, J. McLane and C. Robinson, "Multielectrode nerve cuff stimulation of the median nerve produces selective movements in a raccoon animal model.,"*Journal of Spinal Cord Medicine*, vol. 20, no. 2, pp. 233–243, 1997.

[20] S. Parrini, J. Delbeke, V. Legat, and C. Veraart, "Modelling analysis of human optic nerve fibre excitation based on experimental data," *Medical and Biological Engineering and Computing volume*, vol. 38, no. 4, pp. 454-464, Jul. 2000.

[21] C. Veraart, C. Raftopoulos, J. T. Mortimer, J. Delbeke, D. Pins, *et al.* ,"Visual sensations produced by optic nerve stimulation using an implanted self-sizing spiral cuff electrode.," *Brain Research*, vol. 813, no. 1, pp. 181-186, Nov. 1998.

[22] D. D. Zhou, J. D. Dorn and R. J. Greenberg, "The Argus® II retinal prosthesis system: An overview," *IEEE International Conference on Multimedia and Expo Workshops (ICMEW)*, 2013, pp. 1-6.

[23] J. D. Dorn, "Progress with the Orion Cortical Visual Prosthesis," *42nd Annual International Conference of the IEEE Engineering in Medicine and Biology Society (EMBC)*,EMBS Virtual Academy, 20-24 July 2020.

[24] R. A. Normann, E. M. Maynard, K. S. Guillory and D. J. Warren, "Cortical implants for the blind," *in IEEE Spectrum*, vol. 33, no. 5, pp. 54-59, May 1996

[25] R. A. Normann, E. M. Maynard, P. J. Rousche, and D. J. Warren, "A neural interface for a cortical vision prosthesis," *Vision Research*, vol. 39, no. 15, pp. 2577-2587, Jul. 1999.

[26] C. Nguyen and M. Miao, "Design of CMOS RFIC Ultra-Wideband Impulse Transmitters and Receivers,"*Springer International Publishing*, 2017.

[27] M. K. Kang and T. W. Kim, "CMOS IR-UWB Receiver for ±9.7-mm Range Finding in a Multipath Environment," *in IEEE Transactions on Circuits and Systems II: Express Briefs*, vol. 59, no. 9, pp. 538-542, Sept. 2012.

[28] S. Nagaraj and F. G. Rassam, "Improved Noncoherent UWB Receiver for Implantable Biomedical Devices," *in IEEE Transactions on Biomedical Engineering*, vol. 63, no. 10, pp. 2220-2225, Oct. 2016.

[29] R. Vauche, E. Muhr, O. Fourquin, S. Bourdel, J. Gaubert, N. Dehaese, S. Meillere, H. Barthelemy, and L. Ouvry, "A 100 MHz PRF IR-UWB CMOS Transceiver With Pulse Shaping Capabilities and Peak Voltage Detector," *in IEEE Transactions on Circuits and Systems I: Regular Papers*, vol. 64, no. 6, pp. 1612-1625, June 2017.

[30] J. Duan, Q. Hao, Y. Zheng, B. Wei, W. Xu and S. Xu, "Design of an incoherent IR-UWB receiver front-end in 180-nm CMOS technology," *Sixteenth International Symposium on Quality Electronic Design*, Santa Clara, CA, USA.

[31] D. Wentzloff, "Pulse-Based Ultra-Wideband Transmitters for Digital Communication," *Massachusetts Institute of Technology*, 2007.

[32] T. Liu, J. Anders, and M. Ortmanns, "Bidirectional optical transcutaneous telemetric link for brain machine interface," *Electronic Letters*, vol. 51, no. 24, pp. 1969-1971, 2015.

[33] T. Liu, U. Bihr, J. Becker, J. Anders, and M. Ortmanns, "In vivoverification of a 100 Mbps transcutaneous optical telemetric link", *in 2014 IEEE Biomedical Circuits and Systems Conference (BioCAS) Proceedings*, 2014, pp. 580-583.

[34] R. Ritter, J. Handwerker, T. Liu, and M. Ortmanns, "Telemetry for Implantable Medical Devices: Part 1 - Media Properties and Standards," *IEEE Solid-State Circuits Magazine*, vol. 6, no. 2, pp. 47-51, 2014.

[35] S. A. Mirbozorgi, H. Bahrami, M. Sawan, L. A. Rusch, and B. Gosselin, "A Single-Chip Full-Duplex High Speed Transceiver for Multi-Site Stimulating and Recording Neural Implants," *IEEE Transactions on Biomedical Circuits and Systems*, vol. 10, no. 3, pp. 643–653, 2016.

[36] W.H. Dobelle, "Artificial Vision for the Blind by Connecting a Television Camera to the Visual Cortex," *ASAIO J. 2000*, 2000, 46, 3-9.

[37] D. Tsai, D. Sawyer, A. Bradd, R. Yuste, and K. L. Shepard, "A very large-scale microelectrode array for cellular-resolution electrophysiology," *Nature Communications* 2017, *8*, 1802.

[38] A. J. Lowery, J. V. Rosenfeld, P. M. Lewis, D. Browne, A. Mohan, E. Brunton, E. Yan, *et al.* "Restoration of vision using wireless cortical implants: The Monash Vision Group project," *37th Annual International Conference of the IEEE Engineering in Medicine and Biology Society (EMBC)*, Milano, Italy, 25-29 August 2015; pp. 1041-1044.

[39] P. R. Troyk, D. Frim, B. Roitberg, V. L. Towle, K. Takahashi, S. Suh, M. Bak, S. Bredeson and Z. Hu "Implantation and testing of WFMA stimulators in macaque," *38th Annual International Conference of the IEEE Engineering in Medicine and Biology Society (EMBC)*, 2016, pp. 4499-4502.

[40] M. Yin, D. A. Borton, J. Aceros, W. R. Patterson, A.V. Nurmikko, "A 100-Channel Hermetically Sealed Implantable Device for Chronic Wireless Neurosensing Applications," *IEEE Transactions on Biomedical Circuits and Systems* 2013, 7, 115-128.

[41] J. Naumann, "Search for Paradise: A Patient's Account of the Artificial Vision Experiment". USA: *Xlibris*, 2012.

[42] NESTOR, "Neuronal Stimulation for Recovery of Function", Available online: https://nestor-sight.com/ (accessed on August 15th, 2020) .

[43] M. M. H. Shandhi, M. Leber, A. Hogan, R. Bhandari, S. Negi, "A novel method of fabricating high channel density neural array for large neuronal mapping," *18th International Conference on Solid-State Sensors, Actuators and Microsystems*, Anchorage, AK, USA, 21-25 June 2015; pp. 1759-1762.

[44] VISIO, "Royal Visio - Patient Organization ", Available online: https://www.visio.org/ (accessed on February 12th, 2022)

[45] Bartiméus, "Bartiméus - Patient Organization ", Available online: https://www.bartimeus.nl/ (accessed on February 12th, 2022)

[46] De Oogvereniging, "De Oogvereniging - Patient Organization ", Available online: https://www.oogvereniging.nl/ (accessed on February 12th, 2022)

[47] Y. Park et al., "A Wireless Power and Data Transfer IC for Neural Prostheses Using a Single Inductive Link With Frequency-Splitting Characteristic," *in IEEE Transactions on Biomedical Circuits and Systems*, vol. 15, no. 6, pp. 1306-1319, Dec. 2021.

[48] C. Guo, H. Zhang, Z. Ma, J. Zhang, J. Lin, and R. Zhang, "An inductive wireless telemetry circuit with OOK modulation for implantable cardiac pacemakers," *in 2015 IEEE 11th International Conference on ASIC (ASICON)*, 2015, pp. 1–4.

[49] M. M. Shanechi, R. C. Hu, and Z. M. Williams, "A cortical–spinal prosthesis for targeted limb movement in paralysed primate avatars," *Nature Communications*, vol. 5, no. 1, pp. 3237, 2014.

[50] Y.-K. Lo et al., "A Fully Integrated Wireless SoC for Motor Function Recovery After Spinal Cord Injury," IEEE Transactions on Biomedical Circuits Systems, vol. 11, no. 3, pp. 497–509, 2017.

[51] W. Liu et al., "A neuro-stimulus chip with telemetry unit for retinal prosthetic device," *IEEE Journal Solid-State Circuits*, vol. 35, no. 10, pp. 1487–1497, 2000.

[52] S. Mai, C. Zhang, M.Dong, and Z. Wang, "A Cochlear System with Implant DSP," *in 2006 IEEE International Conference on Acoustics Speech and Signal Processing Proceedings*, 2006, vol. 5.

[53] K. Shimizu, "Optical Biotelemetry," *in Handbook of Biomedical Telemetry*, John Wiley and Sons, Ltd, 2014, pp. 301–329.

[54] T. Sun, X. Xie, and Z. Wang, "Design challenges of the wireless power transfer for medical microsystems," *in 2013 IEEE International Wireless Symposium (IWS)*, 2013, pp. 1–4.

[55] M. Zgaren and M. Sawan, "A high-sensitivity battery-less wake-up receiver for 915 MHz ISM band applications," *2015 IEEE International Conference on Electronics, Circuits, and Systems (ICECS)*, 2015, pp. 336-339.

[56] H. Kassiri et al., "Battery-less Tri-band-Radio Neuro-monitor and Responsive Neurostimulator for Diagnostics and Treatment of Neurological Disorders," *in IEEE Journal of Solid-State Circuits,* vol. 51, no. 5, pp. 1274-1289, May 2016.

[57] R. E. Ziemer and W. H. Tranter, *Principles of Communications Systems, Modulation, and Noise*. New York, USA: John Wily and Sons, 2010.

[58] H. Taub and D. L. Schilling, *Principle of Communication Systems*. New York, USA: McGraw-Hill Companies, 1999.

[59] Chua-Chin Wang, Ya-Hsin Hsueh, U Fat Chio, and Yu-Tzu Hsiao, "A C-less ASK demodulator for implantable neural interfacing chips," *in 2004 IEEE International Symposium on Circuits and Systems (IEEE Cat. No.04CH37512)*, 2004, vol. 4, pp. IV–57.

[60] P. R. Troyk and G. A. DeMichele, "Inductively-coupled power and data link for neural prostheses using a class-E oscillator and FSK modulation," *in Proceedings of the 25th Annual International Conference of the IEEE Engineering in Medicine and Biology Society (IEEE Cat. No.03CH37439),* 2003, vol. 4, pp. 3376-3379 Vol.4.

[61] P. M. Lewis, H. M. Ackland, A. J. Lowery, and J. V. Rosenfeld, "Restoration of vision in blind individuals using bionic devices: A review with a focus on cortical visual prostheses," *Brain Research*, vol. 1595, pp. 51–73, 2015.

[62] J. Coulombe, M. Sawan, J. F. Gervais, "A Highly Flexible System for Microstimulation of the Visual Cortex: Design and Implementation," *IEEE Transactions on Biomedical Circuits and Systems* 2007, 1, 258-269.

[63] M. Ghovanloo, K. Najafi, "A wideband frequency-shift keying wireless link for inductively powered biomedical implants,"*IEEE Transactions on Circuits and Systems I: Regular Papers*, 2004, 51, 2374-2383.

[64] A. Ghenim, D. Daoud, M. Ghorbel, A. B.Hamida, J. Tomas, "A dual band wireless power and DPSK data telemetry for biomedical implants," *ICM 2011 Proceeding*, Hammamet, Tunisia, 19-22 December 2011; pp. 1-5.

[65] F. Asgarian and A. M. Sodagar, "Wireless Telemetry for Implantable Biomedical Microsystems, Biomedical Engineering," *Trends in Electronics*; Laskovski, A.N., Ed.; IntechOpen: London, UK, 2011.

[66] F. Asgarian, A. M. Sodagar, "A high-data-rate low-power BPSK demodulator and clock recovery circuit for implantable biomedical devices,"*4th International IEEE/EMBS Conference on Neural Engineering*, Antalya, Turkey, 29 April-2 May 2009; pp. 407-410.

[67] M. Kiani, M. Ghovanloo, "A 13.56-Mbps Pulse Delay Modulation Based Transceiver for Simultaneous Near-Field Data and Power Transmission," *IEEE Trans. Biomed. Circuits Syst.* 2015, 9, 1-11.

[68] M. Zhou, M. R. Yuce, W. Liu, "A Non-Coherent DPSK Data Receiver With Interference Cancellation for Dual-Band Transcutaneous Telemetries," *IEEE Journal of Solid-State Circuits*, 2008, 43, 2003-2012.

[69] A. E. Omisakin, R. M. C. Mestrom, M. J. Bentum, "Low-Power Communication for an Implanted Intracortical Visual Prosthesis," *13th European Conference on Antennas and Propagation EuCAP*, Krakow, Poland, 31 March-5 April 2019.

[70] R. Puers, J. Thoné, "Short Distance Wireless Communications," In *Bio-Medical CMOS ICs*; H.J. Yoo, C. van Hoof, Editors; Springer: New York, NY, USA, 2011.

[71] A. E. Omisakin, R. M. C. Mestrom, M. J. Bentum, "Low-Power BPSK Inductive Data Link for an Implanted Intracortical Visual Prosthesis," *41st Conference on Engineering in Medicine and Biology EMBC*, Berlin, Germany,23-27 July 2019.

[72] F. Shahrokhi, K. Abdelhalim, D. Serletis, P. L. Carlen, R. Genov, "The 128-Channel Fully Differential Digital Integrated Neural Recording and Stimulation Interface," *IEEE Transactions on Biomedical Circuits and Systems* 2010, 4, 149-161.

[73] M. S. Chae, Z. Yang, M. R. Yuce, L. Hoang, and W. Liu, "A 128-Channel 6 mW Wireless Neural Recording IC With Spike Feature Extraction and UWB Transmitter," *IEEE Transactions on Neural Systems and Rehabilitation Engineering* 2009, 17, 312-321.

[74] K. E. Jones and R. A. Normann, "An advanced demultiplexing system for physiological stimulation," *IEEE Transactions on Biomedical Circuits and Systems* 1997, 44, 1210-1220.

[75] A.I. Al-Kalbani, M. R. Yuce, J. M. Redouté, "Safe SAR levels in inductively powered brain implanted visual prostheses," *International Symposium on Electromagnetic Compatibility*, Rome, Italy, 17-21 September 2012; pp. 1-6.

[76] B. Lenaerts and R. Puers, "Biological Tissue Interaction," *Omnidirectional Inductive Powering for Biomedical Implants*, 1 ed.; Springer: Berlin/Heidelberg, Germany, 2009.

[77] J. Delbeke and C. Veraart, "Visual Prostheses", *Encyclopedia of Medical Devices and Instrumentation*, 2nd ed.; John Wiley & Sons, Inc.: Hoboken, NJ, USA, 2006, pp. 530-549.

[78] L. W. Couch, *Digital and Analog Communication Systems*, 8th ed.; Prentice Hall: Upper Saddle River, NJ, USA, 2012.

[79] M. Zhou, W. Liu,"A Non-Coherent PSK Receiver with Interference-Canceling for Transcutaneous Neural Implants,"*IEEE International Solid-State Circuits Conference,* San Francisco, CA, USA, 11-15 February 2007; pp. 156-593.

[80] M. A. Hannan, S. M. Abbas, S. A. Samad, A. Hussain"," Modulation techniques for biomedical implanted devices and their challenges,"*Sensors*, 2012, 12, 297-319.

[81] L. D. Xing, S. Shafie, and H. Ramiah,"Low power BPSK modulator for the application of capsule endoscope," *In Proceedings of the 2011 Fourth International Conference on Modeling, Simulation and Applied Optimization,* Kuala Lumpur, Malaysia, 19-21 April 2011; pp. 1-4.

[82] F. E. Terman, Radio Engineers' Handbook; *McGraw-Hill Book Company:* New York, NY, USA, 1943.

[83] M. Zgaren and M. Sawan,"A Low-Power Dual-Injection-Locked RF Receiver With FSK-to-OOK Conversion for Biomedical Implants,"*IEEE Transaction of Circuits and System I: Regular Papers* 2015, 62, 2748-2758.

[84] Y. Hu and M. Sawan, "A fully integrated low-power BPSK demodulator for implantable medical devices," *IEEE Transaction of Circuits and System I: Regular Papers*, 2005, 52, 2552-2562.

[85] C. Gong, D. Liu, Z. Miao, W. Wang, and M. Li, "An NFC on Two-Coil WPT Link for Implantable Biomedical Sensors under Ultra-Weak Coupling," *Sensors*, 2017, 17, 1358.

[86] C. Aprile, K. Ture, L. Baldassarre, M. Shoaran, G. Yilmaz, F. Maloberti, C. Dehollain, Y. Leblebici, and V. Cevher, "Adaptive Learning-Based Compressive Sampling for Low-power Wireless Implants,"*IEEE Transaction of Circuits and System I: Regular Papers*, 2018, 65, 3929-3941.

[87] L. Navaii, M. Sadjedi, H. and A. Sarrafzadeh, "Efficient ASK Data and Power Transmission by the Class-E With a Switchable Tuned Network," *IEEE Transaction of Circuits and System I: Regular Papers* 2018, 65, 3255-3266.

[88] T. M. Seese, H. Harasaki, G. M. Saidel, and C. R. Davies, "Characterization of tissue morphology, angiogenesis, and temperature in the adaptive response of muscle tissue to chronic heating," *Lab Investig.* 1998, 78, 1553-1562.

[89] S. Kim, R. A. Normann, R. Harrison, and F. Solzbacher, "Preliminary Study of the Thermal Impact of a Microelectrode Array Implanted in the Brain,"*International Conference of the IEEE Engineering in Medicine and Biology Society*, New York, NY, 30 August-3 September 2006; pp. 2986-2989.

[90] D. Liu, H. Hu, and S. V Georgakopoulos, "Misalignment Sensitivity of Strongly Coupled Wireless Power Transfer Systems," *IEEE Transactions on Power Electronics*, vol. 32, no. 7, pp. 5509–5519, 2017.

[91] A. De Marcellis, E. Palange, M. Faccio, G. Di Patrizio Stanchieri, and T. G. Constandinou, "A 250Mbps 24pJ/bit UWB-inspired optical communication system for bioimplants," *in 2017 IEEE Biomedical Circuits and Systems Conference (BioCAS)*, 2017, pp. 1–4.

[92] T. Liu, J. Anders, and M. Ortmanns, "Bidirectional optical transcutaneous telemetric link for brain machine interface," *Electronics Letters*, vol. 51, no. 24, pp. 1969–1971, 2015.

[93] R. R. Harrison, P. T. Watkins, R. J. Kier, D. J. Black, R. O. Lovejoy,R. A. Normann, and F. Solzbacher, "Design and Testing of an Integrated Circuit for Multi-Electrode Neural Recording," *in 20th International Conference on VLSI Design held jointly with 6th International Conference on Embedded Systems (VLSID'07)*, 2007, pp. 907–912.

[94] Federal Communications Commission, "FCC First Report and Order 02-48," 2002.

[95] H. Bahrami, L. A. Rusch, and B. Gosselin, "Biological channel modeling and implantable UWB antenna design for neural recording systems," *Handb. Bioelectron. Directly Interfacing Electron* Biol. Syst., vol. 62, no. 1, pp. 379–388, Jan. 2015.

[96] A. Bevilacqua and A. M. Niknejad, "An ultrawideband CMOS low-noise amplifier for 3.1-10.6-GHz wireless receivers," *IEEE Journal of Solid-State Circuits*, vol. 39, no. 12, pp. 2259–2268, Dec. 2004.

[97] B. Razavi, RF Microelectronics, 2nd ed. Prentice-Hall Inc, 2012.

[98] H. Arslan, Z.N. Chen, M.G. Di Benedetto, Ultra Wideband Wireless Communications, *John Wiley and Sons Inc*, Hoboken, NJ, 2006.

[99] C. Yoon et al., "Design of a Low-Noise UWB Transceiver SiP," *IEEE Des. Test Comput.*, vol. 25, no. 1, pp. 18–28, Jan. 2008.

[100] D.Andreuccetti, R.Fossi and C.Petrucci, "An Internet resource for the calculation of the dielectric properties of body tissues in the frequency range 10 Hz - 100 GHz. IFAC-CNR", Florence (Italy), 1997. Based on data published by C.Gabriel et al. in 1996. [Online]. Available: http://niremf.ifac.cnr.it/tissprop/

[101] C. Gabriel, S. Gabriel, and E. Corthout, "The dielectric properties of biological tissues: I. Literature survey," *Physics in Medicine and Biology,* vol. 41, no. 11, pp. 2231–2249, Nov. 1996.

[102] S. Gabriel, R. W. Lau, and C. Gabriel, "The dielectric properties of biological tissues: II. Measurements in the frequency range 10 Hz to 20 GHz," *Physics in Medicine and Biology,* vol. 41, no. 11, pp. 2251–2269, Nov. 1996.

[103] D. Anzai, K. Katsu, R. Chavez-Santiago, Q. Wang, D. Plettemeier, J. Wang, and I. Balasingham, "Experimental Evaluation of Implant UWB-IR Transmission With Liv-

ing Animal for Body Area Networks," *in IEEE Transactions on Microwave Theory and Techniques*, vol. 62, no. 1, pp. 183-192, Jan. 2014.

[104] Y. P. Zhang and Q. Li, "Performance of UWB Impulse Radio With Planar Monopoles Over On-Human-Body Propagation Channel for Wireless Body Area Networks,"*in IEEE Transactions on Antennas and Propagation*, vol. 55, no. 10, pp. 2907-2914, Oct. 2007.

[105] A. Zaric, J. R. Costa and C. A. Fernandes, "Low profile UWB antenna for Wireless Body Area Networks," *The 8th European Conference on Antennas and Propagation (EuCAP 2014)*, The Hague, Netherlands, 2014, pp. 3105-3107.

[106] M. Y. Cho, S. S. Tiang, W. H. Lim and M. Mokayef, "Compact Trapezoidal-Shaped Monopole-Like Slot UWB Antenna for WBAN Applications," 2019 *2nd World Symposium on Communication Engineering (WSCE)*, Nagoya, Japan, 2019, pp. 93-97.

[107] M. A. Rahman and M. F. Hossain, "CPW-fed Ultra-wideband Flexible Disc Monopole Antenna Design for Early Detection of Brain Stroke," *2019 International Conference on Computer, Communication, Chemical, Materials and Electronic Engineering (IC4ME2)*, Rajshahi, Bangladesh, 2019, pp. 1-6.

[108] Y. Zheng, M. A. Arasu, K. Wong, Y. J. The, A. P. H. Suan, D. D. Tran, W. G. Yeoh, and D. Kwong, "A 0.18μ m CMOS 802.15.4a UWB Transceiver for Communication and Localization," *2008 IEEE International Solid-State Circuits Conference - Digest of Technical Papers*, San Francisco, CA, USA, 2008.

[109] L. Zhou, Z. Chen, C. Wang, F. Tzeng, V. Jain and P. Heydari, "A 2-Gb/s 130-nm CMOS RF-Correlation-Based IR-UWB Transceiver Front-End," *in IEEE Transactions on Microwave Theory and Techniques,* vol. 59, no. 4, pp. 1117-1130, April 2011.

[110] A. Ebrazeh and P. Mohseni, "30 pJ/b, 67 Mbps, Centimeter-to-Meter Range Data Telemetry With an IR-UWB Wireless Link," *in IEEE Transactions on Biomedical Circuits and Systems*, vol. 9, no. 3, pp. 362-369, June 2015.

[111] M. Ha, Y. Park, and Y. Eo, "A inductorless non-coherent IR-UWB CMOS receiver for 3–5GHz band applications," *2008 Asia-Pacific Microwave Conference*, Hong Kong, China, 2008.

[112] F. S. Lee and A. P. Chandrakasan, "A 2.5 nJ/bit 0.65 V Pulsed UWB Receiver in 90 nm CMOS," *IEEE Journal of Solid-State Circuits*, vol. 42, no. 12, pp. 2851–2859, Dec. 2007.

[113] Coaxial Bandpass Filter, *VBFZ-3590-S+*. [Online]. Available: https://www.minicircuits.com/pdfs/VBFZ-3590+.pdf

[114] 20 MHz to 6 GHz RF/IF Gain Block, *ADL5542 Evaluation board*. 2015. [Online]. Available: https://www.analog.com/media/en/technical-documentation/datasheets/ADL5542.pdf

[115] 1 MHz to 8 GHz, 70 dB Logarithmic Detector/Controller, *AD8318 Evaluation board*. 2017. [Online]. Available: https://www.analog.com/media/en/technical-

documentation/data-sheets/AD8318.pdf

[116] Rail-to-Rail, Very Fast, 2.5 V to 5.5 V,Single-Supply TTL/CMOS Comparators, *ADCMP600*. 2011. [Online]. Available: https://www.analog.com/media/en/technical-documentation/data-sheets/ADCMP600_601_602.pdf

[117] SIMULIA Studio Suite, "Dassault Systèmes SIMULIA," 2019. http:// www.3ds.com

[118] Cadence Virtuoso Software, "Cadence Systems," 2017. http:// www.cadence.com

[119] P. Uthaichana and E. Leelarasmee, "Low power CMOS dynamic latch comparators,"*IEEE TENCON 2003. Conference on Convergent Technologies for Asia-Pacific Region,* 2003, pp. 605-608 Vol.2.

[120] X. Chen, F. Wang, E. Fernandez, and P. R. Roelfsema, "Shapeperception via a high-channel-count neuroprosthesis in monkey visualcortex," *Science*, vol. 370, no. 6521, pp. 1191–1196, 2020.

[121] A. E. Omisakin, R. M. C. Mestrom, and M. J. Bentum, "System Design of a Low-power Wireless Link for Neural Recording in a Visual Prosthesis," *in 2019 IEEE AFRICON*, Accra, Ghana, 2019.

[122] A. E. Omisakin, R. M. C. Mestrom, and M. J. Bentum, "Low-Power Wireless Data Transfer System for Stimulation in an Intracortical Visual Prosthesis," *Sensors*, vol. 21, no. 3, 2021.

[123] H. Bahrami, B. Gosselin, and L. A. Rusch, "Realistic modeling of the biological channel for the design of implantable wireless UWB communication systems," *in 2012 Annual International Conference of the IEEE Engineering in Medicine and Biology Society*, 2012, pp. 6015–6018.

[124] S. Suman, K. G. Sharma, and P. K. Ghosh, "Analysis and design of current starved ring VCO," *in 2016 International Conference on Electrical, Electronics, and Optimization Techniques (ICEEOT),* 2016, pp. 3222–3227.

[125] M. Miao and C. Nguyen, "On the Development of an Integrated CMOS-Based UWB Tunable-Pulse Transmit Module," *IEEE Transactions on Microwave Theory and Techniques,* vol. 54, no. 10, pp. 3681–3687,2006.

[126] N. Weste and D. Harris, CMOS VLSI Design: A Circuits and Systems Perspective, 4th ed. USA: *Addison-Wesley Publishing Company*, 2010.

[127] P. Cenci, M. Bolatkale, R. Rutten, G. Lassche, K. Makinwa, andL. Breems, "A 28 nm 2 GS/s 5-b single-channel SAR ADC with gm-boosted Strong ARM comparator," *in ESSCIRC 2017 - 43rd IEEE European Solid State Circuits Conference*, 2017, pp. 171–174.

[128] P. Toledo, R. Rubino, F. Musolino, and P. Crovetti, "Re-Thinking Analog Integrated Circuits in Digital Terms: A New Design Concept for the IoT Era," *IEEE Transactions on Circuits and Systems II: Express Briefs*, vol. 68, no. 3, pp. 816–822, 2021.

[129] R. B. Staszewski, "Digital RF and digitally-assisted RF (invited)," *in 2011 IEEE International Symposium on Radio-Frequency Integration Technology*, 2011, pp. 9–16.

[130] S. Lee, K. Song, J. Yoo, and H.-J. Yoo, "A Low-Energy Inductive Coupling Transceiver With Cm-Range 50-Mbps Data Communication in Mobile Device Applications," *IEEE Journal of Solid-State Circuits*, vol. 45, no. 11, pp. 2366–2374, 2010.

[131] S. Maity, B. Chatterjee, G. Chang, and S. Sen, "BodyWire: A 6.3-pJ/b30-Mb/s - 30 dB SIR Tolerant Broadband Interference-Robust Human Body Communication Transceiver Using Time Domain Interference Rejection," *IEEE Journal of Solid-State Circuits,* vol. 54, no. 10, pp. 2892–2906, 2019.

[132] Q. Hu, X. Tang, and W. Tang, "Integrated Asynchronous Ultrawide-band Impulse Radio With Intrinsic Clock and Data Recovery," *IEEE Microwave and Wireless Components Letters*, vol. 27, no. 4, pp. 416–418, 2017.

[133] X. Y. Wang, R. K. Dokania, and A. B. Apsel, "A Crystal-Less Self-Synchronized Bit-Level Duty-Cycled IR-UWB Transceiver System," *IEEE Transactions on Circuits and Systems I: Regular Papers*, vol. 60,no. 9, pp. 2488–2501, 2013.

[134] W. Tang, S. Chen, and E. Culurciello, "Live demonstration: A FSK-OOK ultra wide-band impulse radio system with spontaneous clock anddata recovery," *in 2012 IEEE International Symposium on Circuits andSystems (ISCAS)*, 2012, pp. 696–700.

[135] H. Lyu, X. Liu, and A. Babakhani, "A 100-m/s 2.6-pj/pulse compact uwbimpulse transmitter based on antenna-and-pulse-generator codesign," *IEICE Electronics Express*, vol. 16, no. 24, pp. 20 190 672–20 190 672, 2019.

[136] S. Hu, P. Chen, P. Quinlan, and R. B. Staszewski, "A 0.7-V Sub-mW Type-II Phase-Tracking Bluetooth Low Energy Receiver in 28-nmCMOS," *IEEE Transactions on Circuits and Systems I: Regular Papers* ,vol. 68, no. 6, pp. 2317–2328, 2021.

[137] S. Hu, J. Du, P. Chen, H. M. Nguyen, P. Quinlan, T. Siriburanon, and R. B. Staszewski,"A Type-II Phase-Tracking Receiver," *IEEE Journal of Solid-State Circuits*, vol. 56, no. 2, pp. 427–439, 2021.

[138] M.-C. Lee, A. Karimi-Bidhendi, O. Malekzadeh-Arasteh, P. T. Wang,A. H. Do, Z. Nenadic, and P. Heydari,"A CMOS MedRadio Transceiver With Supply-Modulated Power Saving Technique for an Implantable Brain -Machine Interface System," *IEEE Journal of Solid-State Circuits*,vol. 54, no. 6, pp. 1541–1552, 2019.

[139] W. Saadeh, M. A. B. Altaf, H. Alsuradi, and J. Yoo, "A 1.1-mW Ground Effect-Resilient Body-Coupled Communication Transceiver With Pseudo OFDM for Head and Body Area Network," *IEEE Journal of Solid-State Circuits*, vol. 52, no. 10, pp. 2690–2702, 2017.

[140] Diligent Inc., "Analog Discovery 2," Sep. 2015.

[141] Teledyne LeCroy, "Wavemaster 8 zi-B oscilloscopes 4 GHz - 30 GHz," May 2019.

[142] D. Liu, S. Geng, W. Rhee, and Z. Wang, "A high efficiency robust IR-UWB receiver design for high data rate CM-range communications,"*in2014 IEEE International Symposium on Circuits and Systems (ISCAS)*, 2014, pp. 1901–1904.

[143] Z. Zhang, Y. Li, K. Mouthaan, and Y. Lian, "A Miniature Mode Reconfigurable Inductorless IR UWB Transmitter Receiver for Wireless Short Range Communication and Vital Sign Sensing," *IEEE Journal on Emerging and Selected Topics in Circuits and Systems*, vol. 8, no. 2, pp. 294–305, 2018.

[144] F. Kuo, S. Binsfeld Ferreira, H. R. Chen, L. Cho, C. Jou, F. Hsueh, I. Madadi, M. Tohidian, M. Shahmohammadi, M. Babaie, and R. B. Staszewski, "A Bluetooth Low-Energy Transceiver With 3.7-mW All- Digital Transmitter, 2.75-mW High-IF Discrete-Time Receiver, and TX/RX Switchable On-Chip Matching Network," *IEEE Journal of Solid- State Circuits*, vol. 52, no. 4, pp. 1144–1162, Apr 2017.

[145] D. Liu, X. Ni, R. Zhou, W. Rhee, and Z. Wang, "A 0.42-mW 1-Mb/s 3- to 4-GHz Transceiver in 0.18um CMOS With Flexible Efficiency, Bandwidth, and Distance Control for IoT Applications," *IEEE Journal of Solid-State Circuits*, vol. 52, no. 6, pp. 1479–1494, 2017.

[146] K. Teng and C. Heng, "A 370-pJ/b Multichannel BFSK/QPSK Transmitter Using Injection-Locked Fractional-N Synthesizer for Wireless Biotelemetry Devices," *IEEE Journal of Solid-State Circuits*, vol. 52, no. 3, pp. 867–880, 2017.

[147] J. Bae, K. Song, H. Lee, H. Cho, and H. Yoo, "A 0.24-nJ/b Wireless Body-Area-Network Transceiver With Scalable Double-FSK Modulation," *IEEE Journal of Solid-State Circuits*, vol. 47, no. 1, pp. 310–322, Jan 2012.

[148] Y. Liu, C. Bachmann, X. Wang, Y. Zhang, A. Ba, B. Busze, M. Ding, P. Harpe, G. van Schaik, G. Selimis, H. Giesen, J. Gloudemans, A. Sbai, L. Huang, H. Kato, G. Dolmans, K. Philips, and H. de Groot, "13.2 A 3.7mW-RX 4.4mW-TX fully integrated Bluetooth Low- Energy/IEEE802.15.4/proprietary SoC with an ADPLL-based fast frequency offset compensation in 40nm CMOS," *in 2015 IEEE International Solid-State Circuits Conference - (ISSCC) Digest of Technical Papers*, feb 2015, pp. 1–3.

[149] H. Cho, H. Lee, J. Bae, and H. Yoo, "A 5.2 mW IEEE 802.15.6 HBC Standard Compatible Transceiver With Power Efficient Delay-Locked- Loop Based BPSK Demodulator," *IEEE Journal of Solid-State Circuits*, vol. 50, no. 11, pp. 2549–2559, nov 2015.

[150] M. Oshiro, T. Maruyama, T. Tokairin, Y. Tuda, T. Wang, N. Koide, Y. Ogasawara, T. T. Ta, H. Yoshida, and K. Sami, "A 3.2 mA-RX 3.5 mA-TX fully integrated SoC for Bluetooth Low Energy," *in 2016 IEEE Asian Solid-State Circuits Conference (A-SSCC)*, nov 2016, pp. 1–4.

[151] K. M. S. Thotahewa, J. M. Redout, and M. R. Yuce, "Electromagnetic and thermal effects of IR-UWB wireless implant systems on the human head," *in 2013 35th Annual International Conference of the IEEE Engineering in Medicine and Biology Society (EMBC)*, 2013, pp. 5179– 5182.

[152] T. P. G. van Nunen, H. J. Visser and R. M. C. Mestrom . "Wireless Power Transfer to a Visual Prosthesis: 100 mW at 6.78 MHz", *in 2021 IEEE International Symposium on Antennas and Propagation and USNC-URSI Radio Science Meeting*, December 2021.

[153] J. N. Fayad, S. R. Otto, R. V. Shannon and D. E. Brackmann, "Cochlear and Brainstem Auditory Prostheses "Neural Interface for Hearing Restoration: Cochlear and Brain Stem Implants", *in Proceedings of the IEEE*, vol. 96, no. 7, pp. 1085-1095, 2008.

[154] INTENSE, "Innovative NeuroTEchNology for SociEty", Available online: https://intenseproject.eu/ (accessed on September 15th, 2021)

Acknowledgments

A journey of a thousand miles begins with a single step. So it was with my four years of doctorate research work. That first step was my contact with the Dean of my faculty, Bart Smolders, to whom I express gratitude. He found an opportunity interesting for me, believing in my capacity to handle challenging research projects.

One is too small a number to accomplish great things. I want to thank my first promotor Mark Bentum for his outstanding leadership and supervision to finish my PhD work on time. My daily supervisor Rob Mestrom deserves several applauds for his efficiency and remarkable way of setting me on track and keeping me focused. I appreciate their detailed comments and reviews in several of my publications, including this thesis, to bring them to a high standard of expression to experts and non-experts in my field.

I would like to appreciate the Electromagnetic group of the Department of Electrical Engineering where I worked. Including Suzanne Kuijlaars for her assistance with administrative tasks and Ad Reniers for his support with the labs associated with the group enabling me to carry out early prototyping.

It is very satisfying to know that your work is part of a larger context, in my case, the NESTOR consortium. I want to thank the NESTOR project's user committee, including Pieter Roelfsema and Xing Chen from The Netherlands Institute for Neuroscience, Florian Solzbacher from Blackrock Microsystems , Mark Boer from AEMICS and Bert Monna from Tiberian, for shaping the context of my research and giving insight into the overall application. The multiple meetings at The Netherlands Institute for Neuroscience with Pieter, Xing and the entire NESTOR team motivated me to deliver quality research. I enjoyed my visit to the USA for a discussion with Blackrock Microsystems. Thanks to Florian, I got some inspiration from the visit.

Furthermore, I would like to thank the committee members, prof. Bart Smolders, prof. Wouter Serdijn, prof. Florian Solzbacher, prof. Huib Visser and dr. Pieter Harpe for their time reading and reviewing the thesis. Their valuable comments and constructive criticism have kept me alert till the very end.

Doing a PhD research sometimes requires you to gain new expertise in areas related to the study. In my case was that of miniaturization and Integrated Circuits. Therefore, I would like to thank Georgi Radulov, Pieter Harpe, and Rainier van Dommele of the Integrated circuit

Curriculum Vitae

Adedayo Eberechukuwu Omisakin was born on the 3rd of March, 1994, in Lagos, Nigeria. Starting in 2010, he studied electrical and electronic engineering at Eastern Mediterranean University, Famagusta, Cyprus, where he graduated with a maximum possible grade point average. He later moved to the Netherlands in 2015 to start his Master program at Eindhoven University of Technology (TU/e). As part of his master's program, he was also an intern at Philips Lighting and later at Philips Innovation Services. He worked on Indoor positioning and novel metamaterial backed antennas for body-worn application, respectively. He earned a Broadband Telecommunication Technology certificate in addition to his MSc degree.

In 2017, Adedayo immediately continued his academic career as a doctoral candidate in the Electromagnetic group of the Department of Electrical Engineering, TU/e. He worked on the NESTOR project focusing on wireless system development. The main results of this project are presented in this thesis. He also collaborated with the integrated circuit group of his department to miniaturize part of the wireless system he developed. He is working as a Design Flow and Modelling Engineer at NXP Semiconductors.